creative commons
COMMONS DEED

저작자표시-비영리-변경금지 2.0 대한민국

이용자는 아래의 조건을 따르는 경우에 한하여 자유롭게

- 이 저작물을 복제, 배포, 전송, 전시, 공연 및 방송할 수 있습니다.

다음과 같은 조건을 따라야 합니다:

저작자표시. 귀하는 원저작자를 표시하여야 합니다.

비영리. 귀하는 이 저작물을 영리 목적으로 이용할 수 없습니다.

변경금지. 귀하는 이 저작물을 개작, 변형 또는 가공할 수 없습니다.

- 귀하는, 이 저작물의 재이용이나 배포의 경우, 이 저작물에 적용된 이용허락조건을 명확하게 나타내어야 합니다.
- 저작권자로부터 별도의 허가를 받으면 이러한 조건들은 적용되지 않습니다.

저작권법에 따른 이용자의 권리는 위의 내용에 의하여 영향을 받지 않습니다.

이것은 이용허락규약(Legal Code)을 이해하기 쉽게 요약한 것입니다.

Disclaimer

dCollection

공학박사학위논문

Fabrication and Characterization of the Atomic Layer Deposited Yttria Stabilized Zirconia on Ceria Electrolytes

세리아 상의 이트리아 안정화 지르코니아 원자막 증착을 통한 이중층 전해질의 제작과 분석

2012 년 8 월

서울대학교 대학원

기계항공공학부

지 영 석

Abstract

The fact that hydrogen will be the last energy source became no more attractive to us. The main issue is which kind of energy conversion device will be going to survive in the future. Since many researchers highlighted the fuel cell as the next generation power source, a lot of researched have been conducted to commercialize it.

SOFCs have many advantages in comparison with typical PEMFCs which have shown water management problem, usage of novel catalyst, patent issue for polymer electrolyte, expansive graphite bipolar plate and CO poisoning. So many researchers in energy field have been thought SOFC would be the promising device.

But the main bottle neck for the commercialization of SOFC has been its high operation temperature. It can cause thermal mismatch between MEA, nickel agglomeration, reactions between component materials, restricted sealant choice and expensive interconnecter material. So we focused our interest to IT-SOFC. Its temperature position can avoid many problems of HT-SOFC and LT-SOFC maintaining the competitiveness of original SOFC's characteristics.

We started this study to lower the operation temperature of SOFCs using representative two methods; thin film layer and high conductive electrolyte material. To conduct electrochemical characterization, we made

and modified the customized experimental setup and the cell supporting fixture.

The attempt to fabricate bi-layered electrolyte cells via ALD method could prove great feasibility that a nano-scaled YSZ thin layer was able to enhance the performance and the durability of GDC-based SOFCs for intermediate temperature operation.

First, we deposited YSZ on bulk GDC via ALD successfully, and we confirmed the thickness, growth rate and composition were as expected with FIB-SEM and XPS depth profile characterization. We found out that the thin YSZ layer survived the electrode sintering process and the reducing operation condition. With the 690 cycles (about 100nm) ALD-YSZ electrolyte cell, we observed increases of over 50% in the peak power density and of about 5% in OCV under identical gas flow rates at 600°C, and constant OCV behavior over about 8 hours under 5% hydrogen-concentration unlike the case of the pure GDC electrolyte cell. The origin of the enhanced power density was presumed to be the protective ALD-YSZ layer that could prevent the ceria reduction which might result in electron conductivity and micro crack generation on GDC; thus, it could enable to prevent the voltage drop and the increase of ohmic resistance.

Second, we observed the surfaces of ALD-YSZ/GDC bi-layered electrolytes that were exposed various temperatures and hydrogen gas. Through the AFM results we confirmed ALD-YSZ layer could suppress the

roughness changing in hydrogen gas and there was critical thickness limit for this functionality according to temperature. At 1200°C, the tendency that YSZ melted and move to GDC's grain boundary started. We confirmed the start of YSZ/GDC mixing at this temperature with XPS depth profile results. We could know the cell fabrication temperature limit must exist between 800°C and 1200°C and that wet ceramic process must be prohibited in electrodes fabrication for this structure cells. The hydrogen exposure results said that in 600°C H_2 the surface stability of bi-layered structure was preserved from 50nm YSZ thickness. But at in 800°C H_2 the thickness limit increased to 100nm.

Third, in the results of comparison ALD-YSZ bi-layered cells with PLD-YSZ bi-layered cells, we confirmed the effect of ALD-YSZ layer started from 100nm, where the effect of PLD-YSZ layer started from 100nm. We thought this result came from the different surface morphology and the film property due to the different deposition unit and process between ALD and PLD. Besides, in the experiment of the 1mm GDC electrolyte with 100nm PLD-YSZ layer, we concluded 100nm PLD-YSZ functioned as a GDC cracking preventer which could maintains contact resistance not as an electron insulator because the thick GDC itself had high electron resistance.

After confirming the high functionality of ALD-YSZ layer and the cell fabrication limit, the last experiment was the fabrication thin film free-standing bi-layered electrolyte cell. We made the cells from ALD-YSZ,

sputtering-GDC and sputtering-Pt on AAO substrate and all of the fabrication temperature did not exceed 500°C. The results were satisfactory. The OCV was about 1V and the peak power density was about 77mW/cm^2 at 450°C. From this experiment, we confirmed our electrolyte structure could be adoptable to thin film SOFCs in LT operation.

Keywords: solid oxide fuel cell (SOFC), intermediate temperature, gadolinia doped ceria (GDC), atomic layer deposition (ALD), bi-layered electrolyte

Identification Number: 2008-30200

Contents

List of Figures

List of Tables

1. Introduction

1.1 Research background

From 1st and 2nd oil shock, we could know that high oil price would threaten the stability of world economy crucially. The worries to depletion of natural resources and the rapid resource consumption from the fast industrialization of BRICs, have become direct and indirect origins of international conflicts. Some reports said that the leadership of future depends on the securement of energy resources. And energy became a big issue more than past 10 years for an individual from the increase of the demand for portable power due to the spread of mobile information devices.

Because the world win the sympathy that destruction of the environment is due to the hydrocarbon fuel production and usage, so many discussions and congresses have been open for example Kyoto protocol that regulates the usage of carbon dioxide (CO_2), methane (CH_4), nitrogen dioxide (NO_2), fluorocarbon (PFC), hydrofluorocarbon (HFC) and sulfur nexafluoride (SF_6) but promotes the conversion to hydrogen economy.

The future energy paradigm suggested by Department of Energy (DOE) starts from hydrogen production from solar energy and finishes the circulation with electric production / hydrogen consumption by fuel cells. Through this

plan, the field of fuel cell has been studied for a promising substitution energy device by worldwide laboratories and enterprises.

A fuel cell is a device which can change the chemical energy from chemical species into the electric energy that can be used for us directly. This direct energy conversion system is distinct from a conventional internal combustion engine (or generator). In an engine, the form of energy has been converted from chemical energy into heat energy into kinetic energy then finally into electric energy. These complex and multi-step conversion procedure cause lots of energy loss. So the efficiency lowered down thus more fuel must be needed. Because an engine is based on fossil fuel combustion, it is inevitable to pollute the air.

A direct energy conversion device exists not for from us. Batteries are good example. But they show some disadvantages for example heavy weight, relatively small energy density for long operation, slow recharging, short life due to often charging and discharging cycle and difficult capacity scale up/down. Fuel cells called 3rd generation battery can get continuous fuel supplying that is fuel cell get the liberation from recharging time and space restriction. For a portable application, it means changing fuel cartridges that have much more capacity than batteries. For an electric vehicle application, it means more distance per fueling and more fuel efficiency from light weight.

Fuel cells first introduced first by William Grove in 1839 in England. The first fuel cell had the simple platinum electrodes structure reacting hydrogen and oxygen each. Figure 1.1 is the operation principal of his fuel cell (and of conventional fuel cells). Hydrogen gas fed to anode divided to proton ions and electrons. Electrons flow through circuit and load then arrive to cathode. Protons flow through electrolyte which was intended to conduct ion only. Protons and electrons meet oxygen in the air at cathode. Producing water, reaction cycle is finished. Reaction formula is shown below.

$$H_2 + \frac{1}{2}O_2 \rightarrow 2H_2O$$

$$\begin{aligned} &\text{Anode} \quad : \quad H_2 \rightarrow 2H^+ + 2e^- \\ &\text{Cathode} \quad : \quad 2H^+ + 2e^- + \frac{1}{2}O_2 \rightarrow 2H_2O \end{aligned} \qquad (1.1)$$

Fuel cells have three kinds of loss, activation loss, ohmic loss and mass transport loss. These losses expressed heat dissipation, can vary operation condition (current output, feed gas rate, temperature and etc.) and affect the efficiency of the fuel cell. [2]

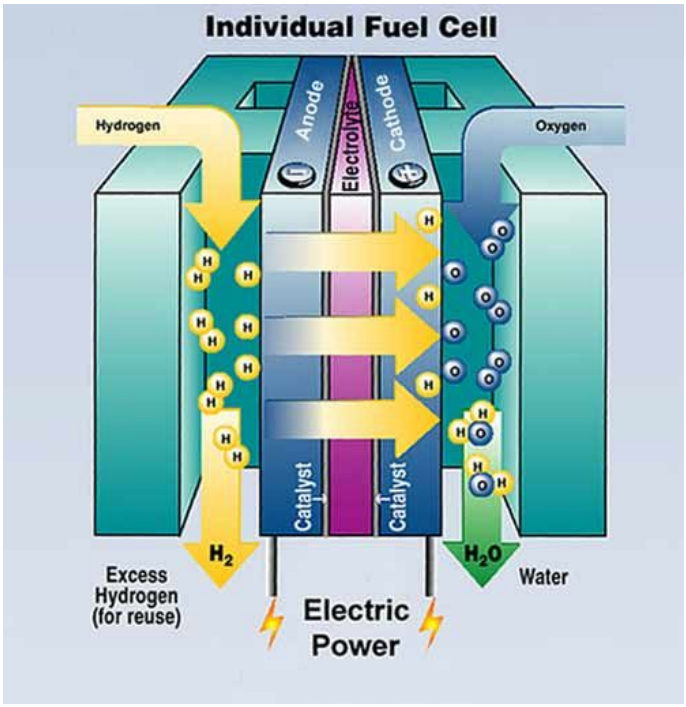

Figure 1.1 Operation principal of a fuel cell [1]

1.2 Kinds of fuel cells

Kinds of fuel cells are classified according to the material of electrolyte, fuel type and operation temperature. Shown in Table 1.1, many kinds of fuel cells are studied but the researches on PEMFC, DMFC and SOFC are more active that are superior than others in comparisons of the performance and the possibility of commercialization.

Table 1.1 Various kinds of fuel cells [2]

	HT - Fuel Cell		LT - Fuel Cell			
	Molten Carbonate Fuel Cell (MCFC)	Solid Oxide Fuel Cell (SOFC)	Phosphoric Acid Fuel Cell (PAFC)	Alkaline Fuel Cell (AFC)	Proton Exchange Membrane Fuel Cell (PEMFC)	Direct Methanol Fuel Cell (DMFC)
operation temp.	550-700°C	800-1000°C	150-250°C	50-120°C	50-100°C	50-100°C
catalyst	Perovskites	Nickel	Platinum	Platinum	Platinum	Platinum
electrolyte	Li/K Alkali Carbonate Mixture	YSZ and etc.	H_2PO_4	KOH	Nafion and etc.	Nafion and etc.
conducting ion	CO_3^{2-}	O^{2-}	H^+	OH^-	H^+	H^+
fuel	H_2, CO, hydrocarbon gas	H_2, CO, hydrocarbon gas	H_2, CO, MeOH, hydrocarbon gas	H_2	H_2	MeOH
efficiency (LHV)	50-60	50-60	40-45		<40	
application	large / intermediate power plant	large / intermediate power plant, portable power	intermediate power plant, biogas plant	space shuttle power source	vehicle power household power portable power	portable power
feature	high efficiency, internal repferming, combined heat power generation	high efficiency, internal repferming, combined heat power generation, easy scale up/down	high CO tolerence, combined heat power generation		low temperature operation, high power density	low temperature operation, high power density, high energy density fuel
problem	corrosion, CO_3^{2-} volatilization	high temperature degradation, thermal stress	corrosion, H_2PO_4 spill	water spill at electrolyte	difficult water management, high material / manufactureing price, low efficiency	difficult water management, high material / manufactureing price, methanol crossover

1.2.1 Proton exchange membrane fuel cell

A PEMFC (proton exchange membrane fuel cell) uses polymer electrolyte which has commercial name Nafion® (Dupont Co., Ltd.), Gore-select® (Gore Co., Ltd.), Aciplex (Asahi Chemical Industry Co., Ltd.), Flemion (Asahi Glass Co., Ltd.), Dow® (Dow Chemical Co., Ltd.), 3M® (3M Co., Ltd.) or etc... The reaction in PEMFC progresses with moving of proton (H+) from anode to cathode. It has fast start-up time due to the low operating temperature mainly below 100°C. Relatively thin MEA(membrane electrode assembly) enables high power density following small size and fast response according to the load change. Due to these advantages PEMFCs used in the applications of electric vehicle and small distributed power generation system. Low temperature ease the system configuration, but cooling and water management have been unsolved issues. PEMFC system should manage effectively the water which produced in electrochemical reaction so that the humidity in electrolytes related to proton conductivity maintains the proper level. If the system cannot eliminate the water in channel, flooding which blocks reaction area in gas diffusion layer would happen. Otherwise, the dry electrolyte from poor humidifying causes poor performance from low ionic conductivity. Beside, PEMFC has inevitable cost-raising factor of usage of platinum (Pt) catalyst and graphite interconnecter. Carbon monoxide (CO) poisoning is also the one of PEMFC's critical problems. [3]

1.2.2 Direct methanol fuel cell

DMFC (direct methanol fuel cell) has identical configuration to PEMFC using polymer electrolyte, but has the difference of which the fuel is methanol. DMFC system doesn't need reformer which converts hydro carbon into hydrogen and only needs simple fuel supplying parts, so it can be compact. It can be used in various applications especially for the substitute of rechargeable batteries of laptop or cell phone. In this field, using time and charging rate problem can be solved with DMFC's specialty of simply changing methanol cartridge. Now, catalyst activation ability, electrodes, electrolytes and cell stacking are research theme for DMFC. However DMFC has problems of poor catalyst activation ability, fuel crossover which means unused methanol moves from anode to cathode through polymer electrolyte. Methanol crossover is main origin of performance degradation, because it reduces cathode potential and it disturbs oxygen reduction reaction. [3]

1.2.3 Molten carbonate fuel cell

MCFC (molten carbonate fuel cell)'s electrolyte is a molten mixture of alkali carbonates: Li_2CO_3 and K_2CO_3, immobilized in a $LiOAlO_2$ matrix. The carbonate ion, CO_3^{2-} moves through the electrolyte. MCFC systems extract the CO_2 from the anode and recirculate it to the cathode because CO_2 is produced at the anode and consumed at the cathode. A schematic diagram of a MCFC is

shown in Figure 1.2. The anode usually consists of a mixture of nickel and chromium. And the cathode is a lithiated nickel oxide.

The relatively high operating temperature (650°C) of the MCFC provides fuel flexibility. That is, MCFCs are able to be fed hydrogen, hydrocarbons and alcohols. So CO tolerance is not an issue for MCFCs like SOFCs. Due to stresses created thermal cycle during start-up and shutdown, the MCFC is best solution for stationary, continuous power applications. The electrical efficiency of a typical MCFC unit is near 50%. In combined heat and power applications efficiencies could reach close to 90%. But the necessity of CO_2 recycling structure can raise the system cost which already has high cost material components. The corrosive molten electrolyte can affect metallic interconnecter and degradation/lifetime issues.

1.2.4 Solid oxide fuel cell

SOFC (solid oxide fuel cell) is a fuel cell using ceramic electrolyte conducting oxygen ion in the temperature of 800~1000°C. The representative electrolyte material is yttria stabilized zirconia (YSZ). In a SOFC, water is produced at the anode, rather than at the cathode as in a PEMFC. A schematic diagram of a SOFC is provided in Figure 1.2. The anode is a cermet of nickel and electrolyte material. The cathode is usually a mixed ion-conducting and electronically-conducting ceramic material. Typical cathode materials include

strontium-doped lanthanum manganite (LSM), lanthanum strontium ferrite (LSF), lanthanum strontium cobaltite (LSC), and lanthanum strontium cobaltite ferrite (LSCF).

Although overall reaction is same, the reaction in each electrode is some different from other conventional fuel cells.

$$\text{Anode} \quad : \quad H_2 + O^{2-} \rightarrow H_2O + 2e^- \tag{1.2}$$

$$\text{Cathode} \quad : \quad \frac{1}{2}O_2 + 2e^- \rightarrow O^{2-}$$

Shown in upper reactions, water is produced at the anode, rather than at the cathode.

Unlike PEMFC, it is the advantage that SOFC do not suffer water management problem, but SOFC's high temperature also cause poor stability, low durability, thermal compatibility problem and restrict choice of component materials. [4] SOFC is the most efficient among various fuel cells. At the system scale, it can be used for power generation system due to the possibility to re-use waste heat for household application or for cogeneration plant with highest efficiency. It can operate with direct hydrocarbon so reformer is not essential so we can simplify the system components and get high efficiency, too. SOFC can lower down the material cost. The platinum catalyst and graphite bipolar plates in low temperature fuel cells are not used in SOFC. And non-royalty electrolytes are necessary for this fuel cell. Indeed,

scale up/down is easier than any other fuel cell. It means various applications can be applicable from the power source of portable and mobile devices through vehicle application to power plant.

Due to these strong points, SOFC is a promising energy conversion device and is one of the most active research areas in fuel cell field. So this study deals with the methods of commercialization of SOFC.

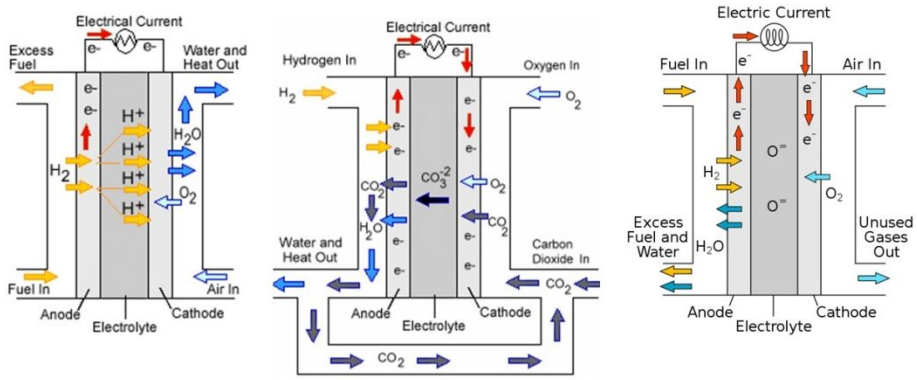

Figure 1.2 Schematics of PEMFC, MCFC and SOFC [5]

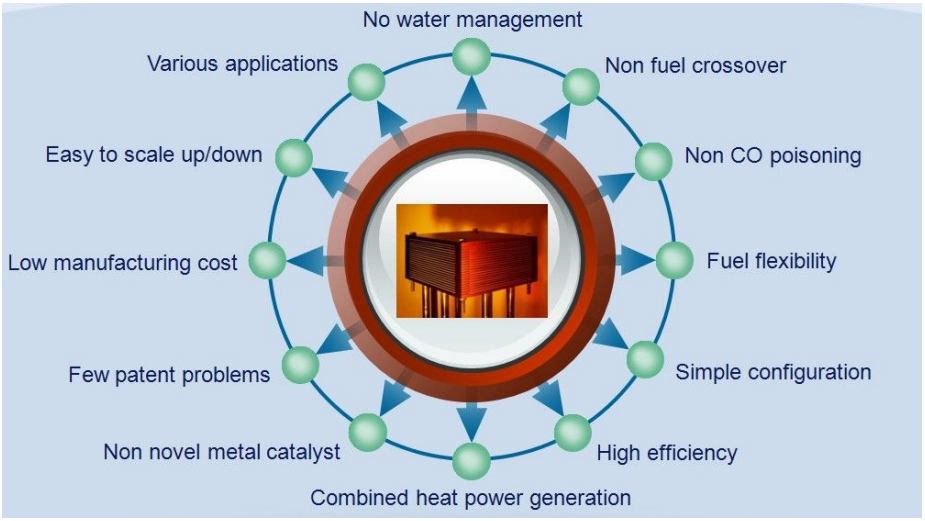

Figure 1.3 Strong points of SOFCs

1.3 Lowering the operation temperature of SOFCs

Written above, the conventional SOFC has some weak points in high temperature. The most critical problem is thermal mismatch between MEA (membrane electrodes assembly). This means electrodes and electrolyte can be separated or broken on elevated temperature due to the different thermal expansion coefficient of materials. It has been the first issue for the stability and durability of SOFCs. Another problem is nickel agglomeration in anodes. This behavior can disconnect the electron conduction roots in MIEC (mixed ionic electronic conduction material) and can reduce the TPB (triple phase boundary) area in which the electrochemical reaction occurs so that performance would be drop. The reactions between component materials at the interface in high temperature have been a problem of degradation, too. Above 800°C we cannot use most metal sealant and at about 1000°C using glass based sealant can be restricted. Sealing fuel and air is very important to maintain cell voltage and to prevent component reduction or oxidation. 750°C is the limit temperature for the usage of steel alloy components. Now most of interconnecter materials are expensive Inconel® and Crofer® that occupy 75% of a SOFC price. A stainless steel based bipolar plate has been a key to cost down a fuel cell system price. So the typical operating temperature range can be a bottle neck for the commercialization of SOFCs. [6] Thus a lot of researches have been conducted to lower the operation temperature.

We divided SOFCs into low temperature (LT, ~500°C) SOFC, intermediate temperature (IT, 500°C~800°C) SOFC and high temperature (HT, 800°C~) SOFC. LT-SOFC is most attractive but it is not free for realizing a large area cell, finding the proper conductivity electrolyte material, the poor stability problem, using novel metal catalyst. So it needs more matured technology now. We focused our interest to IT-SOFC. Its temperature position can avoid many problems of HT-SOFC and LT-SOFC maintaining the competitiveness of original SOFC's characteristics. Thus we could expect IT-SOFC's high commercialization possibility.

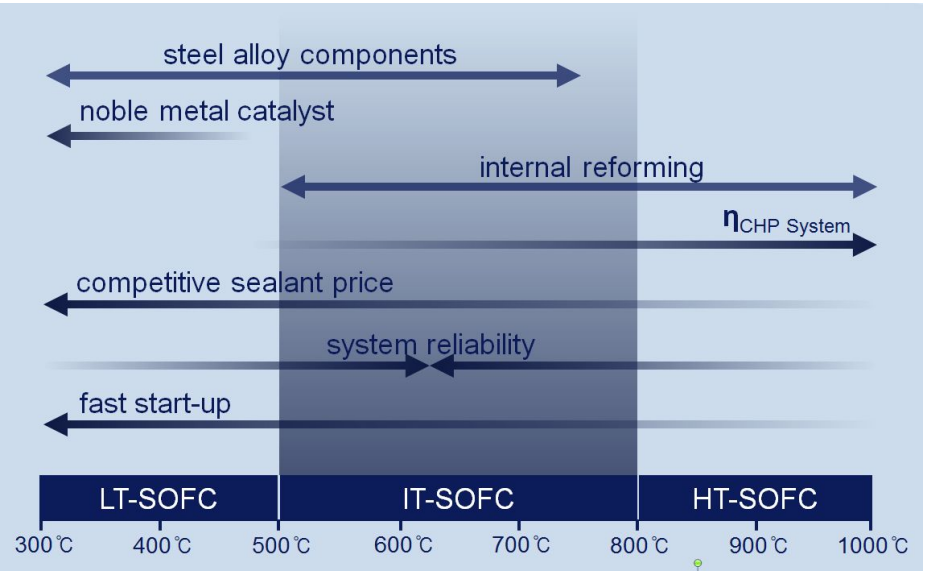

Figure 1.4 Competitiveness of IT-SOFCs

Among the main three losses of fuel cells; activation loss, ohmic loss and mass transport loss, ohmic loss is the main for SOFCs. It is directly connected to ionic transport loss of electrolyte. That is, the resistance comes when ions pass through the electrolyte and it is the exactly same idea of resistance in wire which conducts electrons.

1.3.1 Reducing the thickness of electrolytes

The first method to lower the operation temperature maintaining its performance is reducing the thickness of electrolyte. It means that one makes wire short so that the resistance value is minimized.

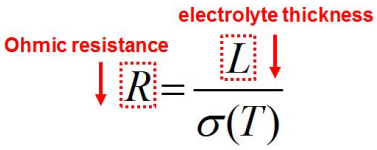

(1.3)

In case of SOFC, proper process is required to form a extremely thin, dense and uniform layer which can prevent any gas permeability. Actually typical wet ceramic processes have thickness minimum limit and the possibility of micro pore cannot be ignorable. [7] So the promising technology for reduced thickness electrolyte is thin film deposition technique.

Thin film micro-fabrication methods originally have been used to fabricate semiconductor. To use a typical thin film deposition method, we have to choose adequate one regarding the next conditions. SOFC components have very complex composition where the materials of

semiconductor are very simple. If we want to make a porous layer, thin film deposition would not be a good choice. If a substrate which we want to coat with target material is weak, PVD (physical vapor deposition) can be dangerous.

Below Figure 1.5 shows the thinner electrolyte (red line, 50nm) which was fabricated via atomic layer deposition has far less iR loss than the thicker electrolyte (dark blue line, 20μm) which was fabricated via screen printing. Figure 1.6 is the experimental conductivity results from the various YSZ thickness layers that means ultra-thin electrolytes can show much lower resistance than the thickness ratio. [8]

The kinds of thin film deposition methods are mentioned below.

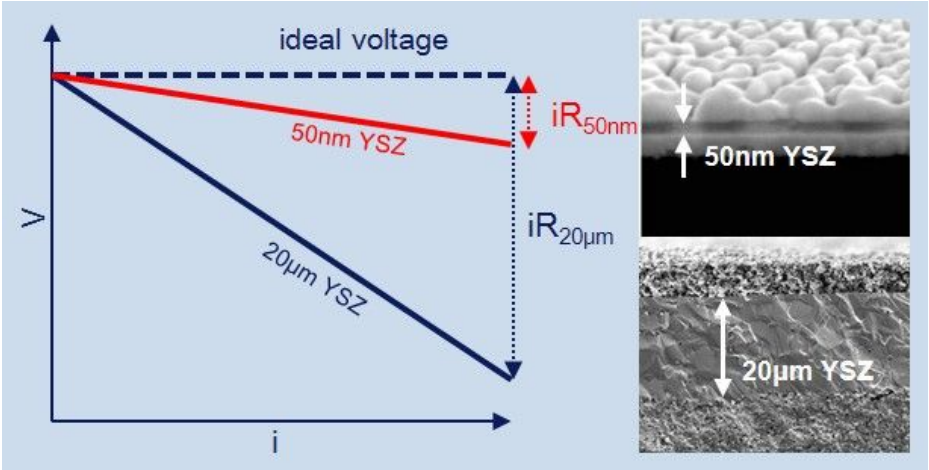

Figure 1.5 Principal of the thickness reduction and examples

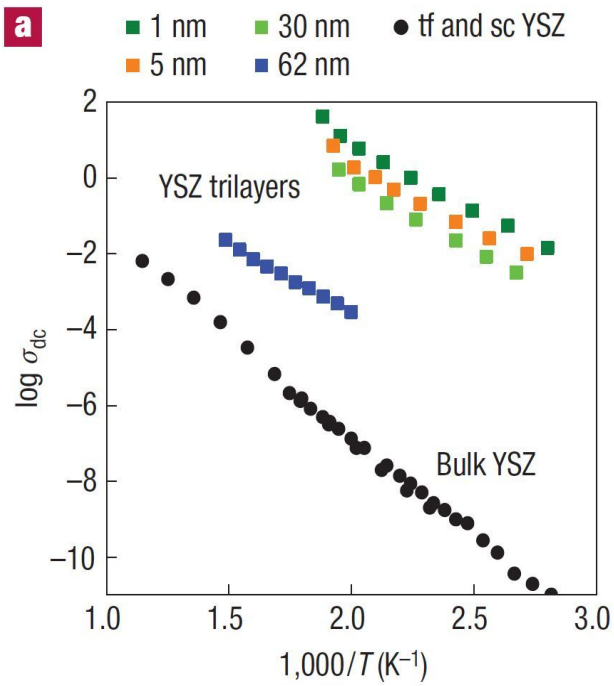

Figure 1.6 Dependence of the logarithm of the ionic conductivity of the STO/YSZ/STO tri-layers [8]

1.3.1.1. Sputtering

Sputtering is one of the most usual techniques to deposit a thin film electrolyte of SOFC. It is the deposition method that particles run out from a target due to the high energy which caused from DC or RF plasma in vacuum deposits the substrate. [9] It is possible in low temperature environment because particles from a target get high plasma ion energy, but substrate surface can be hurt due to the plasma. To prevent this, magnetic field activated by magnetron trap electrons so that it can protect substrate. Using magnetron reduces current. Indeed typical sputtering operates in several mTorr which cause lowering deposition rate due to atoms from target. But magnetron can avoid this problem so it can reduce the pressure in chamber and deposition rate can be higher in the same chamber pressure.

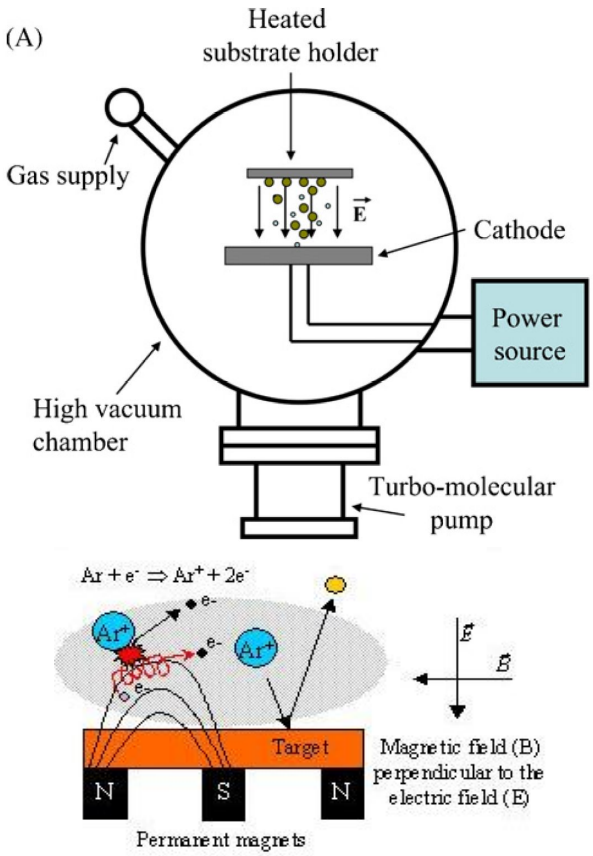

Figure 1.7 Schematics of the sputtering [10],[11]

1.3.1.2. Pulsed laser deposition

In a vacuum chamber, concentration of laser through lens to target material causes particle separation and deposition on substrate. The most non-metal materials observe strong 200~400nm ultraviolet rays. Observed laser energy converted into heat energy, chemical energy and mechanical energy then finally excites electrons.

PLD (pulsed laser deposition) has advantage to maintain the composition because of cluster unit separation not of atom unit separation. Due to this character, it is used recently when complex composition is needed. [9] It can deposit porous perovskite structure (ABO_3) electrodes or dense electrolyte materials like GDC (gadolinia doped ceria), SDC (samaria doped ceria), YSZ (yttria stabilized zirconia) and LSGM (lanthanum strontium gallate magnesite). Amorphous dense layer or nano sized crystal structure can be obtained in low oxygen partial pressure (<10mTorr) and low temperature, then we can crystalize them through annealing process in the air. Chamber pressure can affect porosity or crack generation of GDC and YSZ. Generally low pressure is connected to high density. [12]

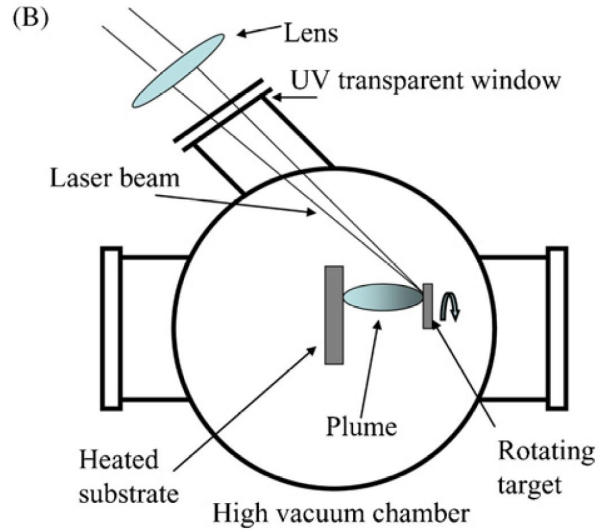

Figure 1.8 Schematic of the pulsed laser deposition [10]

1.3.1.3. Atomic layer deposition

ALD (atomic layer deposition) is one of the variants of CVD (chemical vapor deposition) which can deposit substrate with gas phase precursor. [13] ALD has cyclical precursor input where CVD has continuous precursor input to the reaction chamber. Precursor combines through a reaction with ligand on substrate surface or through chemisorb with substrate surface. If we adjust reaction condition properly, self-limiting reaction can occur on surface, so that we can get the precisely controlled thin film.

ALD process can be explained like this. The first reaction proceeds on the substrate surface at same rate to form a uniform monolayer. At this time, molecules that cannot chemisorb with surface exist in the state of physisorb or no-combined in any form. Purging with inert gas eliminate these physisorb or no-combined molecule. To form another atomic layer first reaction and purging repeats one cycle.

From this mechanism, ALD enables sub-nm thickness control, excellent uniformity, good step coverage, dense layers and pinhole free layers. Moreover, low deposition temperature under 300℃ can be achieved.

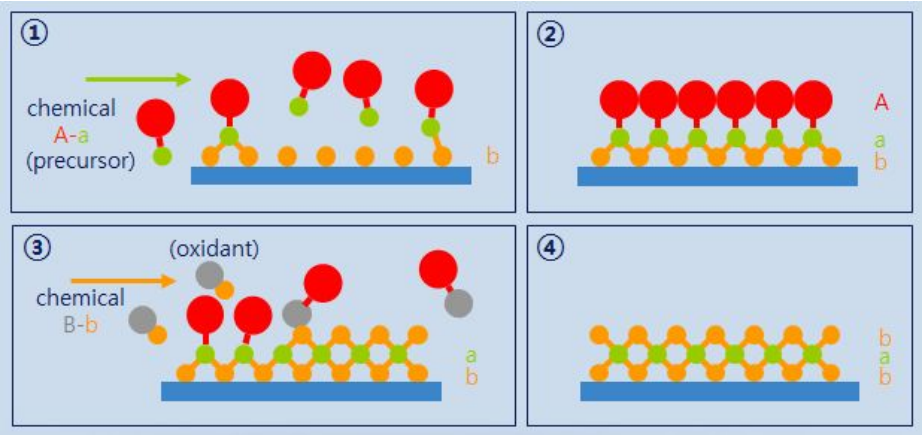

Figure 1.9 Schematic of the ALD cycle with 2 kinds of precursors

Table 1.2 Various thin film deposition methods [10]

Vacuum deposition	Physical vapor deposition (PVD)	sputtering
		Pulsed laser deposition (PLD)
	Chemical vapor deposition (CVD)	conventional CVD
		atomic layer deposition (ALD)
		electrochemical vapor deposition (EVD)
Liquid-precursor-based thin film deposition	Spray deposition	Electrostatic spray deposition (ESD)
		Flame spray deposition (FSD)
		Pressurized gas spray deposition (PSD)
		Ultrasonic spray pyrolysis (USP)
		Mist spray pyrolysis (MSP)
	Electrophoretic deposition (EPD)	
	Spin- and dip-coating	Metal organic decomposition (MOD)
		Polymeric precursors / sol–gel method
		Impregnation
		Slurry-coating

1.3.2 High conductivity electrolytes material

The second method to lower the operation temperature is raise the conductivity of electrolyte. That is, changing the material of wire.

$$\text{Ohmic resistance} \downarrow \quad R = \frac{L}{\sigma(T)} \quad \uparrow \text{ionic conductivity} \tag{1.4}$$

Conventional ZrO_2 based electrolyte materials including YSZ, ScSZ (scandium stabilized zirconia) have wide oxygen partial pressure (P_{O_2}) range, strong mechanical property and chemical stability. But it operates only in high temperature due to poor ionic conductivity.

Bi_2O_3 based materials have 1~2 order higher ionic conductivity than ZrO_2 based. But narrow electrolytic P_{O_2} range and weak mechanical property, especially reduction into metallic phase Bi below the oxygen partial pressure of 10^{-13}atm at 600°C have been problems to be used for electrolyte. [14]

LSGM electrolyte can be operated in wide P_{O_2} range with high ionic conductivity. However, if A:B ratio in perovskite structure is off the original point, secondary phase like $LaSrGa_3O_7$, $LaSrGaO_4$ and La_2O_3 can be generated. [14]

CeO_2 based materials including GDC, SDC secure higher ionic conductivity than YSZ. They also have La blocking character from cathode. But in the low P_{O_2} environment, it shows electron conductivity in the reducing

process from Ce^{4+} to Ce^{3+}.

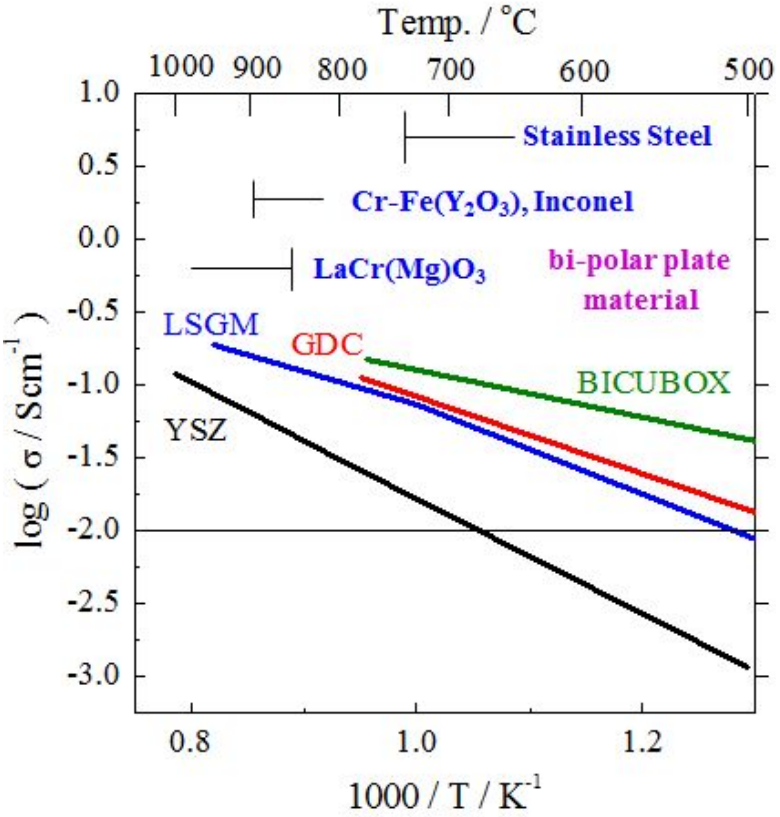

Figure 1.10 Comparison of conductivity of various materials

1.4 Bi-layered electrolyte SOFCs

We decided to fabricate bi-layered electrolyte SOFC for intermediate temperature operation. Base electrolyte material should be high ionic conductive and occupies most electrolyte thickness. And functional electrolyte material should supplement the demerits of main material and be thin. This idea is that combines above two temperature lowering methods.

From 1988 a lot of researchers have been shared bi-layered electrolyte structure technology.

H. Yahiro, Y. Babu, K. Eguchi and H. Arai fabricated YSZ and YDC (yttria doped ceria) bi-layered electrolyte. [15] 1.5μm YSZ was deposited via RF sputtering on 1.5mm YDC. OCV value was 0.82V for pure YDC cell and 0.95V for YSZ/YDC cell at 600°C. At 700°C OCV increased by 0.17V. K. Eguchi and H. Arai made YSZ/SDC bi-layer via RF ion plating. Thickness ratios were 1.86μm/1.825mm and 2μm/1.658mm. At 800°C bi-layered cell showed 0.25V higher OCV. [16],[17]

A. V. Virkar calculated P_{O_2} between bi-layer from a simple equivalent circuit. [18] And he formed YSZ/YDC bi-layer with K. Mehta and R.Xu via spin coating. There were 0.2V OCV increase at 600°C and 0.15V OCV increase at 700°C. [19] R.Xu, K. W. Chour and J. Chen made YSZ/YDC bi-layer via MOCVD (metalorganic vapor deposition), EVD+sputtering, sputtering and sol-gel and compared OCV from these methods.

EVD+sputtering showed 0.32V OCV increase at 750°C and MOCVD showed 0.27V OCV gap. [20]

Y. Tsai, E. Perry and S. Barnett obtained 0.12V increased OCV with sputtered YSZ/YDC. [21] P. Soral, U. pal and W. L. Worrell made 2μm YSZ and 100μm/10μm GDC bi-layered cell with 0.96V OCV. [22]

An authority on bi-layered electrolyte, E. D. Wachman had interest to ceria and bismuth oxide bi-layered electrolyte. YSB/YDC (yttria doped bismuth oxide) showed 0.08V and 0.04V OCV increases at 700°C and 800°C. ESB/SDC (erbia doped bismuth oxide) showed 0.08V, 0.1V, 0.14V and 0.26 OCV increases at 800°C, 700°C, 600°C and 500°C. [23] With ESB/SDC electrolyte via PLD and spin coating, changing the ESB thickness showed 0.3~0.4V OCV increase. [24] Spray coating 10μm GDC then 4μm ESB on Ni-GDC substrate showed 0.05V more OCV at 650°C. [25]

S. H Chan, X. J. Chen and K. A Khor suggested bi-layered model regarding ion, free electron and electron-hole. [26] S. H Chan, X. J. Chen, K. A Khor and Q. L. Liu measured OCV of the ceramic co-sintered 3μm YSZ and 7μm GDC. The results showed 0.25V, 0.33V and 0.45V increase at 600°C, 700°C and 800°C than 10μm GDC. [27]

Z. Bi, M. Cheng, Y. Dong, H. Wu, Y.She and B. Yi composed 25μm LDC (lanthan doped ceria) / 75μm LSGM electrolyte via dry-pressing. Bi-layered cell showed 1.06V OCV where LDC cell showed 0.67V and LSGM showed 1.1V. [28]

R. Maric, D. Ghosh, X. Zhang, M. Robertson, C. Deces-Petit, Y. Xie, R. Hui, S. Yick, E. Styles, J. Roller and O. Kesler made 5μm YSZ / 15μm SDC via co-firing. They obtain 0.22V and 0.38V increased OCV with bi-layered cell at 600°C and 700°C. [29],[30] R. Maric, D. Ghosh, D. Yang, X. Zhang, S. Nikumb, C. Deces-Petit, R. Hui made 1μm ScSZ / 6μm SDC electrolyte cell with 0.2V higher OCV at 600°C. [31] R. Maric, D. Ghosh added the 20μm anode functional layer between anode and bi-layer via spin-coating and result was 0.2V higher OCV. [32]

T. Yamaguchi, S. Shimizu, T. Suzuki, Y. Fujishiro and M. Awano composed ScSZ/GDC via co-sintering and added LSM-GDC layer between cathode and bi-layer. With LSM-GDC layer power density increases were 5.5mW/cm^2, 30.5mW/cm^2 and 106mW/cm^2 at 500°C, 600°C and 700°C.

Yousei university and KIST made GDC substrate via tape-casting (0.44μm) then deposited 2μm YSZ via sol-gel dip drawing with 0.075V, 0.061V and 0.055V OCV increase at 1000°C, 950°C and 900°C. [33] Spin-coated 2μm YSZ on 1.6mm YDC showed 0.04V, 0.04V, 0.05V and 0.06V OCV increase at 1000°C, 900°C, 800°C and 700°C. [34]

Table 1.3 and Figure 1.11 show the cell data and the power density distribution of various bi-layered electrolyte cells and ceria based electrolyte cells.

Table 1.3 Reported data of ceria based bi/single layered electrolyte SOFCs

Layer type	Deposition method	Thickness	Cell configuration	Temp (°C)	Material	OCV (V)	Max. power (mW /cm^2)	Ref.
YSZ/YDC	RF-sputtering	1μm/1.5mm	H_2, Pt | YSZ/YDC | Pt, O_2	600	YDC	0.82	3	[15]
					YSZ/YDC	0.95	8	
				700	YDC	0.72	10	
					YSZ/YDC	0.89	19	
				800	YDC	0.82		
					YSZ/YDC	1.08		
YSZ/SDC	RF-ion plating	1.86μm/1.825mm	H_2, Pt | YSZ/SDC | Pt, O_2	800	SDC	0.82	38	[16]
					YSZ	1.2	14	
					YSZ/SDC	1.08	33	
YSZ/SDC	RF-ion plating	2μm/0.658mm	H_2, Ni-YSZ | YSZ/SDC | LSM, O_2	800	SDC	0.8	250	[17]
					YSZ	1.1	120	
					YSZ/SDC	1.08	320	
YSZ/YDC	RF-ion plating	0.3μm/-	H_2, Pt | YSZ/YDC | Pt, O_2	600	YDC	0.71		[19]
					YSZ/YDC	0.85		
				700	YDC	0.61		
					YSZ/YDC	0.79		
YSZ/YDC	MOCVD	-	H_2, Pt | YSZ/YDC | Pt, O_2	750	YDC	0.55		[20]
					YSZ/YDC	0.82		

				700	YDC	0.65		
					YSZ/YDC	0.86		
				650	YDC	0.7		
					YSZ/YDC	0.87		
YSZ/YDC	sputtering	1μm/8μm	H_2, Ni-YSZ | YSZ/YDC | LSM-YSZ, O_2	500	YSZ/YDC	1.089	55	[21]
				550	YSZ/YDC	1.068	110	
				600	YSZ/YDC	1.03	155	
		1.5μm/4μm			YSZ/YDC	0.88		
		-			YSZ	1.01		
YSZ/GDC	-	2μm/100μm	10^{-19}, An. | YSZ/GDC | Ca.,10^{-1}	800	YSZ/GDC	0.96	1.5	[22]
		2μm/10μm			YSZ/GDC	0.96	11	
		-			GDC	0.91		
		-			YSZ	0.96		
YDZ/YSB	co-sintering	-	H_2, Pt | YDC/YSB | Au, O_2	700	YDC	0.68		[35]
					YDC/YSB	0.76		
				800	YDC	0.6		
					YDC/YSB	0.64		
SDC/ESB	co-sintering	-	H_2, Pt | SDC/ESB | Au, O_2	500	SDC	0.84		
					SDC/ESB	1.01		
				600	SDC	0.84		
					SDC/ESB	0.98		
				700	SDC	0.84		
					SDC/ESB	0.94		
				800	SDC	0.79	38	

					SDC/ESB	0.87	54	
GDC/ESB	co-sintering	-	H_2, Pt | GDC/ESB | Au, O_2	500	GDC	0.83		
					GDC/ESB	1.01		
				600	GDC	0.85		
					GDC/ESB	0.95		
				700	GDC	0.8		
					GDC/ESB	0.89		
				800	GDC	0.75		
					GDC/ESB	0.83		
SDC/ESB	PLD	1.6μm/0.8μm	H_2, Pt | SDC/ESB | Au, O_2	800	SDC/ESB	0.6		[24]
	PLD	1.76μm/1.3μm				0.63		
	dip-Coating	1.5mm/9μm				0.69		
	dip-Coating	1.5mm/22μm	H_2, Pt | SDC/ESB | Ag-ESB, O_2			0.82		
	dip-Coating	1.0mm/30μm	H_2, Pt | SDC/ESB | Au, O_2			0.92		
	-	-			SDC	0.5		
	PLD	1.6mm/0.8μm	H_2, Pt | SDC/ESB | Au, O_2	700	SDC/ESB	0.65		
	PLD	1.76mm/1.3μm				0.6		
	dip-Coating	1.5mm/9μm				0.74		
	dip-Coating	1.5mm/22μm	H_2, Pt | SDC/ESB | Ag-ESB, O_2			0.87		
	dip-Coating	1.0mm/30μm	H_2, Pt | SDC/ESB | Au, O_2			0.96		
	-	-			SDC	0.5		
	PLD	1.6mm/0.8μm	H_2, Pt | SDC/ESB | Au, O_2	600	SDC/ESB	0.62		
	PLD	1.76mm/1.3μm				0.65		
	dip-Coating	1.5mm/9μm				0.77		

	dip-Coating	1.5mm/22μm	H_2, Pt | SDC/ESB | Ag-ESB, O_2			0.95		
	dip-Coating	1.0mm/30μm	H_2, Pt | SDC/ESB | Au, O_2			0.96		
	-	-			SDC	0.59		
	PLD	1.6mm/0.8μm	H_2, Pt | SDC/ESB | Au, O_2	500	SDC/ESB	0.6		
	PLD	1.76mm/1.3μm				0.65		
	dip-Coating	1.5mm/9μm				0.84		
	dip-Coating	1.5mm/22μm	H_2, Pt | SDC/ESB | Ag-ESB, O_2			1		
	dip-Coating	1.0mm/30μm	H_2, Pt | SDC/ESB | Au, O_2			1		
	-	-			SDC	0.59		
GDC/ESB	PLD	10μm/4μm	H_2, Ni-GDC | GDC/ESB | LSM-GDC, O_2	650	GDC	0.73	1.03	[25]
					GDC/ESB	0.77	1.95	
YSZ/GDC	co-sintering	3μm/7μm	H_2, Ni-GDC | YSZ/GDC | LSM-GDC, O_2	600	GDC	0.86		[27]
					YSZ/GDC	1.107		
				700	GDC	0.76		
					YSZ/GDC	1.081	409	
				750	YSZ/GDC		570	
				800	GDC	0.58		
					YSZ/GDC	1.049	678	
LDC/LSGM	dry-pressing	25μm/75μm	H_2, Ni-GDC | LDC/LSGM | SSC-LDC, O_2	800	LDC	0.67		[28], [29]
					LSGM	1.1		
					LDC/LSGM	1.02		
YSZ/SDC	co-firing	5μm/15μm	H2, Ni-YSZ, Ni-YSZ | YSZ/SDC | SSC, O2	600	SDC	0.88		[30]
					YSZ/SDC	1.1	180	
				700	SDC	0.78		

					YSZ/SDC	1.08	600	
SDC/ScSZ	PLD	6μm/1μm	H_2, NiO-YSZ, Ni-SDC | ScSZ/SDC | SSC, O_2	600	SDC	0.87		[31]
					SDC/ScSZ	1.04	900	
SDC/ScSZ	PLD	2μm/20μm	H_2, SS430, NiO-SDC/AFL | ScSZ/SDC | SSC, O_2	600	SDC	0.87		[32]
					SDC/ScSZ	1.01	161	
YSZ/YDC	sol-gel dip drawing coating	2μm/0.44μm	H_2, Pt | YSZ/YDC | Pt, O_2	900	GDC	0.67		[33]
					YSZ/YDC	0.725	160	
				950	GDC	0.634		
					YSZ/YDC	0.695		
				1000	GDC	0.598		
					YSZ/YDC	0.673		
YSZ/YDC	spin-coating	2μm/1.6mm	H_2, Pt | YSZ/YDC | Pt, O_2	700	YDC	0.92		[34]
					YSZ/YDC	0.86		
				800	YDC	0.85	134	
					YSZ/YDC	0.8	122	
				900	YDC	0.78		
					YSZ/YDC	0.74		
				1000	YDC	0.7		
					YSZ/YDC	0.66		
YSZ/GDC	RF sputtering	2μm/1mm	H_2, An. | YSZ/GDC | Ca., O_2	600	YSZ/GDC	0.88		[36]
				700		0.8		
				800		0.75		
YSZ/GDC	drop coating	5μm/45μm	H2, Ni-GDC | YSZ/GDC | LSM, Air	650	YSZ/GDC	0.84	520	[37]
		45μm/5μm	H2, Ni-GDC | GDC/YSZ | LSC, Air		GDC/YSZ	1.01	140	

YSZ/GDC	screen printing	3μm/5μm	H_2, An. | YSZ/GDC | Ca., O_2	600	YSZ/GDC	1.04		[38]
				650		1.03		
				700		1.02		
				750		1.01		
				800		0.99		
YSZ/GDC	PLD	-	H2, Ni-GDC | GDC/YSZ | LSC, Air	600	GDC	0.56	377	[39]
		25nm/1mm			YSZ/GDC	1.06		
		50nm/1mm				1.09	1010	
		100nm/1mm				1.08	1080	
		200nm/1mm				1.09	1140	
GDC/YSZ	RF sputtering	500nm	H2, Pt-YSZ | YSZ/GDC | Pt-YSZ, Air	400	YSZ/GDC	0.97	1	[40]
				450		0.94	1.25	
GDC	dry-pressing	49μm	H2, Ni-GDC | GDC | LSCF-GDC(40:60wt%), Air	450	GDC	1.08	60	[41]
				500		1.05	139	
				550		1	257	
				600		0.96	422	
				650		0.91	562	
GDC	cold press	210μm	H2, Ni-GDC | GDC | SSC-GDC(70:30wt%), Air	600	GDC	0.96	400	[42]
				700		0.84	225	
GDC	co-pressing	18μm	H2, Ni-GDC | GDC | SSC-GDC(70:30wt%), Air	500	GDC	0.889	230	[43]
				550		0.869	432	
				600		0.852	602	
				650		0.787	694	
	metallic-ion	18μm	H2, Ni-GDC | GDC | SSC-	450	GDC	0.78	50	

	impregnation		GDC(70:30wt%), Air	500		0.79	120	
				550		0.76	240	
				600		0.73	400	
GDC	dry-pressing	98μm	H2, Ni-GDC | GDC | LSCF-GDC, Air	500	GDC	0.99	80	[44]
				550		0.95	150	
				600		0.9	250	
				650		0.86	330	
				700		0.85	415	
	spin-coating	19μm	H2, Ni-GDC | GDC | LSCF-GDC, Air	500	GDC	0.97	125	
				550		0.91	250	
				600		0.88	380	
				650		0.87	490	
GDC	spray-coating	10μm	H2, Ni-GDC | GDC | LSCF-GDC(50:50wt), Air	400	GDC	0.99	25	[45]
				450		0.99	65	
				500		0.95	170	
				550		0.91	350	
				600		0.88	580	
GDC	dry-pressing	26μm	H2, Ni-GDC(65:35wt%) | GDC | SSC-GDC(90:10wt), Air	400	GDC	1	30	[46]
				450		0.95	80	
				500		0.9	140	
				550		0.87	205	
				600		0.8.	260	
				650		0.81	320	
		20μm	H2, Ni-GDC(65:35wt%) | GDC | SSC-	400	GDC	1	25	

			GDC(90:10wt), Air	450		0.92	60	
				500		0.83	140	
				550		0.81	275	
				600		0.8	400	
GDC	spray- co-pressing	10μm	H2, Ni-GDC | GDC | BSCF, Air	400	GDC	1.05	100	[47]
				450		1.01	205	
				500		0.99	450	
				550		0.95	825	
				600		0.92	1320	
GDC	dry-pressing, co-pressing	20μm	H2, Ni-GDC | GDC | LSM-BSCF, Air	500	GDC	0.99	250	[48]
				550		0.95	510	
				600		0.905	900	
SDC	tape casting	20μm	H2, NiO-SDC | SDC | LSCF, Air	500	SDC	0.9	210	[49]
				550		0.88	450	
				600		0.86	750	
				650		0.8	915	
GDC	tape casting	20μm	H2, NiO-SDC | GDC | SSC, Air	600	GDC	0.87	270	[50]

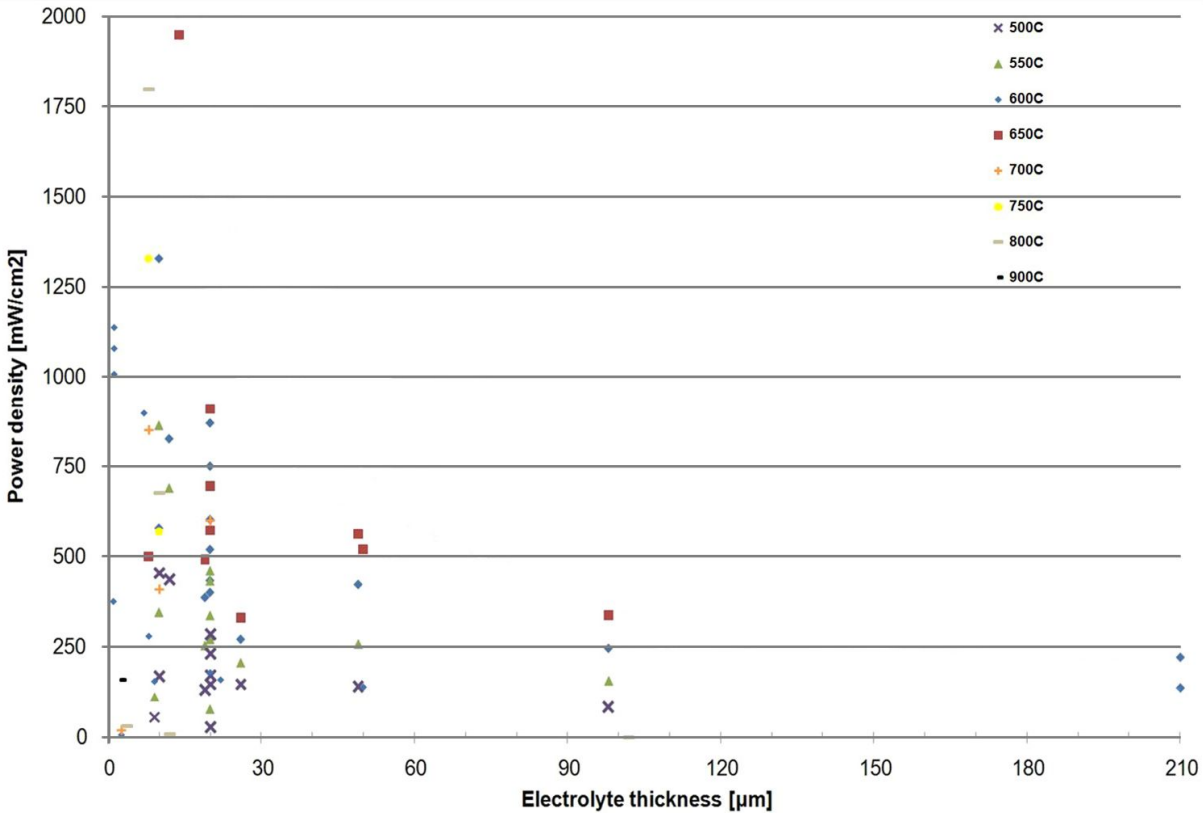

Figure 1.11 Reported power density data of ceria based bi/single layered electrolyte SOFCs.

2. The cell fabrication and experimental process

2.1 The components of bi-layered electrolyte

As written above, we chose high conductive main material and functional thin layer structure. Main electrolyte material was GDC which can secure low ohmic resistance in lowered temperature environment. At the anode side of GDC, YSZ functional thin layer deposited via ALD technique

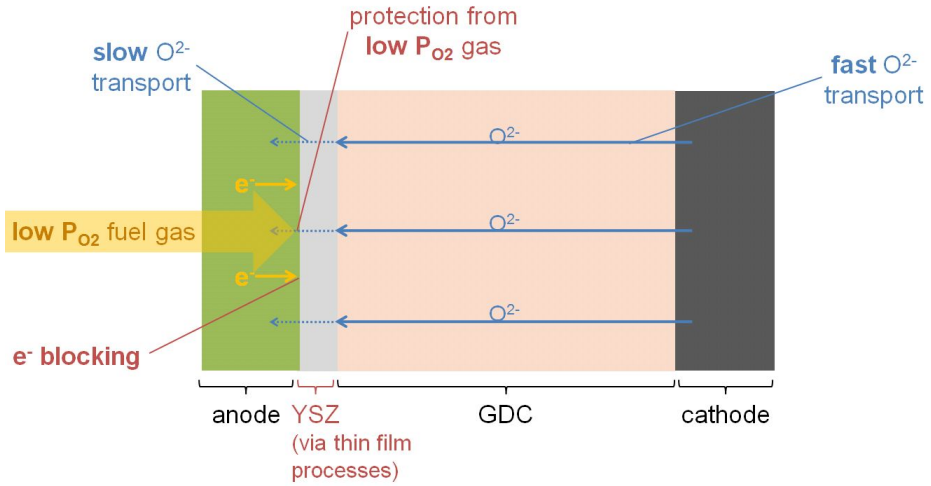

Figure 2.1 Schematic of a YSZ/GDC bi-layered electrolyte SOFC

2.1.1 Bulk GDC electrolyte

GDC is representative high conducting material for SOFC. GDC divided by gadolinia doping ratio to GDC10 (10% gadolinia doped) and GDC20 (20% gadolinia doped). GDC20 shows better performance but GDC10 has better stability. We decided to choose GDC10 bulk pellets for the main electrolyte and substrate of YSZ deposition.

GDC's electron conductivity in reducing environment can be the great cause to lower power density. It is like electric shorting effect, so some part of generated power cannot be delivered to load. Ceria exist originally in the phase of CeO_2. But at low P_{O_2} environment it changes into Ce_2O_3. That is Ce^{4+} ion is reduced to Ce^{3+}. At this time electronic conductivity appears. The lower temperature environment ceria is at, the lower P_{O_2} that electronic conductivity starts to appear at, so electrolytic range gets narrower elevating the operation temperature. And the P_{O_2} of humidifying condition is below the low P_{O_2} limit of electrolytic range. Thus GDC based electrolyte cell should be operated between the low P_{O_2} limit of electrolytic range and oxygen partial pressure of air (0.21atm). When GDC cell is operated out of upper range, electronic conduction naturally appears and this effect is observed more at higher voltage area in the current-voltage (iV) curve. One interesting phenomenon is volume expansion of reduced GDC surface and

micro crack generation. It is due to the internal stress between reduced surface and un-reduced internal part. [51],[52],[53],[54] It can affect the binding of electrode on GDC and the mechanical fracture.

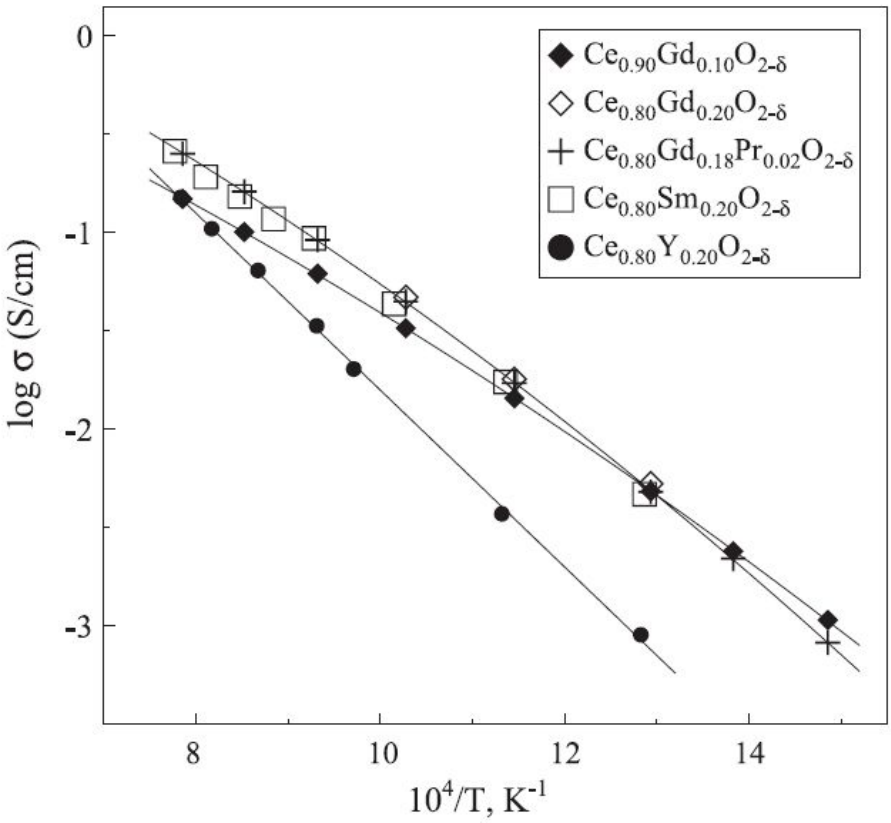

Figure 2.2 Selected data on the total conductivity of ceria-based solid electrolytes in air [14]

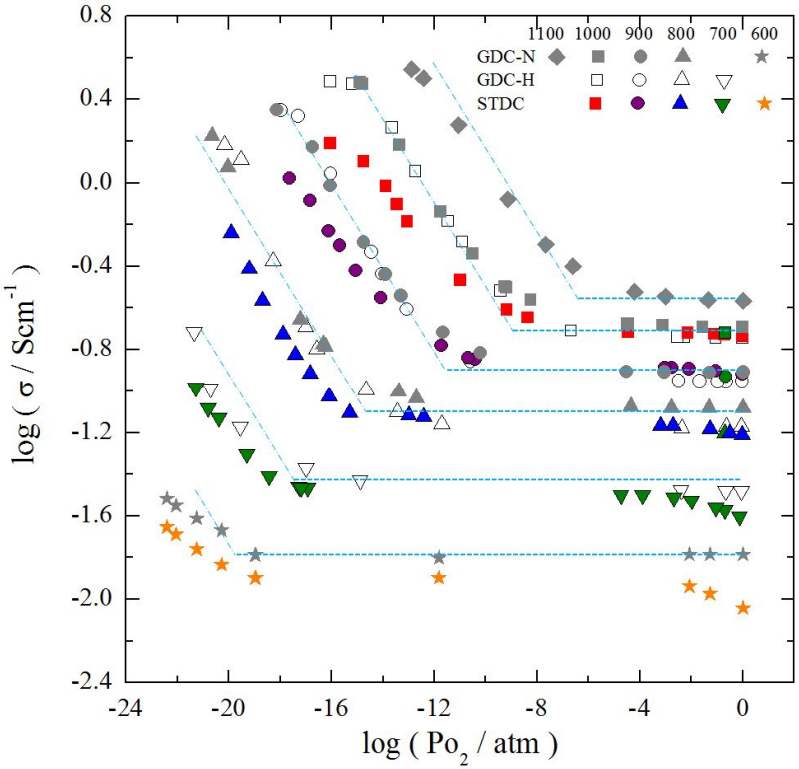

Temp.	O_2 partial pressure range for ion conduction
600˚C	$10^{-19} < Po_2 < 1$
700˚C	$10^{-17} < Po_2 < 1$
800˚C	$10^{-15} < Po_2 < 1$
900˚C	$10^{-12} < Po_2 < 1$
1000˚C	$10^{-9} < Po_2 < 1$
1100˚C	$10^{-7} < Po_2 < 1$

: ion conductivity

: electron conductivity

Figure 2.3 Ion and electronic conductivity at various temperatures and oxygen partial pressures [55]

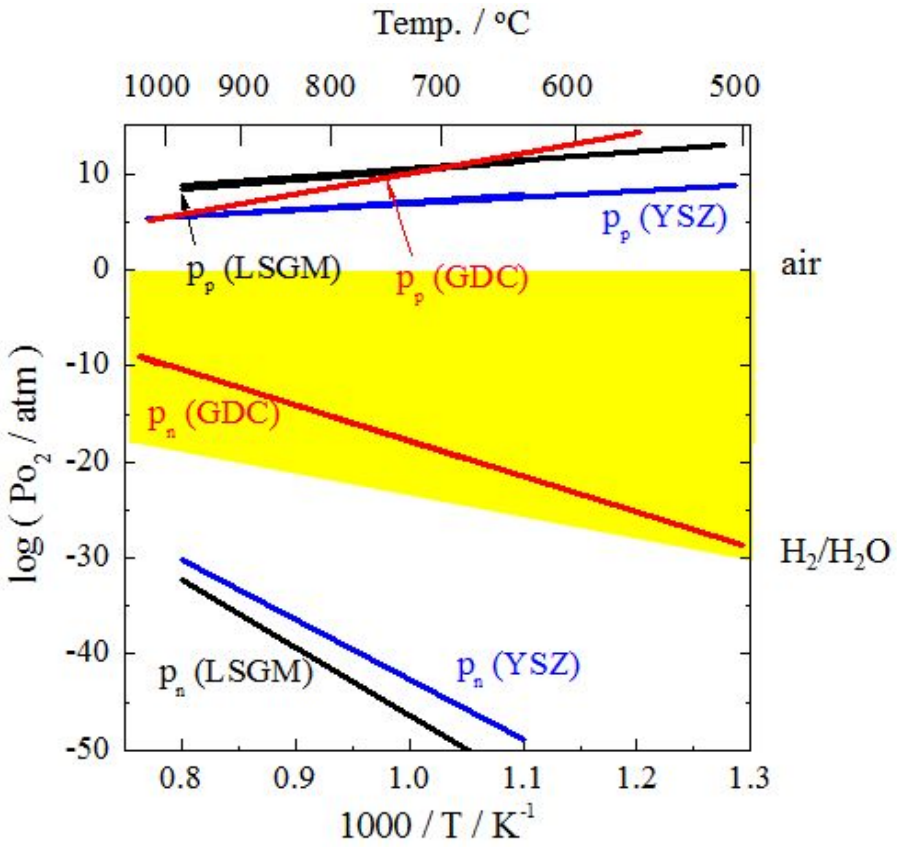

Figure 2.4 Comparison of electrolytic P_{O_2} regions for electrolyte materials [55]

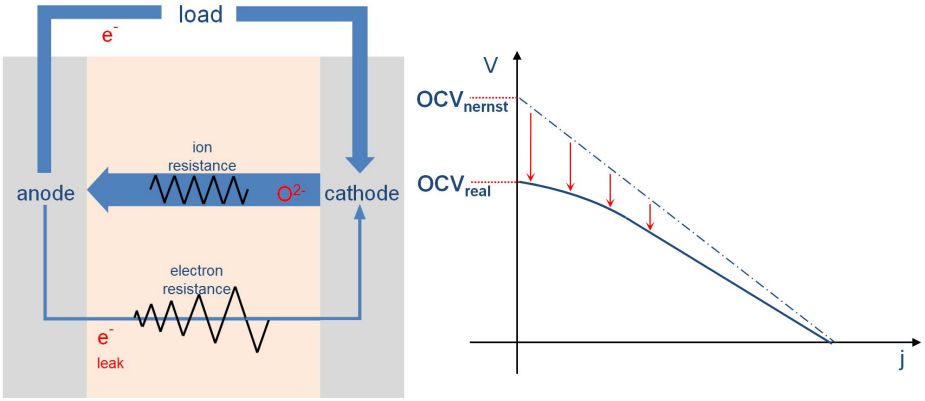

Figure 2.5 Electron conductivity of GDC and voltage drop from it

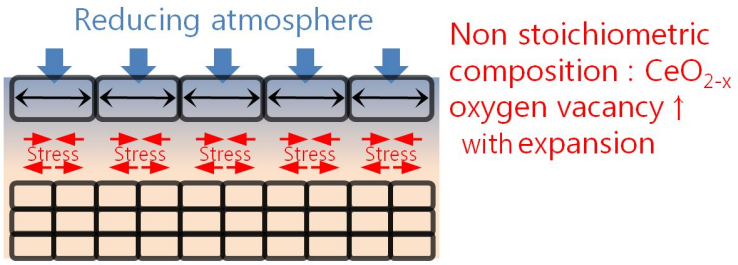

Figure 2.6 Origin of micro crack generation on GDC surface in reducing gas

2.1.2 ALD-YSZ for a functional layer

The key of this study is the ALD deposition of YSZ on the anode side of GDC. The first object of the ALD-YSZ layer is minimized thickness. It is impossible to operate in reduced temperature for low conductive YSZ layer with normal thickness. So minimized YSZ thickness means fast ion transport with minimized ohmic loss and lowered temperature operation possibility. Sub-nm thickness control ability of ALD enables this thin layer and the ALD can guarantee precise thickness control which means repeatability. Second, ALD's high uniformity, high density and good step coverage guarantees blocking the direct contact of hydrogen so that it protects ceria from reducing. The elimination of possibility for hot spot in the operation is important due to the even ion transport distribution. Besides, there is little contact resistance problem. Third, with ALD, there is no secondary phase due to low deposition temperature. Secondary phase at the interface between YSZ and GDC shows low ion conductivity and high electron conductivity. So it is important to prevent the generation of YSZ/GDC mixture. Fourth, we thought chemical stability and mechanical strength of YSZ could be of help to the durability of the cell. Especially the function of preventing micro crack in the interface between electrode and electrolyte can reduce the interfacial resistance. Fifth, we expected YSZ's high electron insulation property could block the electron flow through electrolyte and prevent the reduction of ceria. And we conducted

a case study to confirm maintaining the functionality of ALD-YSZ like bulk YSZ. Prinz et al. in Stanford University composed 60nm ALD-YSZ electrolyte with Pt electrodes. They succeeded to operate this μSOFC at below 500°C. [56] So we can confirm that there is no problem using ALD-YSZ for functional layer.

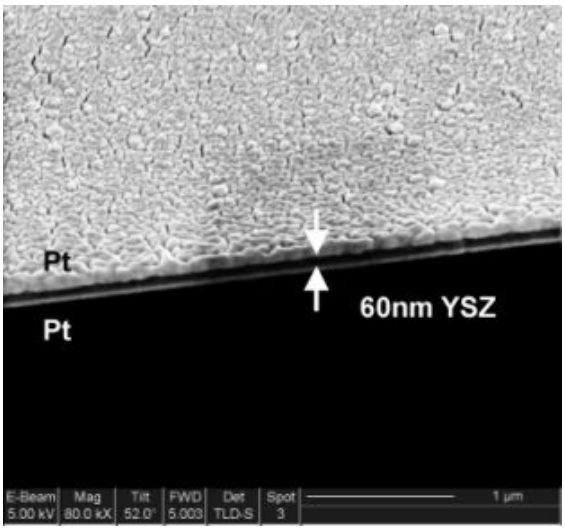

Figure 2.7 Example of ALD-YSZ based µSOFC [56]

2.2 Theoretical study

To put GDC in electrolytic region, P_{O_2} of interface should be positioned at the lower limit of GDC's electrolytic domain at least. So the thickness ratio of YSZ must have minimum value.

In the OCV condition, if bi-layered electrolyte position between air (P'_{O_2}) and fuel (P'''_{O_2}), P_{O_2} gradient which means the permeation of oxygen appears through electrolyte and P''_{O_2} would be generated at the interface between YSZ and GDC. Oxygen flux follows this formula

$$
\begin{aligned}
J_{O^{2-}} &= -\frac{\sigma_{O^{2-}}}{4e^2} t_{e^-} \nabla \mu_O \\
\int_0^L J_{O^{2-}} dx &= -\int_{\mu'_O}^{\mu''_O} \frac{\sigma_{O^{2-}}}{4e^2} t_{e^-} d\mu_O \\
J_{O^{2-}} &= -\frac{\sigma_{O^{2-}}}{4e^2 L} \int_{\mu'_O}^{\mu''_O} t_{e^-} d\mu_O
\end{aligned}
\qquad (3.1)
$$

where, σ_{ion} is ion conductivity, t_{e^-} is transference number which explains the electron conductivity over whole conductivity, and $\nabla\mu_0$ is oxygen chemical potential difference. Chemical potential of oxygen is expressed as

$$
d\mu_O = \frac{1}{2} kT d\ln P_{O_2} \qquad (3.2)
$$

If we suppose the steady state that oxygen fluxes through GDC and

YSZ are same, we can obtain the thickness ratio t.

$$-\frac{\sigma_{ion}^{GDC}}{4e^2 t}\int_{p'_{O_2}}^{p''_{O_2}} t_{e^-}^{GDC} d\ln P_{O_2} = -\frac{\sigma_{ion}^{YSZ}}{4e^2(1-t)}\int_{p''_{O_2}}^{p'''_{O_2}} t_{e^-}^{YSZ} d\ln P_{O_2}$$

$$t = \left[1 + \frac{\sigma_{ion}^{YSZ}\int_{p''_{O_2}}^{p'''_{O_2}} t_{e^-}^{YSZ} d\ln P_{O_2}}{\sigma_{ion}^{GDC}\int_{p'_{O_2}}^{p''_{O_2}} t_{e^-}^{GDC} d\ln P_{O_2}}\right]^{-1} \quad (3.3)$$

t_{e^-} can be re-arranged according to the relationship of electron and ion conductivity with partial oxygen pressure.

$$t_e = \frac{\sigma_{elec.}}{\sigma_{elec.} + \sigma_{ion}} = \frac{P_{O_2}^{-1/4}}{P_n^{-1/4} + P_{O_2}^{-1/4}} \quad (3.4)$$

Equation 3.3 and 3.4 can be organized below.

$$t = \left[1 + \frac{\sigma_{ion}^{YSZ} \ln \frac{P_{n,YSZ}^{-1/4} + P_{O_2}^{'''-1/4}}{P_{n,YSZ}^{-1/4} + P_{O_2}^{''-1/4}}}{\sigma_{ion}^{GDC} \ln \frac{P_{n,GDC}^{-1/4} + P_{O_2}^{''-1/4}}{P_{n,GDC}^{-1/4} + P_{O_2}^{'-1/4}}}\right]^{-1} \quad (3.5)$$

At 800°C which is maximum temperature for IT-SOFC, we supposed YSZ/GDC interfacial P_{O_2} was 10^{-15} atm, P_{O_2} at the cathode was 0.21 atm and P_{O_2} at the anode was 10^{-23} atm. The calculation result was t=0.9999, it means the minimum thickness ratio of YSZ is about 10^{-4} of GDC. That is to say 10^{-4} of YSZ layer can protect GDC from reducing P_{O_2}. We calculated the YSZ thickness with 500μm GDC. At 700°C, YSZ's thickness should be more than 1.26nm.

In order to realize this YSZ thickness maintaining its property, we had to use ALD. And we deposited YSZ of 50, 100 and 200nm on 500μm GDC substrate because the real thin film layer would be different from ideal case, although ALD film would be very dense, uniform and conformable to surface morphology.

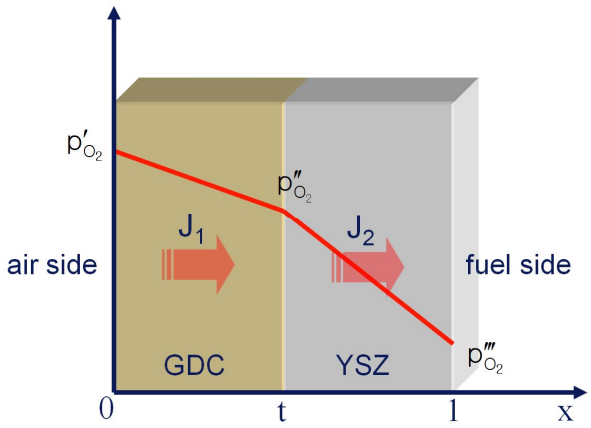

Figure 2.8 P_{O_2} gradient in YSZ/GDC bi-layerd electrolyte [57]

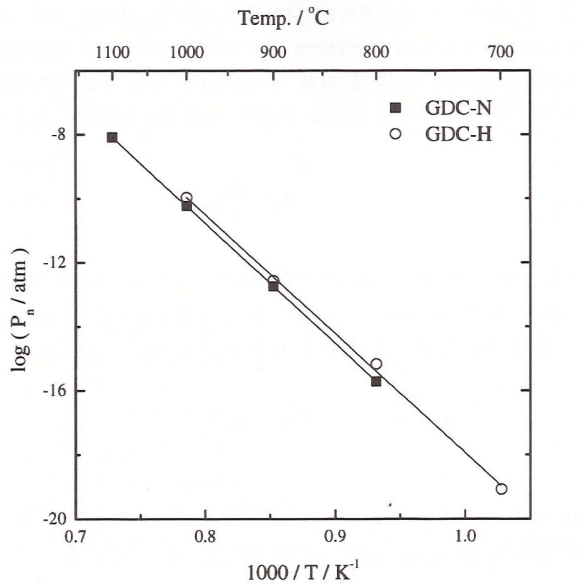

Figure 2.9 Lower boundaries of electrolytic domains of GDCs [55]
(GDC-N:Nextech GDC powder, GDC-H:High purity chemical GDC powder)

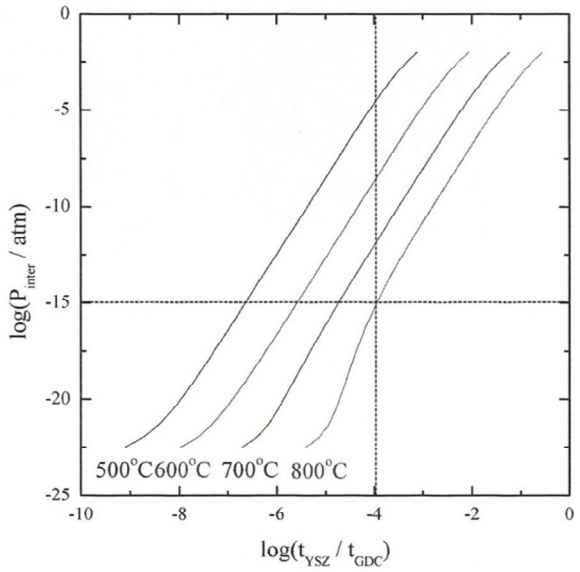

Figure 2.10 Calculation results of YSZ/GDC ratio [57]

2.3 The cell fabrication process

2.3.1 Electrolyte supported type

To carry out the investigation focused on the electrolyte, we planned experiments with electrolyte-supported button cells although the performance would be much poorer (about 500μm thickness electrolyte) than that of typical anode-supported cells.

For SOFCs thin electrolyte directly connects to high performance because ohmic loss is the major polarization factor of SOFCs. So the thinner electrolyte you choose, the lower performance loss can be appeared. Typical electrolyte thickness is under 50μm.

As we said above we have anticipated this low power density and current density due to the thick GDC substrate. The electrolyte thickness of 500μm causing high ohmic loss was not general for intermediate temperature SOFCs. But we did not choose electrode supported cell structure because there could be sealing problems on a porous anode or a cathode. If gas sealing is not perfect, iV curve shift to left side. As a result, overall voltage drops than the situation of perfect sealing. Sealant with a porous surface cannot guarantee gas sealing.

Besides the gas is very permeable hydrogen. So the leakage possibility gets higher and higher. If we have chosen the electrode supported structure, we could not find out the clear origin of OCV and power density drops that could be due to the gas leakage as well as the electron conductivity of ceria. Thus we might be unable to find out the ALD-YSZ layer effect. Figure 2.11 shows an example of voltage drop factors in the experiments for the different ceria electrolyte cell structures.

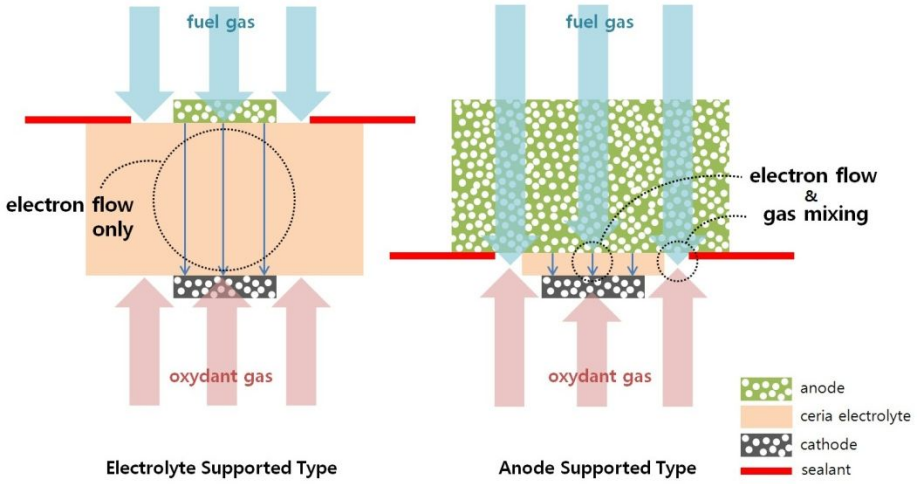

Figure 2.11 Example of voltage drop factors in SOFC experiments for different ceria electrolyte cell structures

2.3.2 Substrate preparation

First, densified 10% gadolinia doped ceria ($Ce_{0.9}Gd_{0.1}$)$O_{1.95}$ in the form of disks with 1 inch diameter and 3mm thickness were obtained from NexTech Materials, Ltd. Then the disks were ground to 200 and 500μm thickness and polished with diamond sand. (200μm type cannot be used in experimental because of the breakage during the pressing process for sealing) After a thermal etching process of GDC disks at 800°C for two hours that can eliminate the grinding oil or sticky components, the roughness was measured to be 134nm RMS value.

2.3.3 YSZ thin film deposition

The coating of YSZ on GDC disks was conducted via ALD process with a zirconium precursor (Tetrakis (dimethylamido) zirconium, $[(CH_3)_2N]_4Zr$, Sigma-Aldrich® and with a yttrium precursor (Tris (methylcyclopentadienyl) yttrium, $(CH_3C_5H_4)_3Y$, Strem Chemicals Inc.).

Deposition conditions were below. The temperature of the ALD reaction chamber was 230°C, and distilled (DI) water was used as an oxidant. [58] For 8 mole %, cycle ratio was 7:1. The YSZ deposition rate was 1.4~1.5 Å per cycle.

After deposition, the annealing process follows at 800°C. The final

electrolyte samples were 500μm pure GDC disks without coating, 345 cycles (50nm) ALD-YSZ film coated 500μm GDC disks, 690 cycles (100nm) ALD-YSZ film coated 500μm GDC disks and 1380 cycles (200nm) ALD-YSZ film coated 500μm GDC disks.

1 : zircornia precursor
2 : yttria precursor

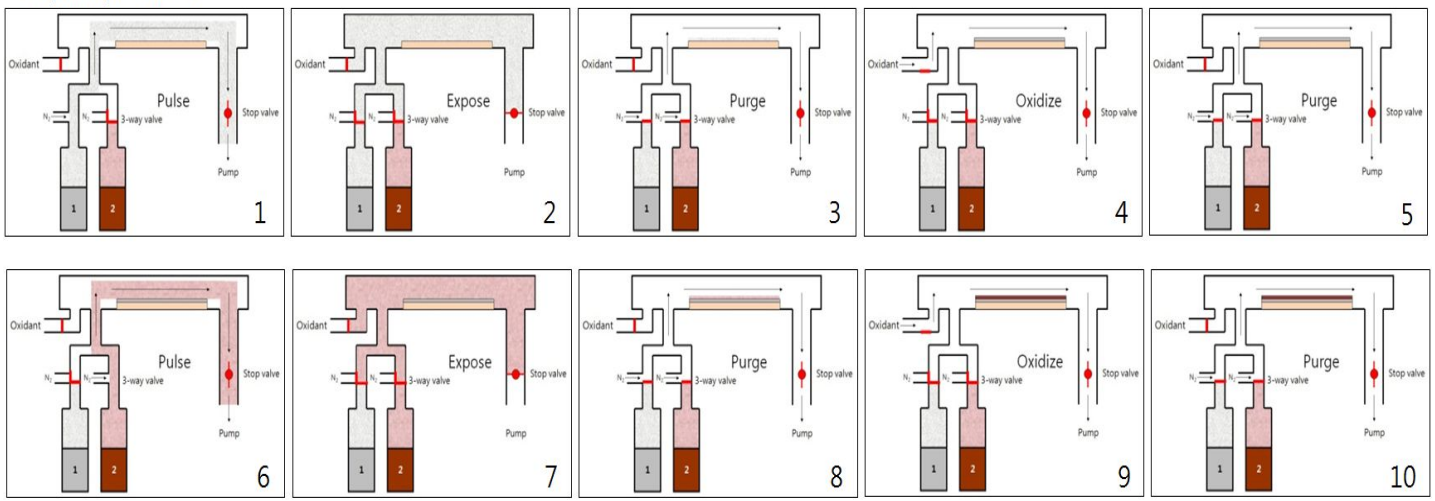

Figure 2.12 ALD-YSZ thin film deposition process

Table 2.1 ALD-YSZ conditions [58]

	ZrO_2	Y_2O_3
Precursor	$Zr(dm\text{-}am)_4$ Tetrakis(dimethylamido)zirconium(IV) Sigma Aldrich	$Y(m\text{-}cpd)_3$ tris-(methylcyclopentadienyl) yttrium $(Y(MeCp)_3)$ Strem Chemical
Oxidant	DI water	
Temperature	230°C	
Rate	1.2 Å/cycle	~2 Å/cycle
Cycle ratio	**7**	**1**
Purity	No contaminant	
YSZ deposition rate	**1.4~1.5 Å/cycle**	

Deposition time	50nm	100nm	200nm
	4h (345cycles)	8h (690cycles)	16h (1380cycles)

2.3.4 Electrodes screen printing

Then, the electrode materials of GDC-NiO cermet for anodes (50:50) and GDC-LSCF for cathodes (50:50) were applied to all the electrolyte samples. The anode was screen-printed on the electrolyte and sintered at 1400°C for 2 hours. The cathode was applied according to the similar procedure but sintered at 1200°C for 2 hours. The heating and cooling rate was 3°C/min and it was enough to release internal residual stress. So we could confirm that there was no crack or fracture in the fabrication process and in the final cells. The dimension of electrodes was 1cm by 1cm and each thickness was about 30μm. To protect the ceria electrolyte from reducing environment, the anode was attached to the YSZ coated side. (Figure. 2.13)

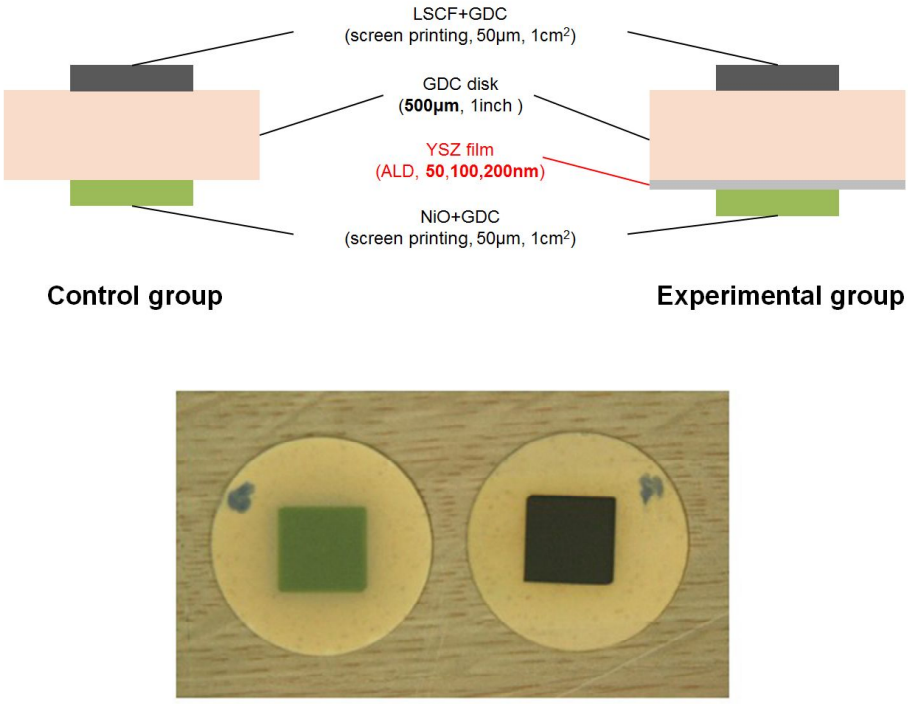

Figure 2.13 Schematics of the ALD-YSZ / GDC cell and the pure GDC cell and actual image of the anode and cathode sides

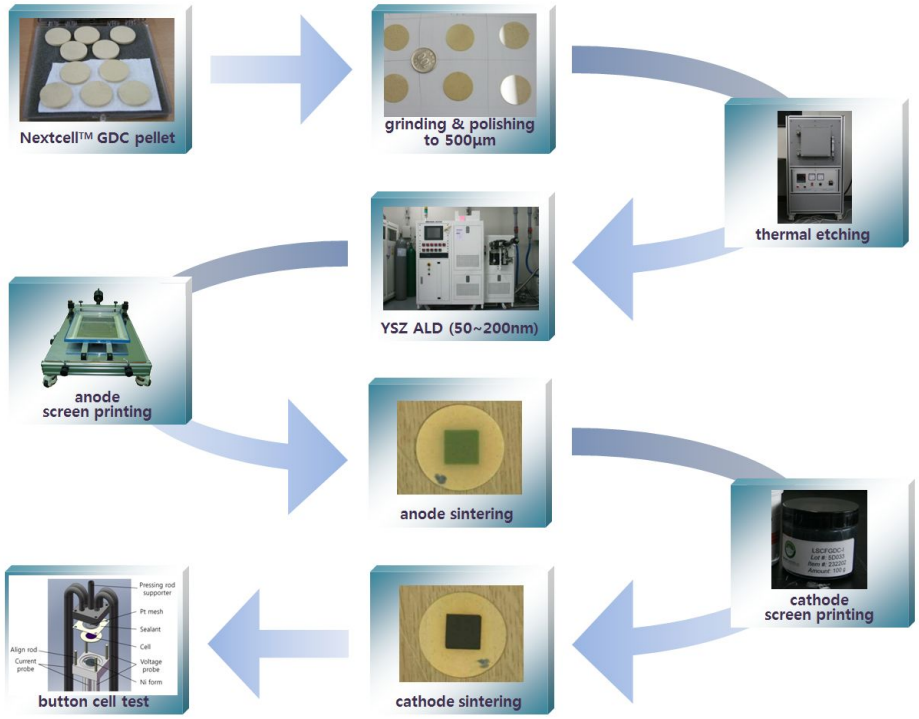

Figure 2.14 ALD-YSZ bi-layered cell fabrication flow

2.4 The experimental process

2.4.1 Final button cell test station setup

The button cell test station was composed of an electric furnace (Korea Furnace Development Co., Ltd.) with temperature controller (Yokogawa, UP550-01), Thermo couples with indicator, cell pressing unit, gas tubes with mass flow controllers (MFC: Mykrolis, FC-280SAV), humidifier in the anode line, electrochemical measurement devices (Solartron, SI 1287 and SI 1260), and cell supporting fixture. (Figure 2.15)

Electric furnace should have minimum internal volume that can accommodate supporting fixture only. If furnace is big, internal might not follow controller's target temperature. Thus it can delay experimental time and affect cell degradation. Furnace controller should be programed to have several temperature segments for sealant de-binding process. Thermo couples (TC) used to measure the temperature of fixture. Because the Furnace temperature could be different from actual cell temperature, K type TCs in contact with the fixture were used. Cell pressing unit is the device to give weight to cell to ensure gas sealing. Rotating handle gives and release pressure. The load cell at the end of pressing unit senses the pressing weight and it should cool down with electric fan. We used 3 kinds of MFC for hydrogen, nitrogen and air. They can control the flow from 0 to 500sccm. Air line to cathode side also should be connected to anode side because gas

should be flow in the fixture at the anode and cathode side in de-binding process. Nitrogen and hydrogen line to the anode side should be merged so that we can control the hydrogen concentration in operation. The bubbler in anode line humidified (about 2% AH) the fuel gas. The gas regulator maintains the pressure of feeding gas. We could measure cell voltage, current and impedance data with electrochemical measurement devices. They connected to the cell supporting fixture by 4 probe type or 2 probe type.

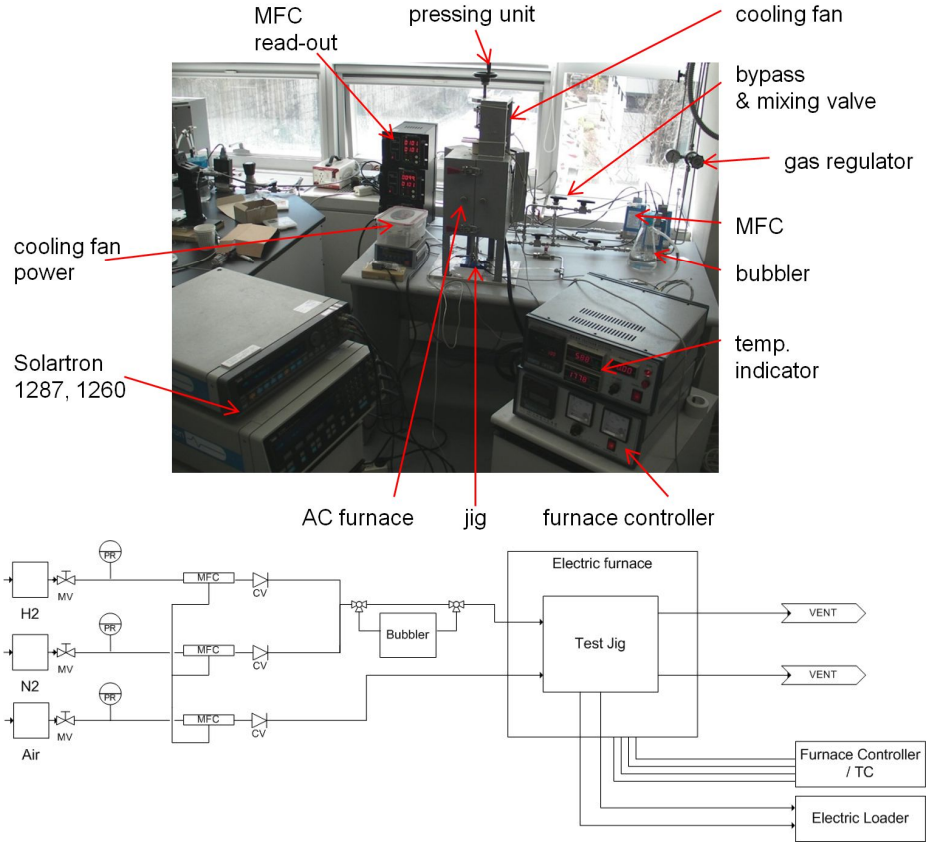

Figure 2.15 Button cell test station and P&ID diagram

Figure 2.16 Electric furnace, controller and TC

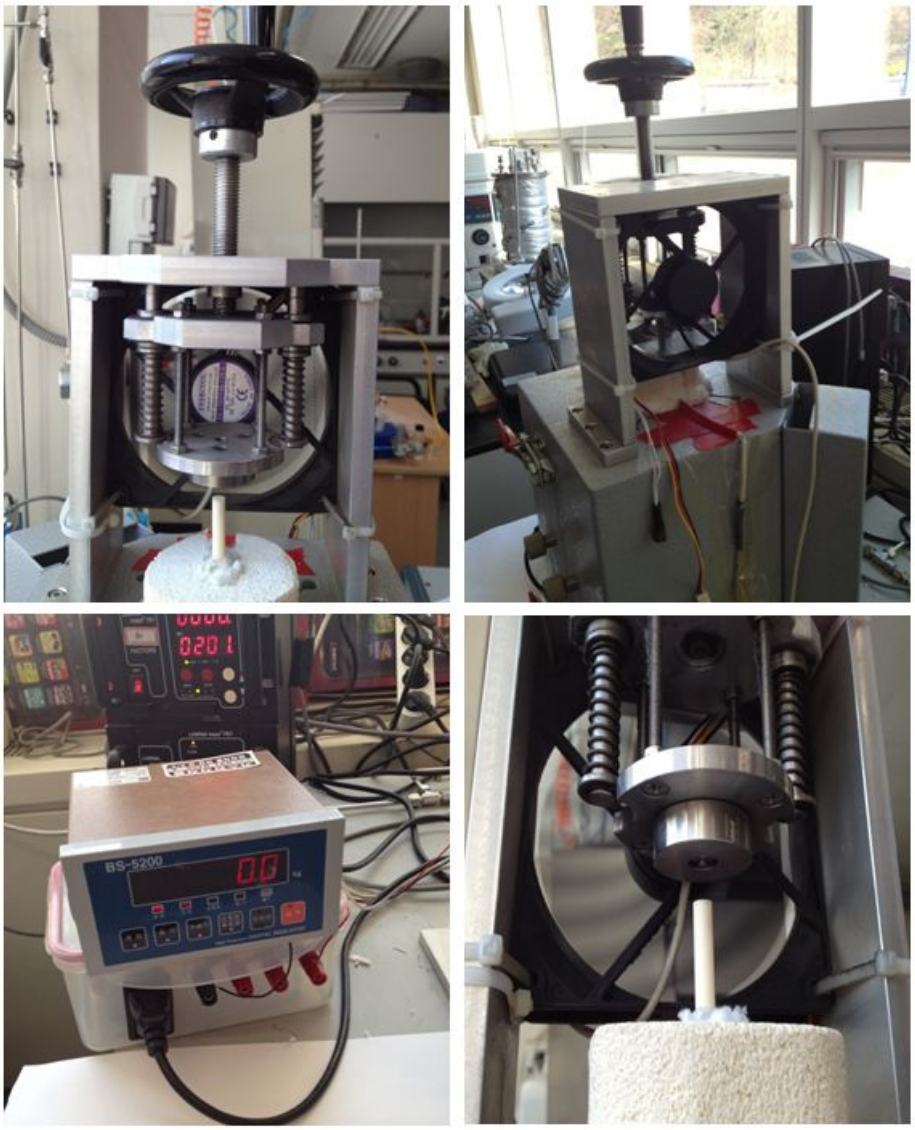

Figure 2.17 Cell pressing unit and indicator

Figure 2.18 MFCs and controllers

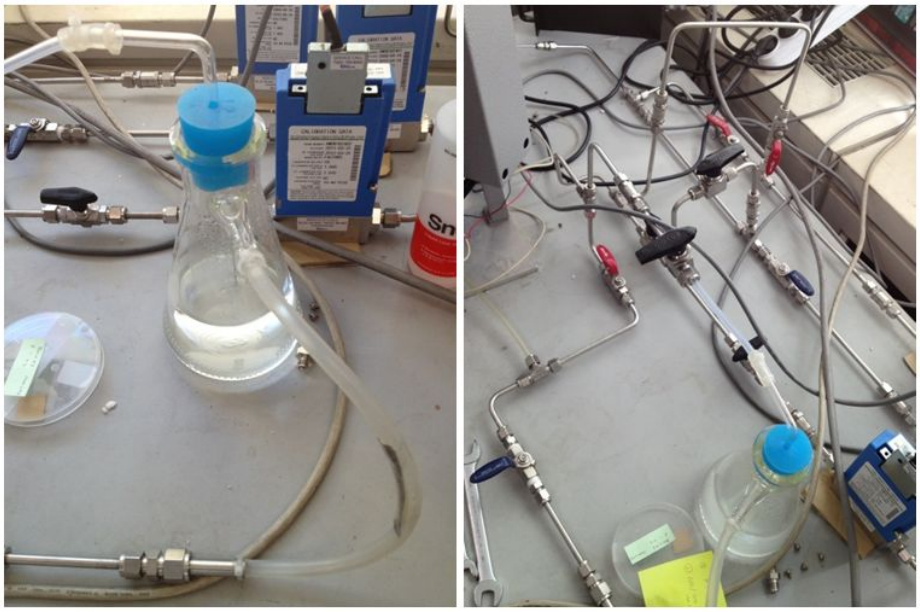

Figure 2.19 Bubbler type humidifier

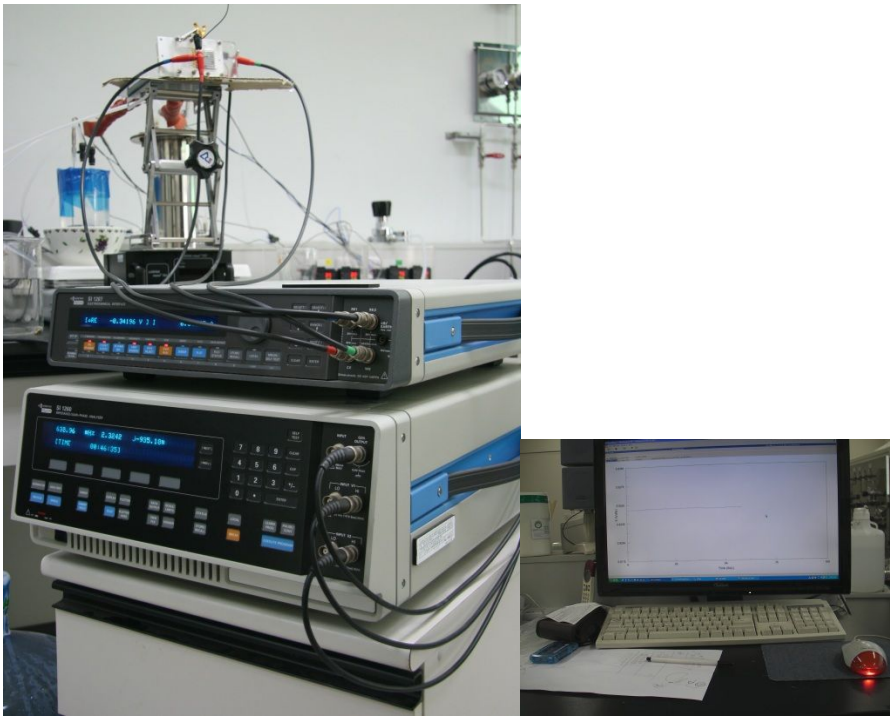

Figure 2.20 Solartron SI 1287 and SI 1260

2.4.2 Fixture design

The cell supporting fixture design changed a lot to secure the maximum performance from cells.

First and second design was focused on the current collection and the transport to load. Current probes and gas in/outlet were in same structure. Fixture is divided into upper plate and lower plate for anode and cathode current collection. Material was Crofer 22 which has better electron conductivity in high temperature than Inconel 600. Sealant was glass paste which is typical to SOFC experiment.

Especially in design 2, we did CFD analysis for the asymmetric shape of gas feeding slope. The result said gentler-exhaust slope case showed that gas discharging was not smooth. There were some vortexes near the exhaust slope. And we confirmed flow in chamber was not uniform. Another case of gentler-feeding slope case showed fluent gas flow and uniform flow distribution.in the chamber. And we calculated voltage offset of this fixture for each case of voltage.

The designs were fitted to 20cm X 20cm X 20cm furnace (Nara cell tech Inc.) But these designs have too heavy weight so that cells were often broken in experiment even if electrolyte thickness was 3mm. And it showed poor performance due to gas sealing and a lot of welding spots.

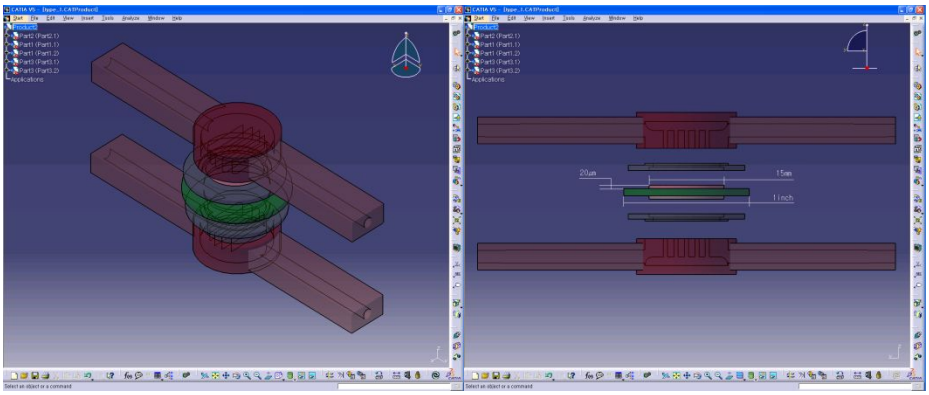

Figure 2.21 First fixture design

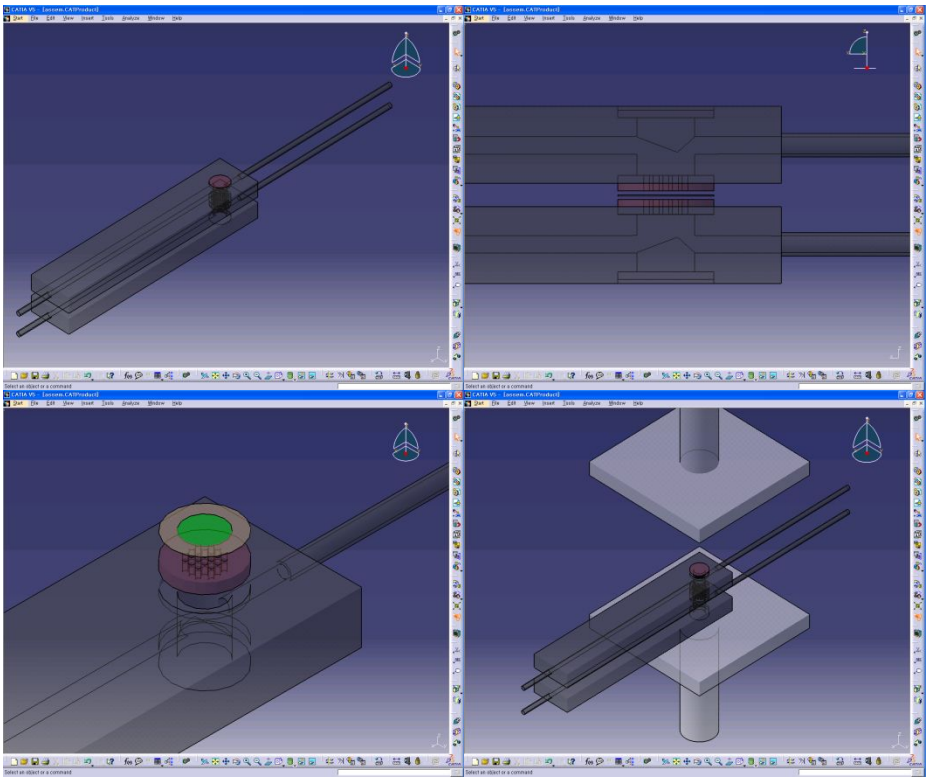

Figure 2.22 Second fixture design

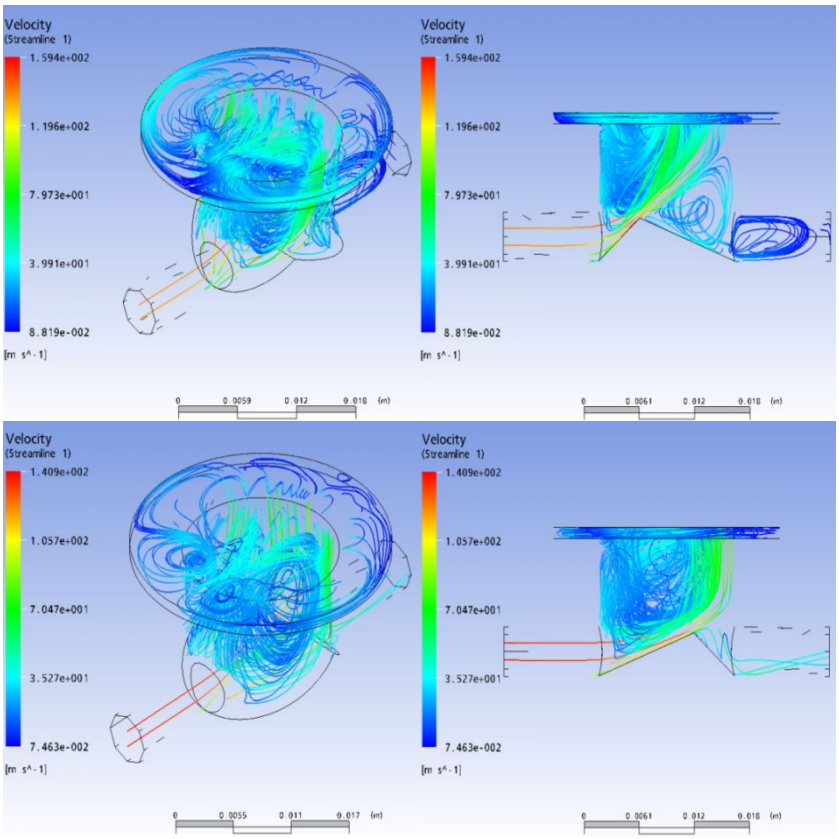

Figure 2.23 CFD analysis for the asymmetric shape of the gas feeding slope, (Upper) gentler-exhaust slope case and (Lower) gentler-feeding slope case

Table 2.2 Electric resistance loss of the second fixture design

Operating voltage	Loss
1.0V	0.002%
0.8V	0.009%
0.6V	0.023%
0.4V	0.054%
0.2V	0.162%

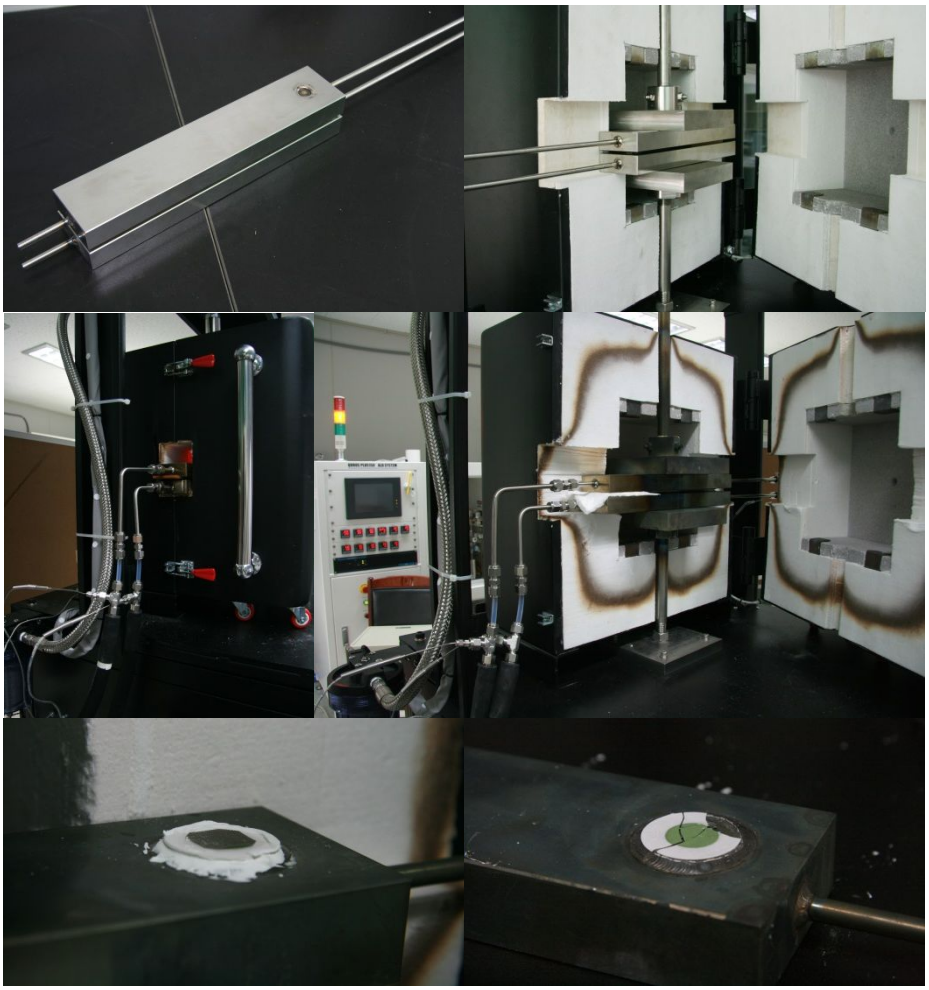

Figure 2.24 Experiment using the second design fixture and the cell fracture

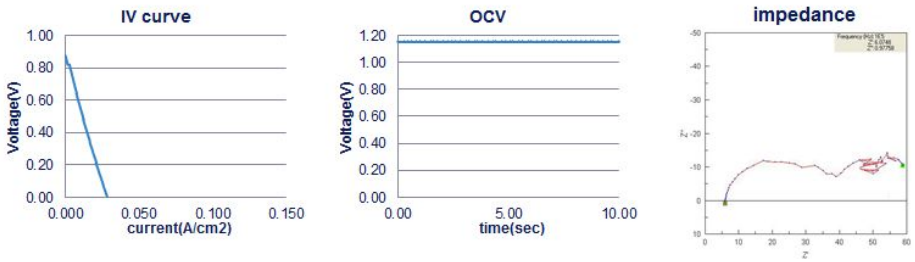

Figure 2.25 Cell performance from the second design fixture

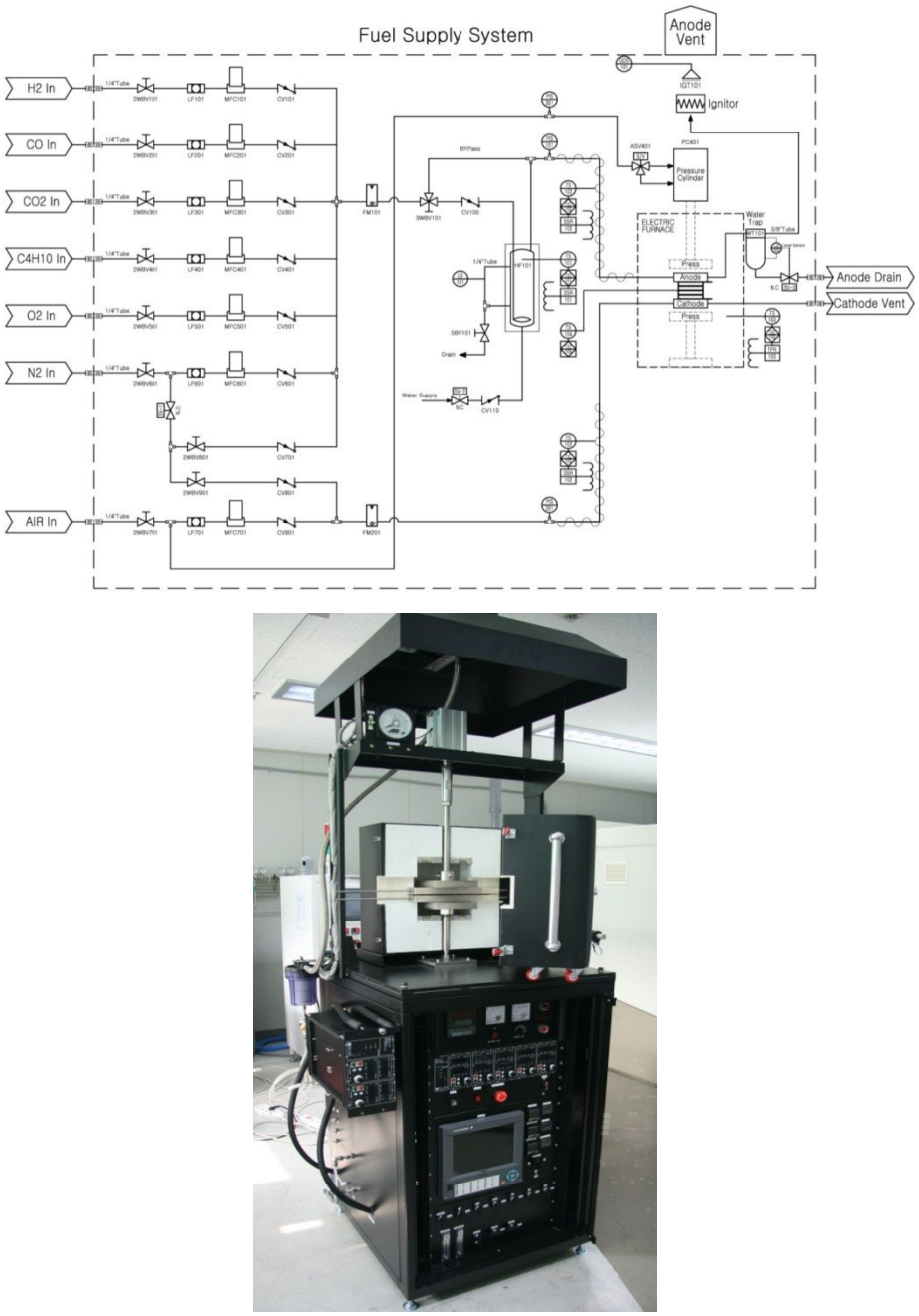

Figure 2.26 Large scale fuel cell test station (Nara Cell Tech)

So the third and fourth designs were changed smaller and compact. Applicable furnace was same as first and second design. The dielectric sealant, ESL type 4460 was used. And the holes for alumina align rod or shorting preventer was added.

With fourth fixture, we did not experience any breakage in the operations. And ScSZ based commercial cell (NexTech Materials, Ltd.) test results were excellent. However after the operation, sealant was hardened so we cannot get the cells without breakage. And it was very difficult to remove the hardened sealant.

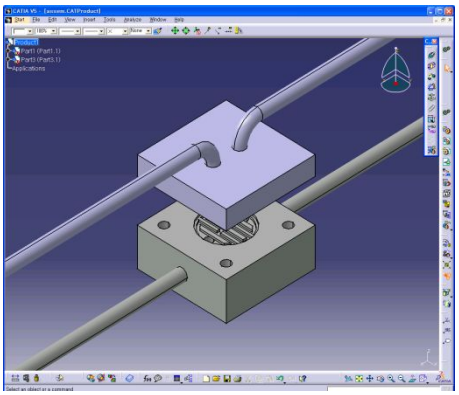

Figure 2.27 Third fixture design

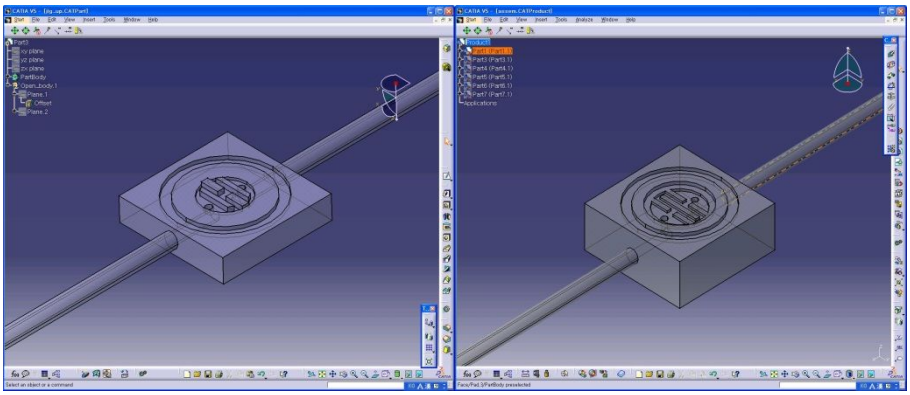

Figure 2.28 Fourth fixture design

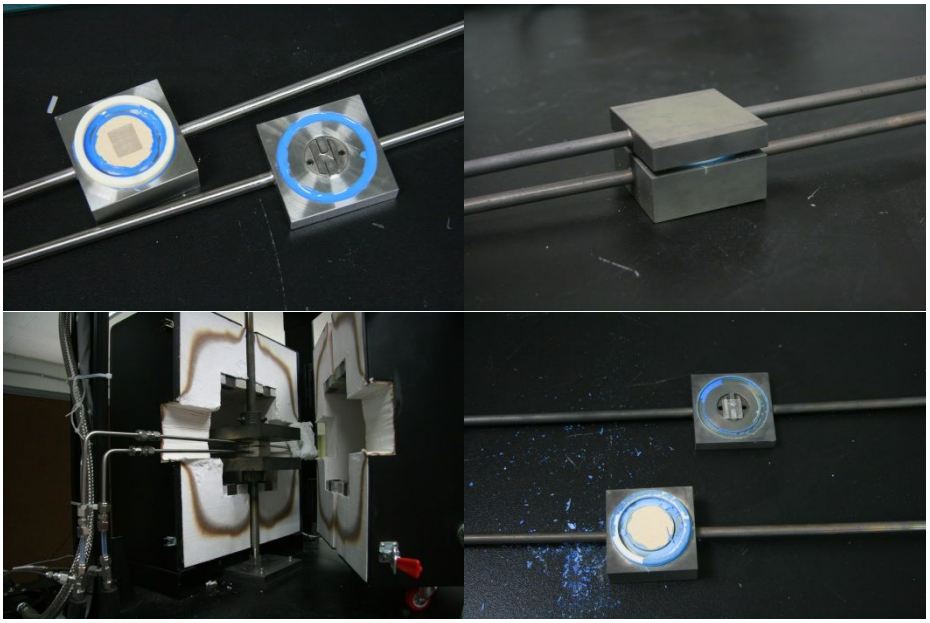

Figure 2.29 Experiment using the fourth design fixture

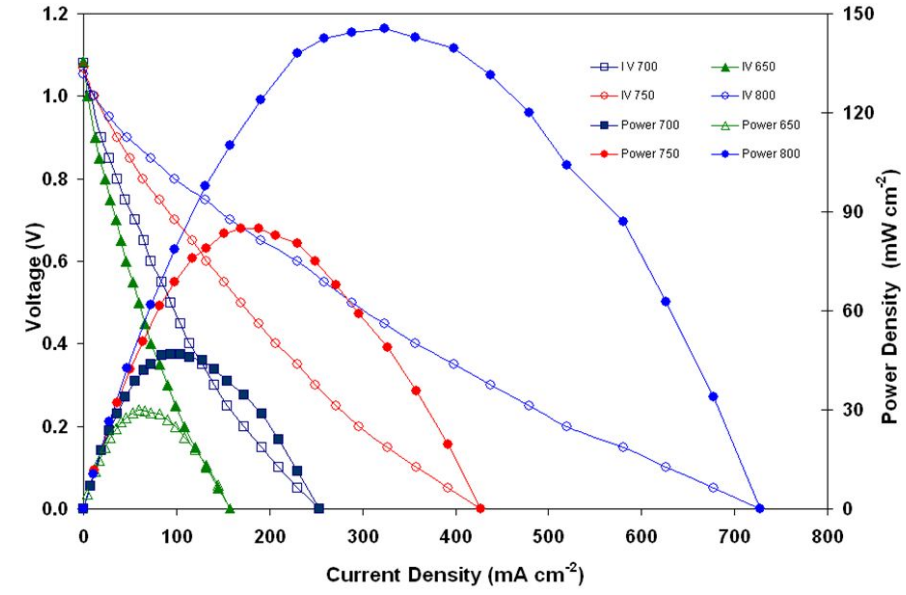

suggested commercial cell data

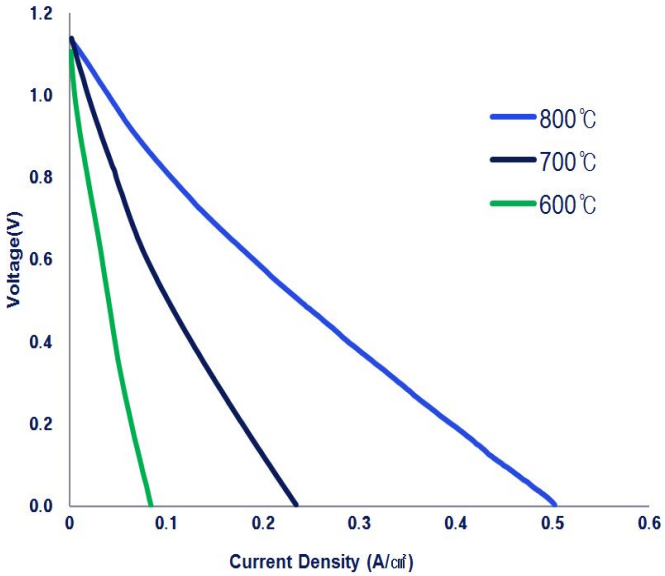

experimental cell data

Figure 2.30 iV data comparison between reference and experiment using the fourth design fixture

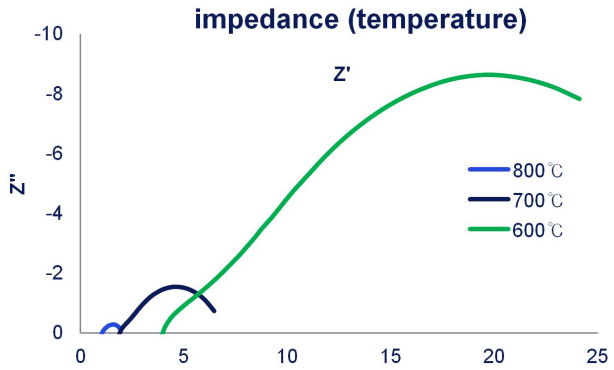

Figure 2.31 Impedance data using the fourth design fixture

The fifth cell supporting fixture design shown in Figure 2.32 was made of Inconel 600 for long time stability. It was fitted to sheet type sealant which was easily removable after the operation. And it needed to press for gas sealing. This fixture consisted of upper and lower structures that were assigned to cathode and anode. The structures include current probes that are rod-shaped to minimize the iR drop and voltage probes that are pipe-shaped to provide fuel and oxidant. Ni form on the anode side and Pt mesh on the cathode side are placed as flexible current collectors according to pressing situation.

This design and small furnace can guarantee fast response to furnace temperature control and need special additional structure on top of furnace. Figure 2.34 shows the cell performance comparison between commercial data and experimental results on this fixture. We got the good results at 650°C and 700°C so that we could trust this fixture system. The performance gap at 800°C came from that the sealant capacity was limited to 700°C.

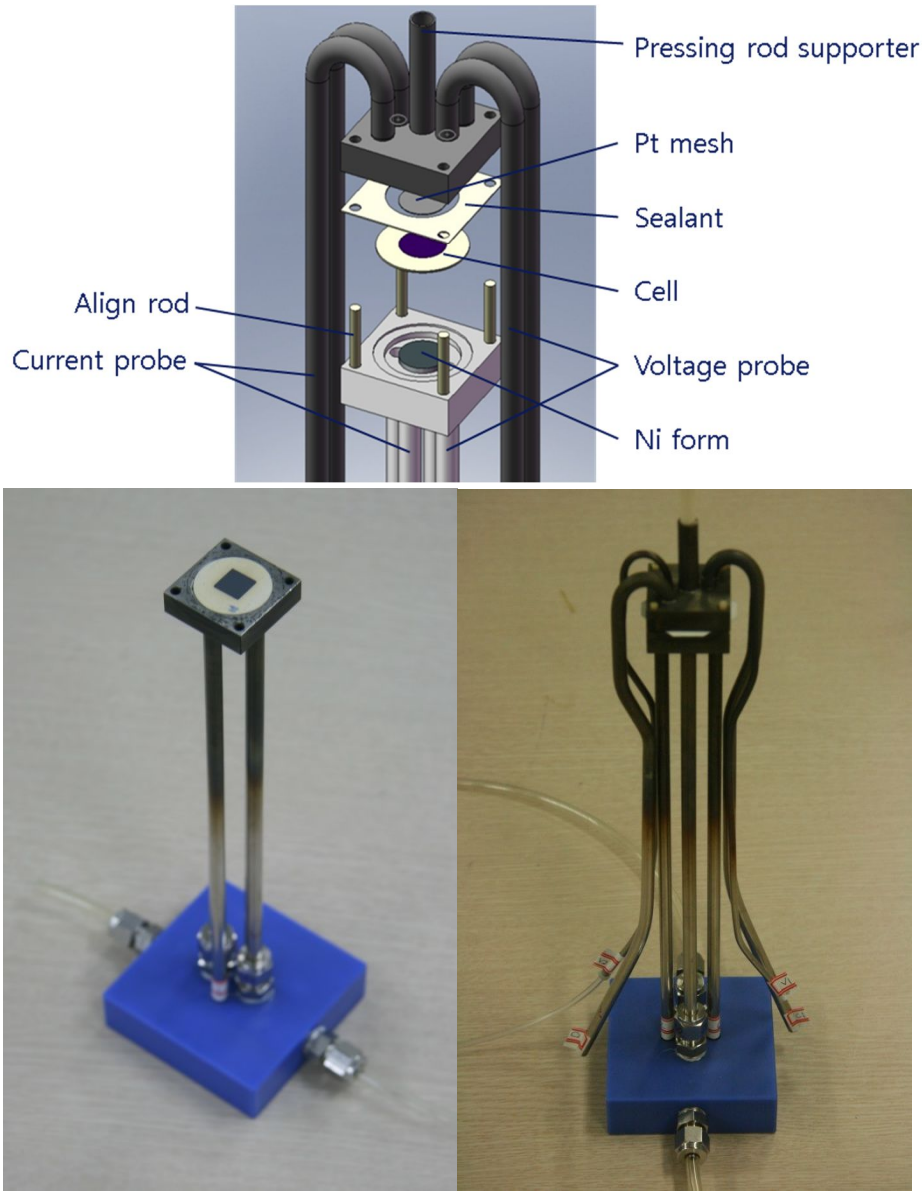

Figure 2.32 Fifth button cell supporting fixture design for experiments

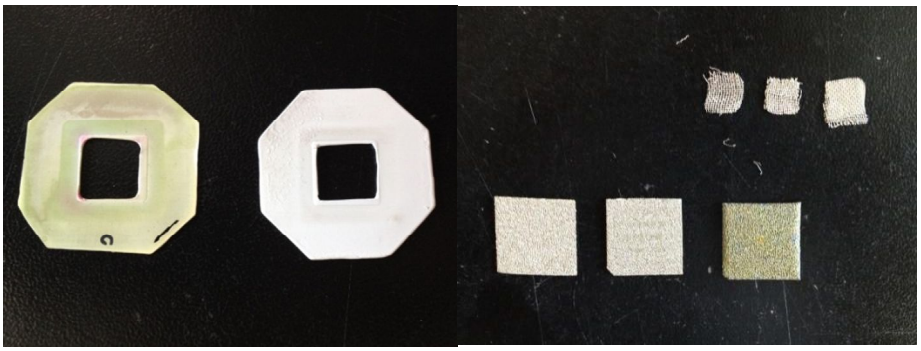

Figure 2.33 Sealants and current collectors for the fifth design fixture

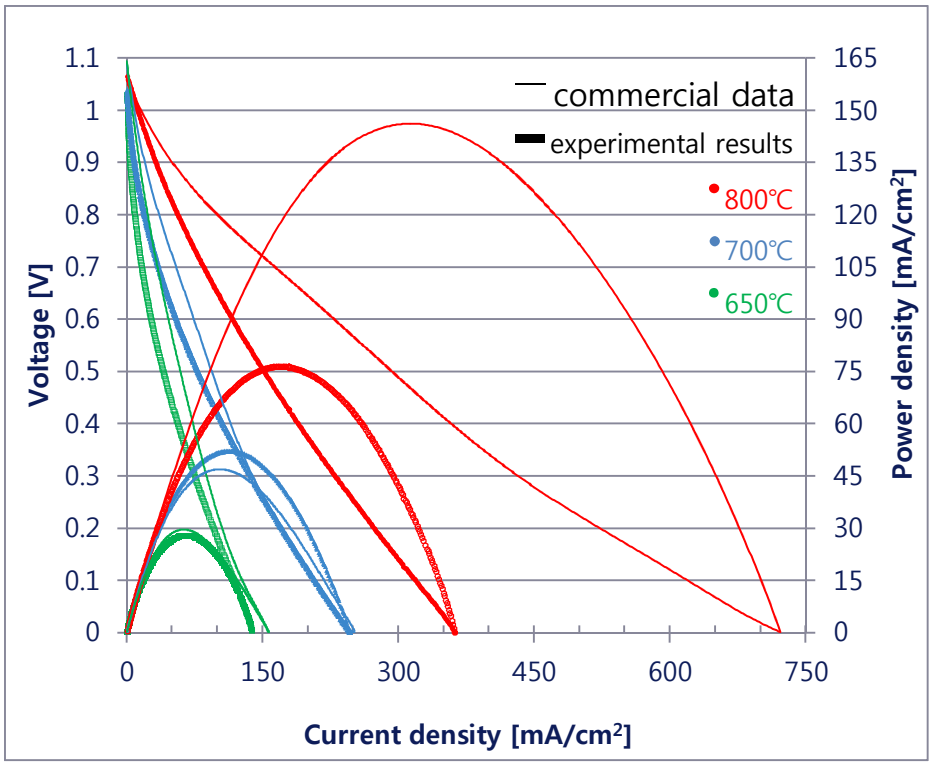

Figure 2.34 iV data comparison between reference and experiment using the fifth design fixture

2.4.3 Cell test procedure

Before heat up, preparation process on this fixture followed this order. First we cut a Ni form into the shape of groove of bottom fixture and pressed it to the thickness of groove. And we put the button cell on the Ni form. After putting alumina align rod into the hole, sheet type sealant was placed. Sealant sheets were laminated 2~4 times. Lamination process was done on 80°C at the hydraulic press. We pressed Pt mesh to the thickness of 80% of sealant because thickness of sealant reduced in de-binding process. The reason of same thicknesses of sealant and Pt current collector is to get the gas tightness and to secure contact between cathode - Pt mesh – upper fixture. If Pt mesh was thicker than another, gas sealing could not be accomplished. Otherwise, thicker sealant cause open circuit situation so that we cannot measure the cell performance. Putting the upper fixture according to the align rods is the final stage of fixture preparation. Figure 2.35 shows the experiment preparation process on this fixture.

The furnace was controlled to heat up slowly to prevent thermal stress and breakage of GDC and to de-bind the organic components in sealant. (Figure 2.36) The heating time was over 18 hours to reach the operating temperature of 600°C. For the sealing property, we maintained temperature for several hours at 170°C, 250°C, 350°C, 500°C, and 620°C during hear-up schedule. Cells were compressed lightly between upper and lower supporting

structures to ensure gas tightness at the cell sealing. We started increasing pressing load from 0.1kgf/cm^2 at 530°C to 1kgf/cm^2 at softening temperature (580°C).

Till the operation temperature, air feeding to anode and cathode side should be done to remove the organic components generated from de-binding process. To prevent sudden oxygen partial pressure changes and to promote reactions on anodes, we humidified the gas fed to the anode with bubbler (2% AH) from the anode-reduction step until the end of the experiments. Also, we carried out a slow anode-reduction process for 8 hours with low hydrogen concentration gas (5% H_2 and 95% N_2). Current-voltage (iV) characterization and electrochemical impedance spectroscopy (EIS) with 100% H_2 fuel gas followed the anode-reduction.

Then we cooled down the furnace slowly feeding H_2 to preserve the changes of electrolytes from reducing environment without thermal stress.

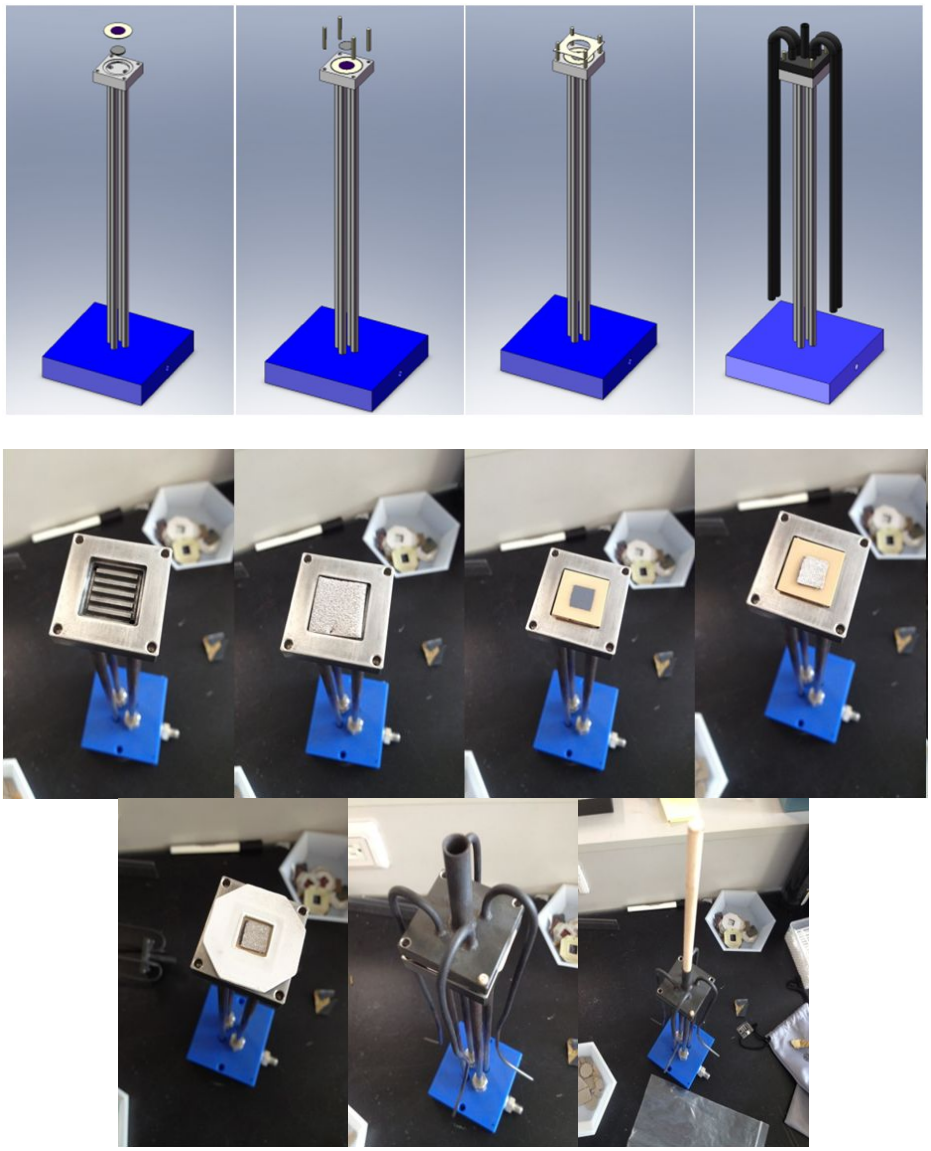

Figure 2.35 Experiment preparation process on the fifth design fixture.

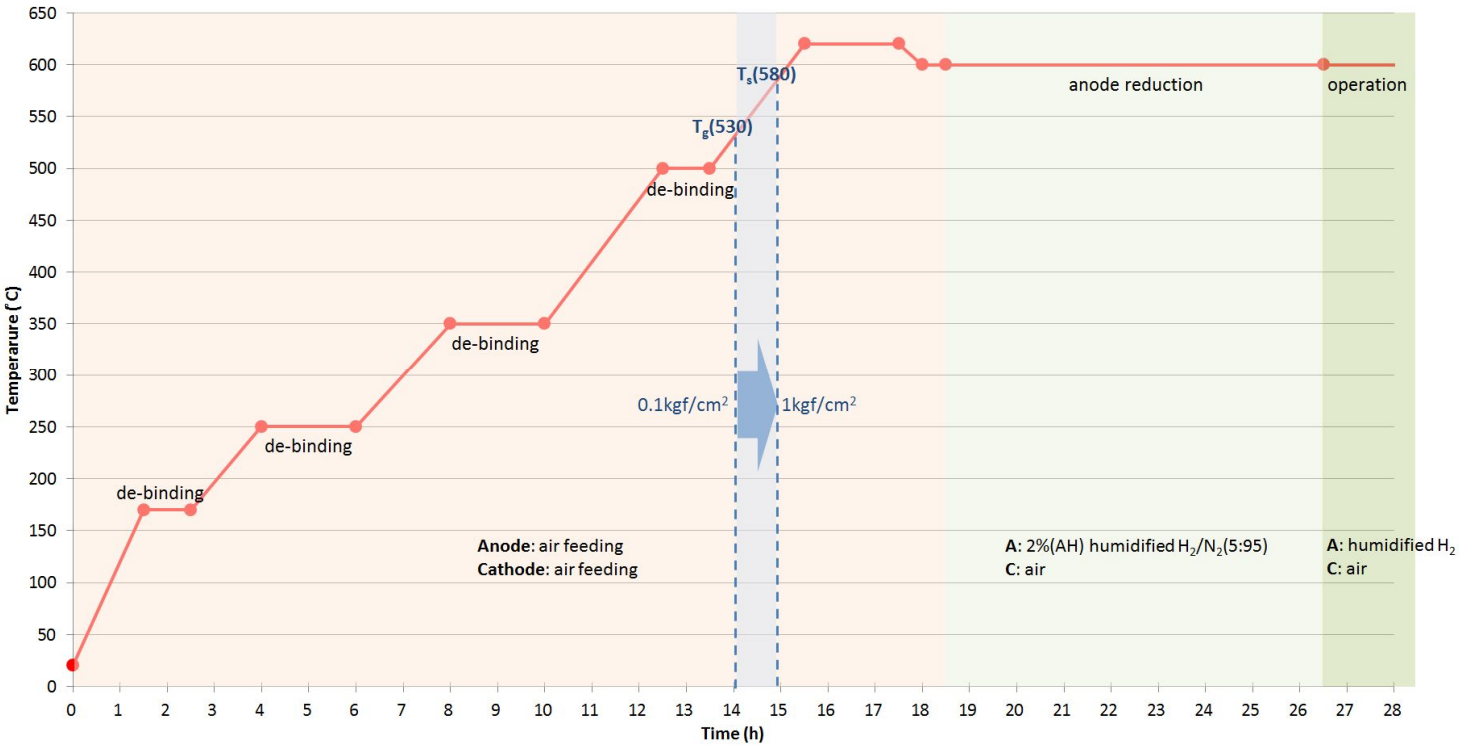

Figure 2.36 The heating-up schedule for button cell tests

.

3. Results and discussions

3.1 Characterization results of ALD-YSZ / bulk GDC cells

3.1.1 Confirmation of the ALD-YSZ layer

We could confirm that the thickness of the as-deposited 1380 cycles ALD-YSZ layer on bulk GDC electrolyte pellet before electrodes sintering step (Figure 3.1 (a)) was about 200nm from the cross section scanning electron microscope (SEM) images with focused ion beam (FIB: FEI, Quanta 3D FEG). From this image, the ALD-YSZ recipe on GDC was successful so we could find out that the growth rate, layer shape, thickness uniformity, and good step coverage were as expected. Together with the FIB-SEM image that includes more backscattered electron (BSE) signal which enabled to distinct YSZ from GDC via high contrast, we could obtain more magnified SEM image (FEI, Strata 235DB dual-beam FIB/SEM) with through the lens detector (TLD) to see the morphology of as-deposited ALD-YSZ film which has pillar-shaped nano structure. (Figure 3.1 (a′)) Then we obtain the FIB-SEM image of the 690 cycles ALD-YSZ layer after the operation. After the operation means YSZ film on GDC suffered electrodes sintering processes (1400°C and 1200°C) and 3 days operation with hydrogen gas. Shown in Figure 3.1 (b) dark YSZ was deposited on GDC as a layer shape with perfect step coverage, too. But the thickness was about 85nm which was less than

100nm of as-deposited step. We thought the reason of this gap came from the slight mixing of YSZ and GDC on electrode sintering temperature. We will discuss this phenomenon later.

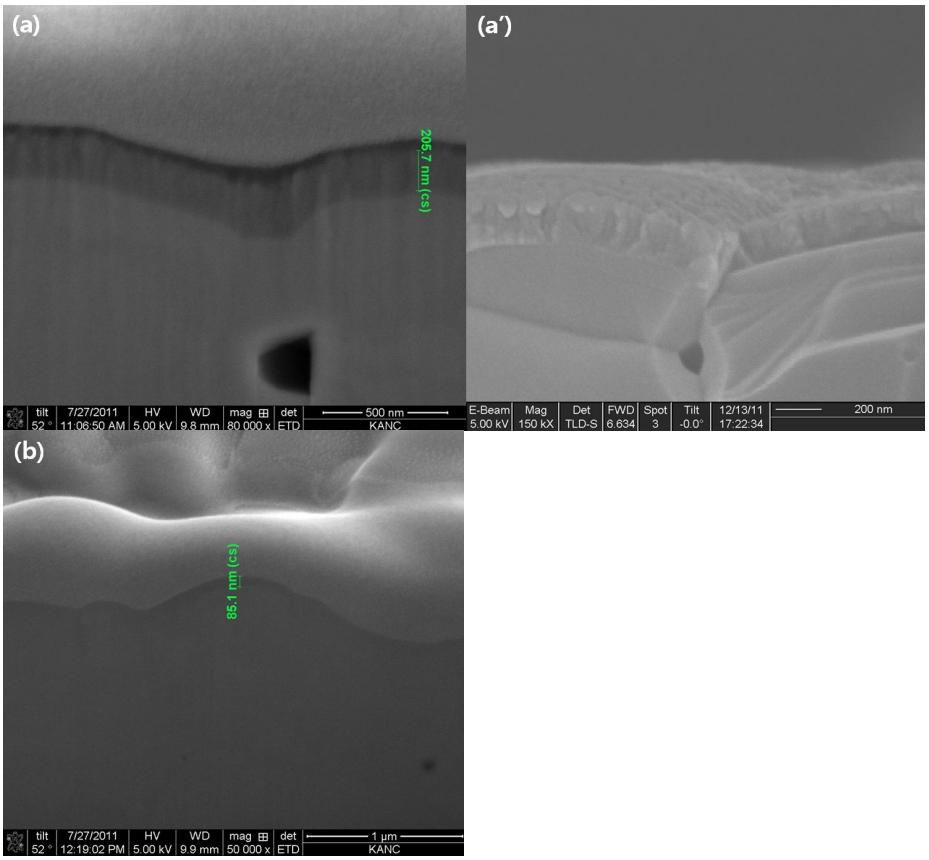

Figure 3.1 SEM images of ALD-YSZ layer on GDC, (a) as-deposited 1380 cycles ALD-YSZ layer on bulk GDC, (b) 690 cycles ALD-YSZ layer after the cell operation

Then we performed X-ray photoelectron spectroscopy (XPS: Kratos Analytical, AXIS-HSi) analysis of the surface of bi-layered electrolytes. ALD-YSZ as-deposited and after the cell operation samples were investigated, too. Figure 3.2 shows clear peaks of yttrium and zirconium for the surfaces of the sample before electrodes sintering and after the operation. The red letters show the locations of main peaks for Ce, Gd, Zr, and Y elements. [59] There is no peak at the location of Ce and Gd., so there was no peak related to gadolinium and cerium. So we could know YSZ covered GDC surface and there was no change after the exposure to high temperature and to reducing gas. Figure 3.3 shows depth profile of bi-layered electrolyte which was deposited 345 cycles (50nm) ALD-YSZ. (PHI, VersaProbe Scanning XPS Microprobe) We could confirmed about 8% (7~8.2%) yttrium mole fraction in YSZ thin layer until 2 min etching. And we could make sure the 50nm thickness of ALD-YSZ layer from the experiences of YSZ etching rate about 25nm/·min with the condition of 5kV beam energy, 1μA beam current, and 1μm X 1μm spot size.

From these SEM and XPS results, we conclude that nano-scaled ALD-YSZ layer could survive the electrode sintering condition of 1200°C and 1400°C as well as the cell operating condition in the reducing atmosphere maintaining its shape and conformability with identical composition ratio as we expected.

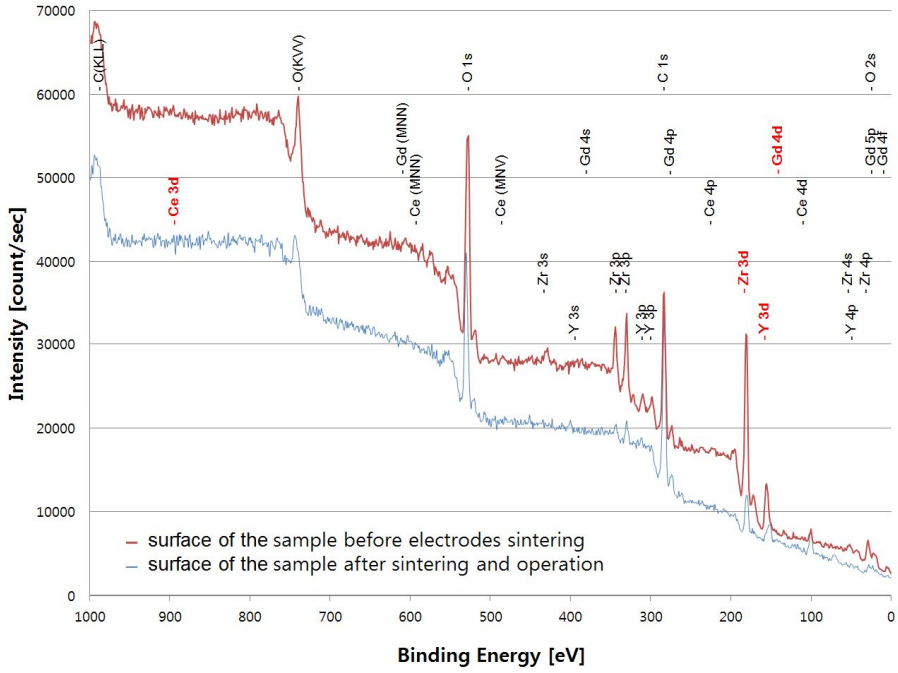

Figure 3.2 XPS spectra on the surfaces of ALD-YSZ / GDC samples (red) before the electrode sintering process and (blue) after the cell operation

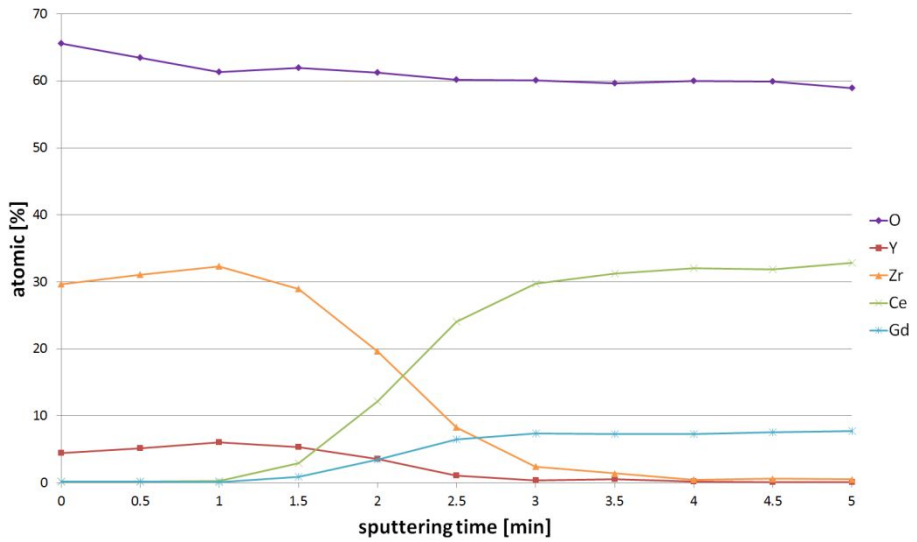

Figure 3.3 XPS depth profile of the bi-layered electrolyte which was 345 cycles (50nm) ALD-YSZ coated GDC

3.1.2 OCV transition results

We investigated the open circuit voltage (OCV) changes of the fabricated cells at a low hydrogen concentration (5% H_2, 95% N_2) corresponding to the anode-reduction step prior to cell operations. As shown in Figure 3.4, at 620°C the pure GDC electrolyte cell showed a voltage drop and saturation at 0.8V after 8 hours from hydrogen feeding whereas the 690 cycles (100nm) YSZ-coated GDC cell showed constant 0.95V. This difference was due to the increase of electronic conductance on the hydrogen side in the electrolyte from the gradual expansion of the domain of reduced cerium ion for pure GDC cell. The voltage of 0.95V could not reach the reported calculation value over 1.0V for humidified hydrogen fuel gas, [60],[61] but we could corroborate the long term electron insulation effect of nano-scale YSZ layer considering typical experimental data for ceria based cell's OCV varied from 0.87V to 0.91V. [62],[50] We could know that the electronic conduction was not perfectly blocked, because typical OCV values from YSZ cells exceeded 1.1V on this temperature even though their results were from the stack scale experiments. [63] Also, at higher hydrogen concentration, during the anode-reduction steps of the 100nm YSZ-coated cell, the OCV drop was observed. So we thought more experiments considering electrolyte thickness variation via ALD were needed for the optimization.

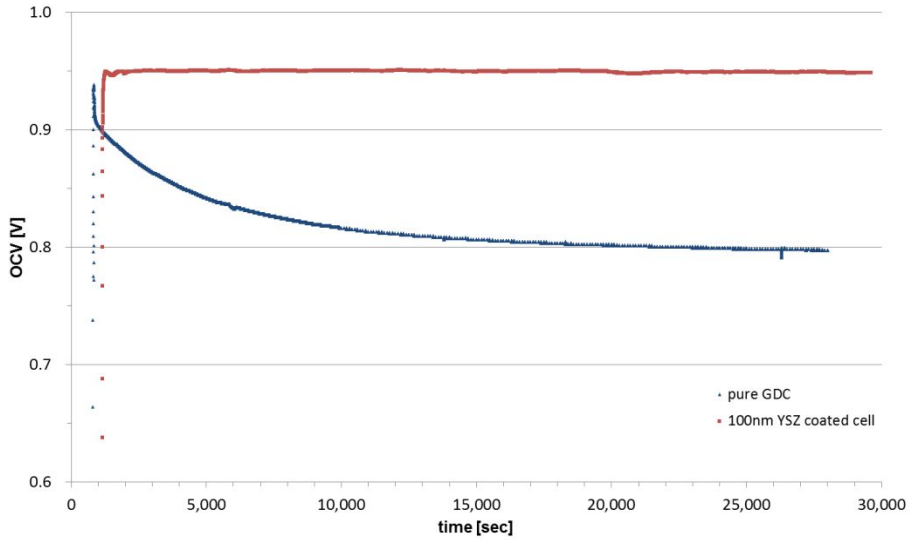

Figure 3.4 OCV transitions of the pure GDC cell and of the 690 cycles (100nm) ALD-YSZ / GDC cell at 620°C using 5% H_2 fuel during the anode reduction step

3.1.3 iV and power density results

After the observation of OCV transition for about 8 hours, the next experiment was iV and power density measurement at 600°C with the same feed rate of hydrogen and air (200sccm each). The peak power density of the 690 cycles (100nm) YSZ-coated cell was 46.1mW and this cell showed 0.83V OCV. In spite of the low performance, 690 cycles (100nm) YSZ-coated cell showed about 5% higher OCV and 53% larger peak power density than pure GDC electrolyte cell. (Figure 3.5)

Together with above OCV change in Figure 3.4, these results prove the electron insulation functionality of the ultra-thin YSZ layer arising from the ALD method. In the case of the 345 cycles (50nm) YSZ-coated cell, we observed almost similar or slightly lower power density performance compared to the case of the pure GDC cell. The slope of the current density curve was similar to that of the pure GDC cell and the OCV value was slightly higher. This suggests that the electron blocking was meaningless through the 345 cycles (50nm) ALD-YSZ layer, of which the reason was not clear at this point, but further investigation is being conducted.

Figure 3.6 displays a comparison of the iV and power density when the hydrogen and air feed rates were increased to 300sccm. The experiments for the 50nm YSZ-coated GDC cell was excluded since the performance improvement was not observed as explained previously. We observed an improvement in OCV and the power density for the 100nm YSZ-coated cell

for increased flow rates, but at the advantageous feed condition for gas, the pure GDC cell did not show any enhancement. We observed the similar trend for other flow rate values, too. Changing the feed rate of gases, we obtained the maximum power of 55.1mW at 0.482V for the YSZ-coated GDC cell under 200sccm hydrogen and 1000sccm air flow rates.

We investigated the performance at various temperatures from 600°C to 700°C and various flow rates. We can confirm that the most effective temperature for YSZ coating was 620°C with 66.7% gap, and that 200/1000sccm (H_2/air) flow rates enhanced the power densities by 19.6%, 35.2% and 414.4% at 600°C, 650°C and 700°C. At 700°C, unstable performance result was due to the temperature limit of sealant and water generation and condensation at the anode side and outlet.

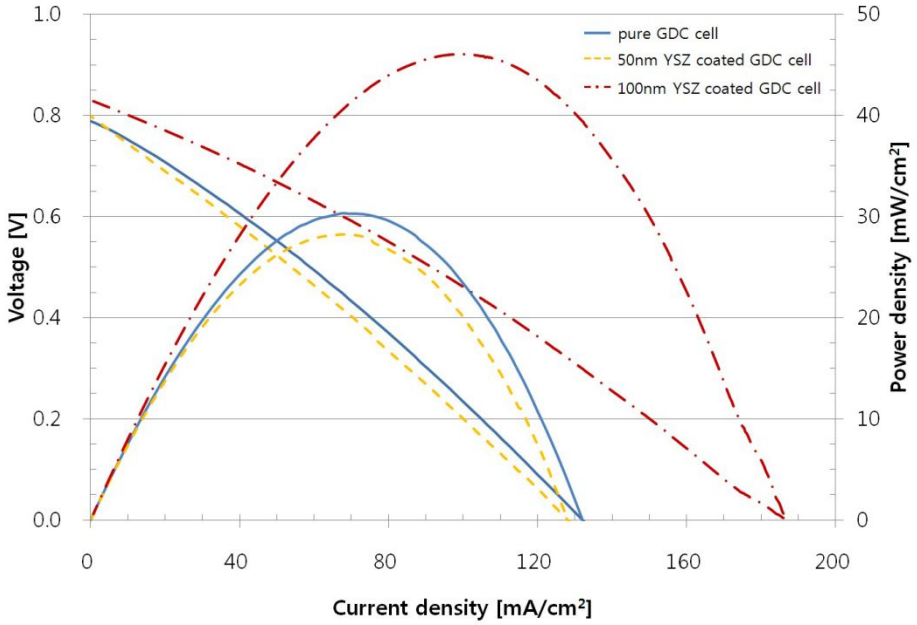

Figure 3.5 iV and power density curves at 600°C for the pure GDC cell, 50nm ALD-YSZ / GDC cell, and the 100nm ALD-YSZ / GDC cell

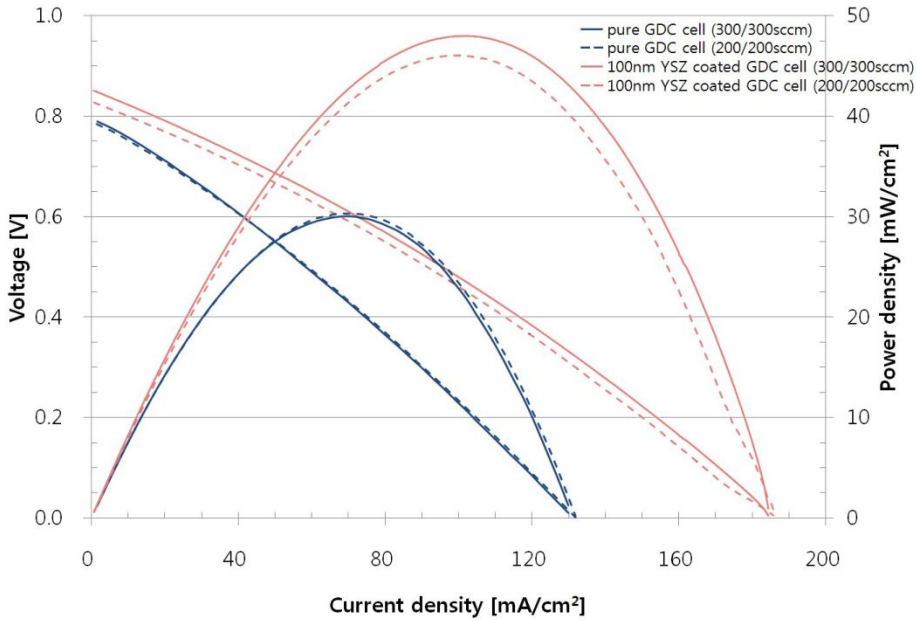

Figure 3.6 Comparison of the iV and power density at 600°C as the hydrogen and air feed rates increased from 200sccm to 300sccm

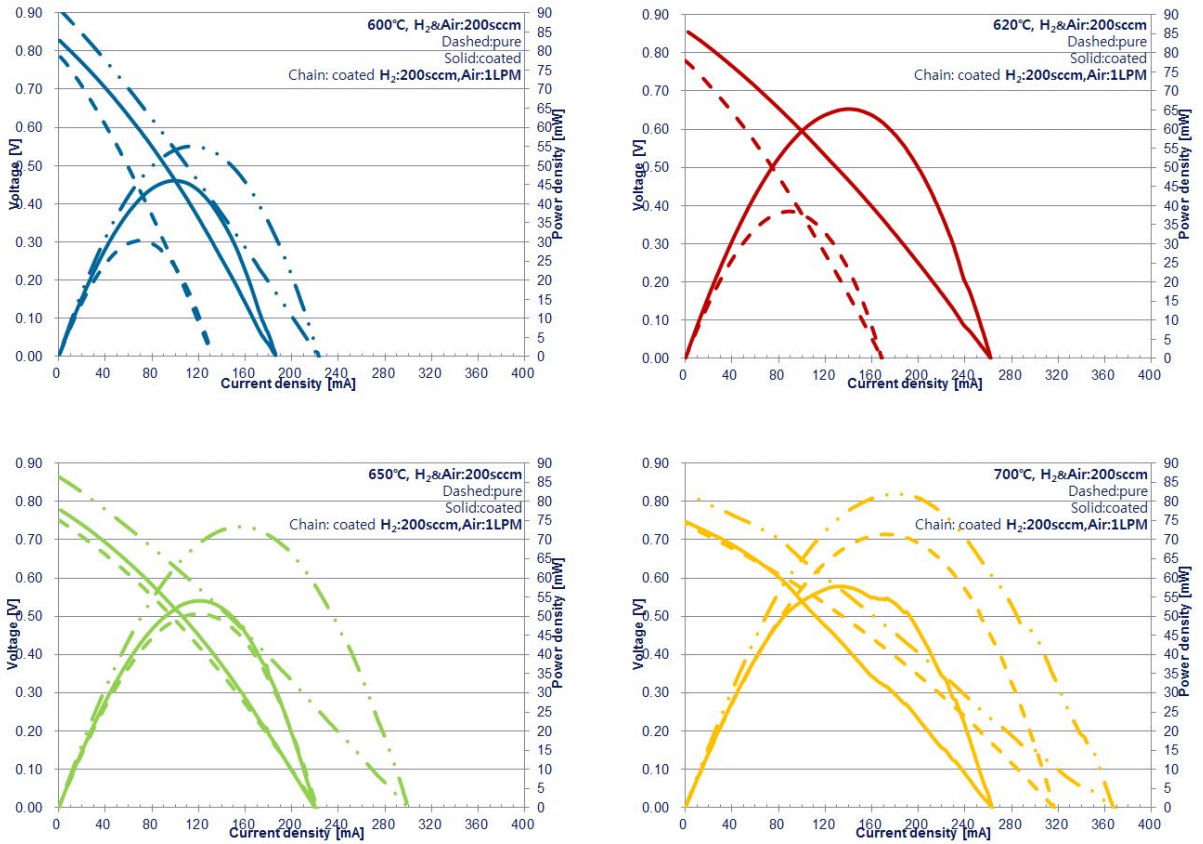

Figure 3.7 iV and power density comparisons at 600~700°C

3.1.4 EIS spectra results

We investigated the effect of the ALD-YSZ functional layer from measuring the electrochemical impedance of the same samples. The gentler slope of the I-V curve for the YSZ-coated cell indicates that its ohmic resistance was lower than pure GDC's. And this observation was confirmed from the EIS Nyquist spectra that were obtained in the frequency range of 2 ~ 106 Hz using the ac amplitude of 30 mV at OCV. In Figure 3.8 (a) the intercept value on real axis of the impedance spectra which means ohmic resistance of cells for the 690 cycles (100nm) ALD-YSZ coated cell was significantly lower than that of the uncoated cell. This was a very interesting result, but the result supports the opposite effect. In general situation, doped ceria exposed to low oxygen partial pressure has both ionic and electronic conductivity. So impedance data must show low ohmic resistance. In addition, because we made cells from pellets of identical thickness GDC, the coated cell which has low conductive YSZ layer must have slightly higher resistance. We thought the reason was that micro cracks were generated at ceria electrolyte near anode due to the long exposure to hydrogen gas so the contact resistance became higher. The enlarged left side half circle in Figure 3.8 (b) than the one in Figure 3.8 (a) that means activation loss of anodes, enabled us to have the same presumption.

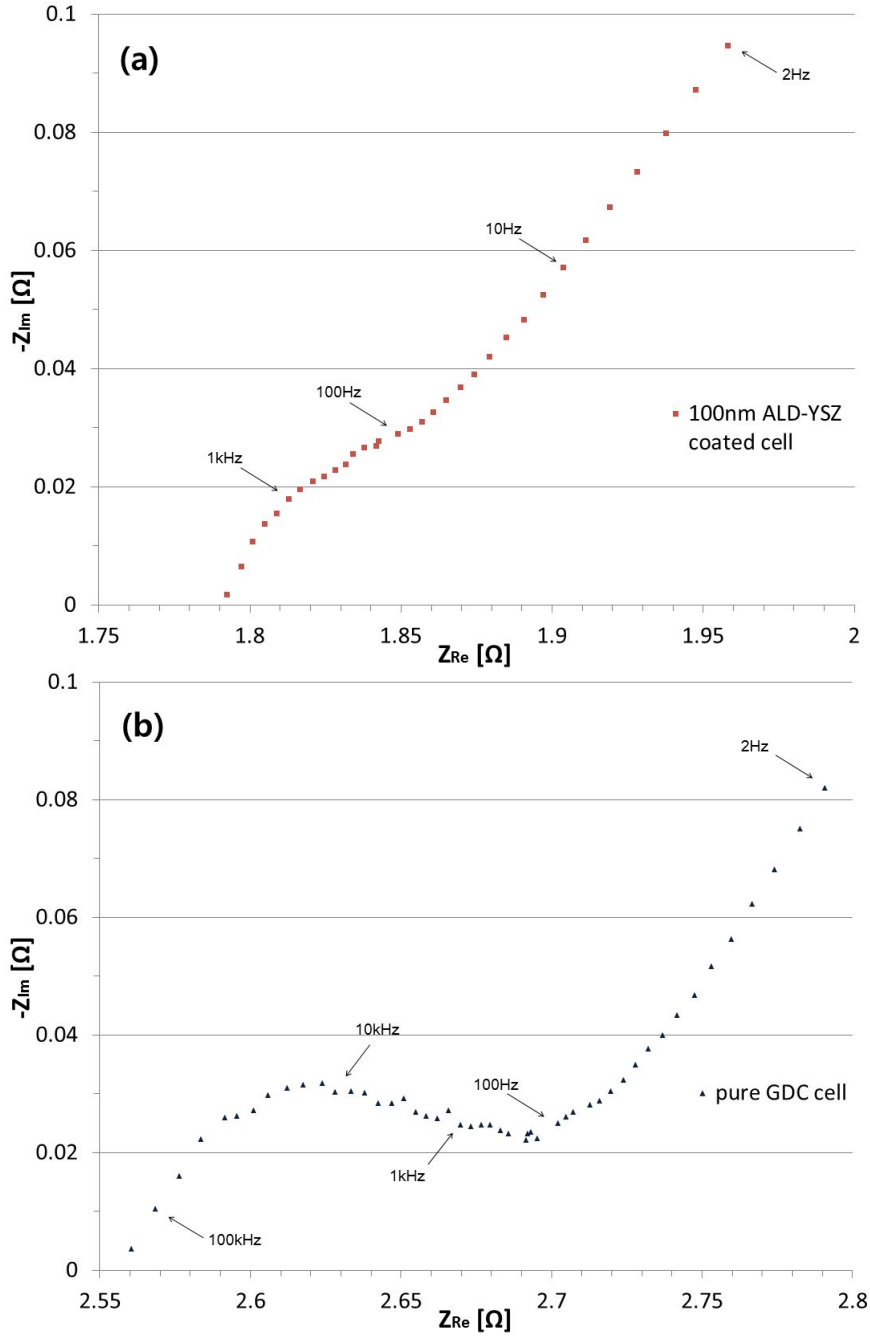

Figure 3.8 EIS Nyquist spectra at 600°C (a) for the 690 cycles (100nm) ALD-YSZ / GDC cell and (b) for the pure GDC cell

3.1.5 SEM results

So we compared the electrolytes before and after the operation. In Figure 3.9 (b) the pure GDC electrolyte cell sample after the operation for 3 days which was exposed to highly reductive hydrogen atmosphere, a lot of cracks were created on the surface regardless of the distance from grain boundary, and it showed relatively high roughness. From SEM images of the pure GDC electrolyte before the operation in Figure 3.9 (a) that did not showed any cracks, we could know this result was not from high temperature in the cell fabrication process. As shown above, these cracks were generated mainly due to internal stress. The local volume expansion of the surface due to the reduction of ceria would cause internal stress with the unreduced interior. [51],[52],[53],[54] In case of ALD-YSZ coated GDC before the operation in Figure 3.9 (c), the grain size and shape were similar to pure GDC case but the contrast of the SEM image fell down like PLD-YSZ case with same thickness due the coating effect. In Figure 3.9 (d), ALD-YSZ coated GDC after the operation for 3 days did not showed dramatic change in comparison to the case of pure GDC in Figure 3.9 (b). From the EIS and the surface observation results, in addition to its high electron insulation property ALD-YSZ thin layer seemed to suppress electron conductivity following disturbance of ceria reduction, so it could cause higher OCV for YSZ coated cells. Also ceria reduction without YSZ layer brought rough electrolyte surface and micro crack near the interface between anode and GDC

electrolyte, thus ohmic loss of pure GDC cells would increase due to the contact resistance and due to the narrow and longer oxygen ion path. (Figure 3.10)

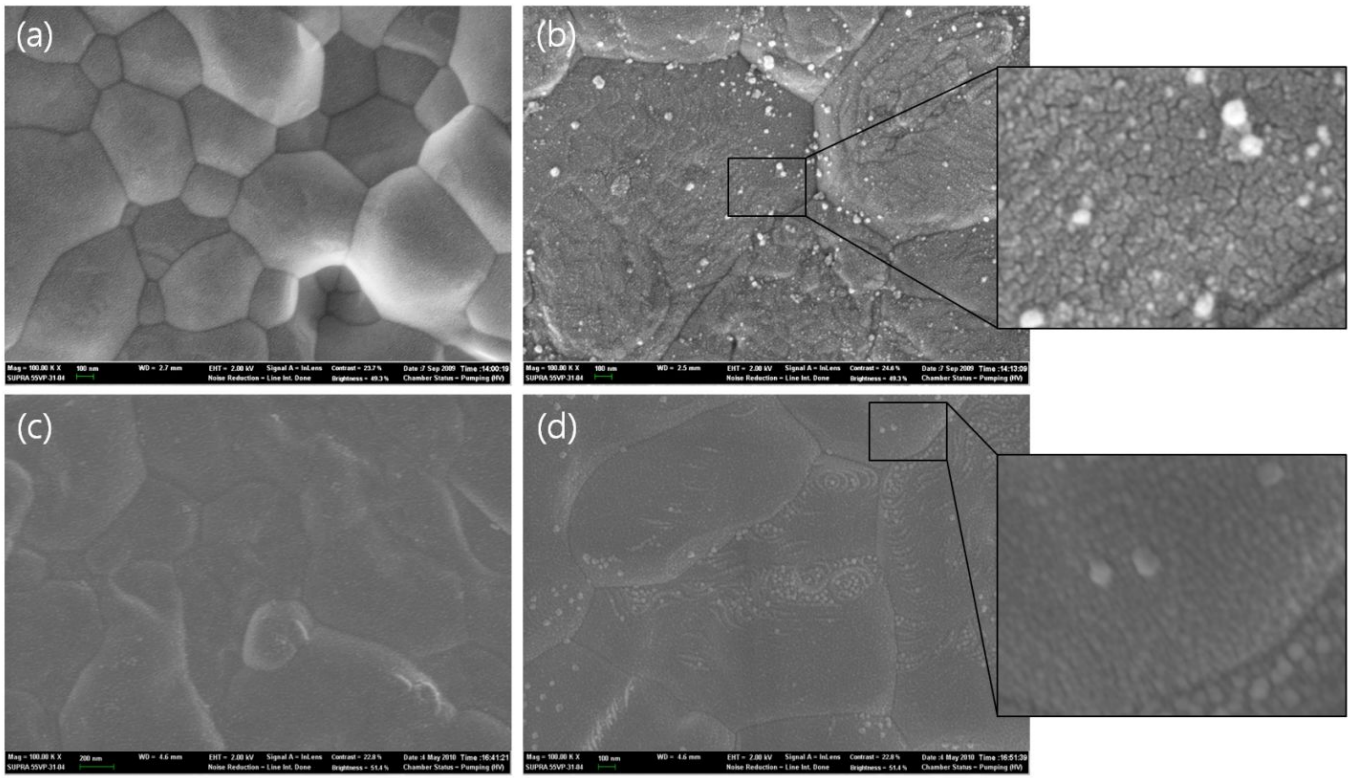

Figure 3.9 Comparison of SEM images of the pure GDC electrolytes and 690 cycles (100nm) ALD-YSZ / GDC electrolytes (a) pure GDC before the operation (after the electrodes sintering), (b) pure GDC after the 3 days operation, (c) ALD-YSZ / GDC before the operation (after the electrodes sintering), (d) ALD-YSZ / GDC after the 3 days operation

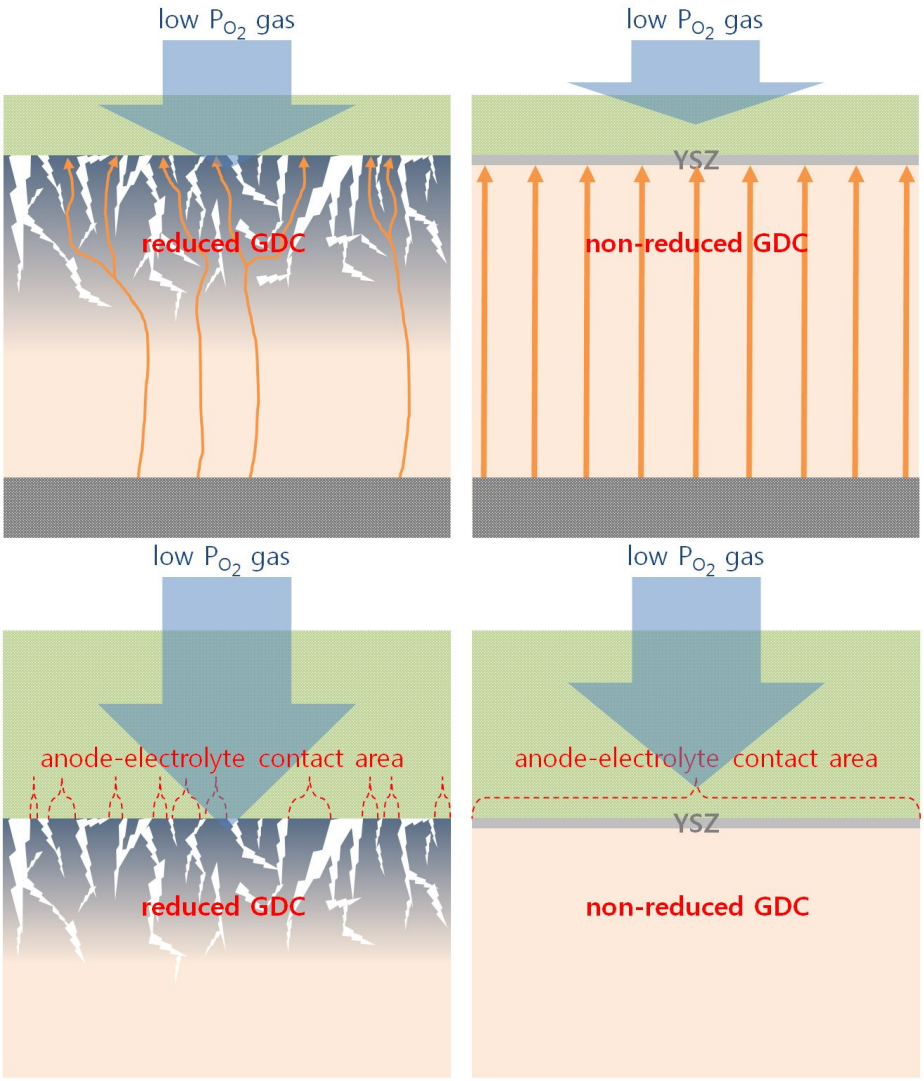

Figure 3.10 Schematics of (upper) the narrow and longer oxygen ion path and (lower) the contact resistance increase for the reduced pure GDC electrolyte cells

3.2 Stability of ALD-YSZ / GDC bi-layered electrolyte

3.2.1 Problems of previous cell experiments

We observed poor ohmic resistance with the pure GDC cell and under 1V OCV with the 100nm ALD-YSZ cell. We should know the exact origin and direct environment of contact resistance increase. And we needed to found out the thickness and compositional change of functional layer.

We planned experiments to know the hydrogen effect on GDC with and without YSZ functional layer. We intentionally exposed the GDC samples with various thickness YSZ functional layers to air and hydrogen. To conduct fair comparison we experimented not on the cell scale which included electrodes. We could find out the crack generation environment and thickness of functional layer to prevent cracks which can affect the ohmic resistance of cells.

Although ALD temperature condition was below 300°C, there could be a high temperature effect due to the electrodes sintering process at 1200°C and 1400°C. We doubted solid state diffusion between YSZ and GDC in sintering process. If it was possible, secondary phase could show low ion conductivity and high electron conductivity. [64],[65] We had to know the critical mixing temperature and mixing thickness according to various temperatures because they are directly connected to the cell fabrication process and to the reliability and the effectiveness of the functional YSZ layer.

3.2.2 Surface roughness observation results

Measuring roughness and observation the surface could let us know the generation of micro cracks. So we decided to use AFM (Atomic force microscopy, NANO Station II, Surface Imaging Systems, Inc.). We needed to prepare GDC samples with maximum polishing to notice the surface differences after the experiments. We compare the polishing results from two companies and we chose one (Stanford university Crystal shop, Figure 3.11 (b)). We deposited 0, 25, 50, 100nm YSZ via ALD on nano polished 350μm bulk GDC. Then we exposed samples to ambient temperature, 600°C air for 5 hours, 800°C air for 5 hours, 1200°C air for 5 hours, 1500°C air, 600°C H_2 for 5 hours, 600°C H_2 for 100 hours and 800°C H_2 for 5 hours. 600°C and 800°C were representative IT and highest limit of IT. 1200°C was cathode sintering temperature and 1500°C was GDC sintering temperature.

Roughness results were arranged in Table 3.1. Just elevating temperature had a little effect until 800°C. (Figure 3.12~3.14) But the clear grain boundaries were generated for pure GDC sample. For 50nm ALD-YSZ coated sample, YSZ layer seemed to melt and move to grain boundaries to minimize surface energy. 100nm ALD-YSZ coated sample showed melting effect only because of thicker YSZ layer. (Figure 3.15) At 1500°C dramatic grain growth and roughness increase were observed. With the XPS and these results, we confirmed YSZ and GDC entirely mixed. (Figure 3.16) The AFM results in air said that the cell fabrication temperature limit must exist between

800°C and 1200°C, thus wet ceramic process must be prohibited in electrodes fabrication for this structured cells. We could know that the origin of low OCV for 100nm ALD-YSZ coated GDC cell was the reduced YSZ thickness due to the high temperature sintering process.

Then we re-confirmed that the increase of surface roughness was mainly due to hydrogen gas and ALD-YSZ layer could suppress the roughness changing. In the case exposed to 600°C H_2 for 5 hours, 0 and 25nm YSZ coated samples showed roughness increase and changing of surface morphology. Although 50nm YSZ coated samples showed the figure near 4nm, it was due to a hole and dirt. (Figure 3.17) In the 100 hours case at 600°C H_2, all of roughness of the samples increased a lot but the gap of 50, 100nm YSZ coated sample was meaningless. (Figure 3.18) 0, 25 and 50nm YSZ coated samples that exposed to 800°C H_2 for 5 hours, showed severe morphological changes and high roughness values. (Figure 3.19)

The hydrogen exposure results said that in 600°C H_2 the surface stability of bi-layered structure was preserved from 50nm ALD-YSZ thickness. This result matched well with the unstable OCV results with 25nm PLD-YSZ coated 1μm GDC cells. [39] But in 800°C H_2, the protective thickness limit increased to 100nm.

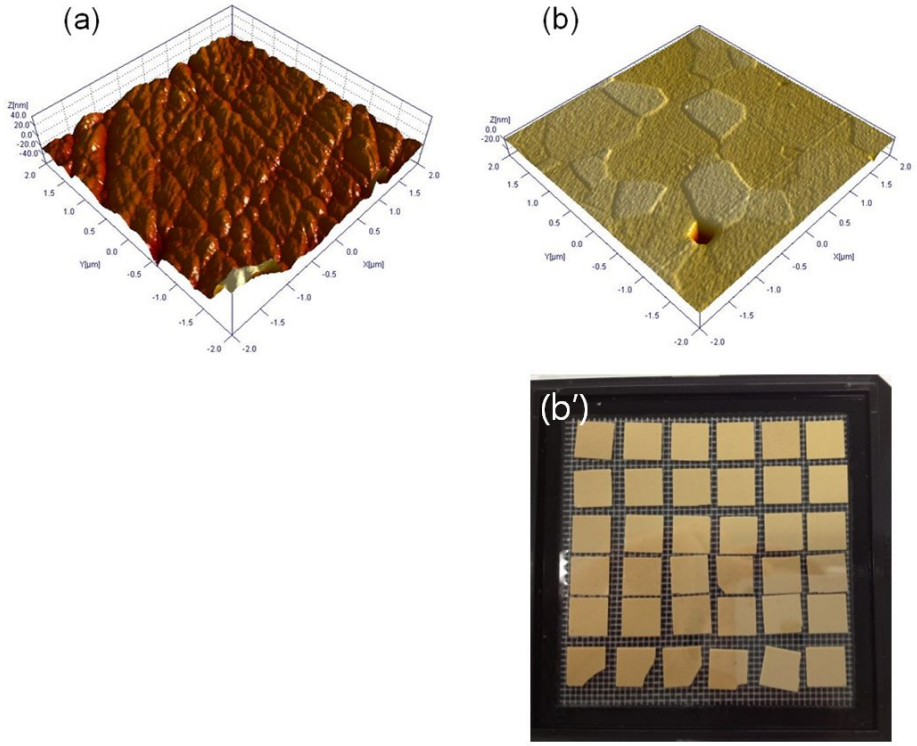

Figure 3.11 Roughness comparison of polished samples showing (a) 6.67nm (Alpha high tech. Inc., Korea) and (b) 1.90nm (Stanford university Crystal shop, US) RMS values

Table 3.1 Roughness results in air/hydrogen with various temperatures

YSZ / GDC		As Dep.	600°C Air 5h	800°C Air 5h	1200°C Air 5h	1500°C Air 5h	600°C H_2 5h	600°C H_2 100h	800°C H_2 5h
		roughness (nm)							
pure GDC	0nm / 350μm	1.90	1.24	3.84	2.92	79.0	5.50	5.94	5.58
YSZ-ALD / GDC	25nm / 350μm	1.59	4.24	4.76	-	73.7	3.34	5.55	5.98
	50nm / 350μm	1.45	1.80	1.87	2.43	108	4.08	2.11	4.62
	100nm / 350μm	1.04	1.05	1.11	3.46	88.7	1.16	2.22	1.47

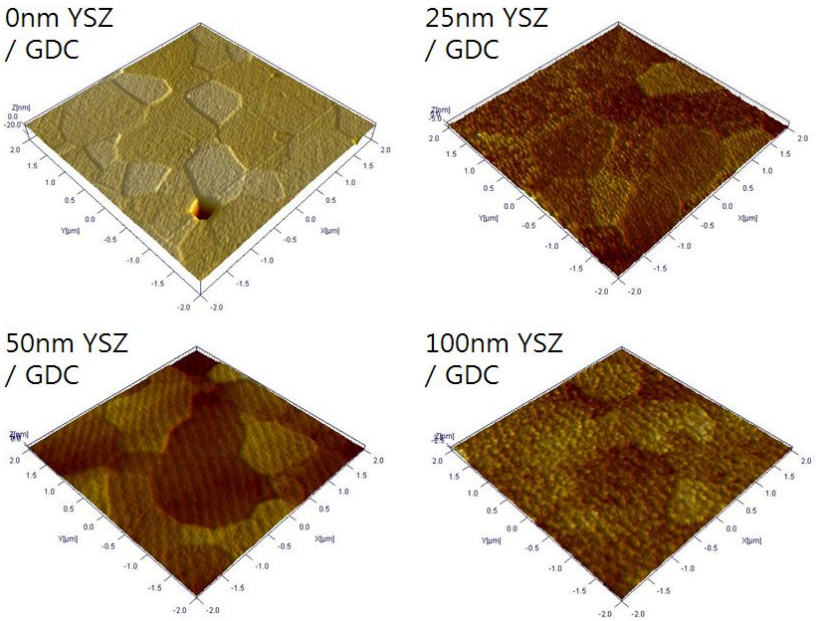

Figure 3.12 YSZ/GDC samples at ambient air (x:y:z=1:1:10)

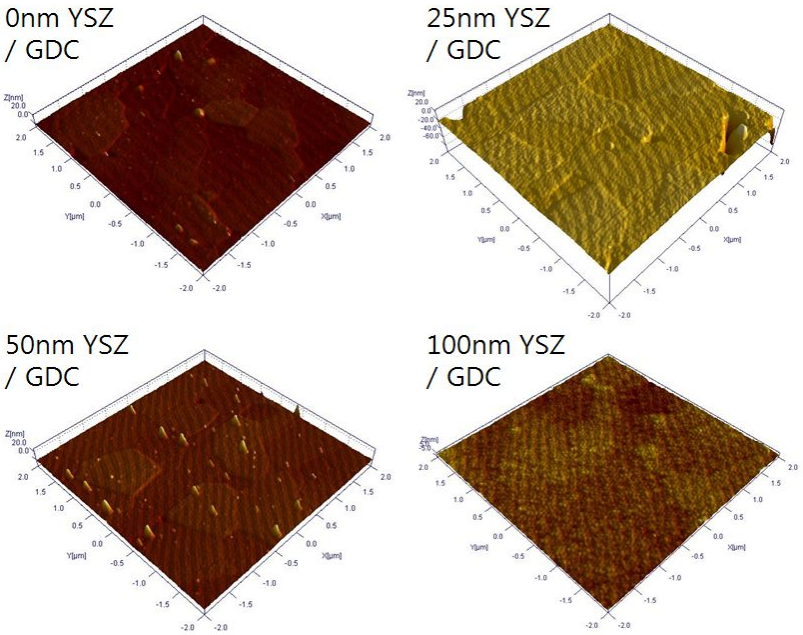

Figure 3.13 YSZ/GDC samples at 600°C air for 5 hours (x:y:z=1:1:10)

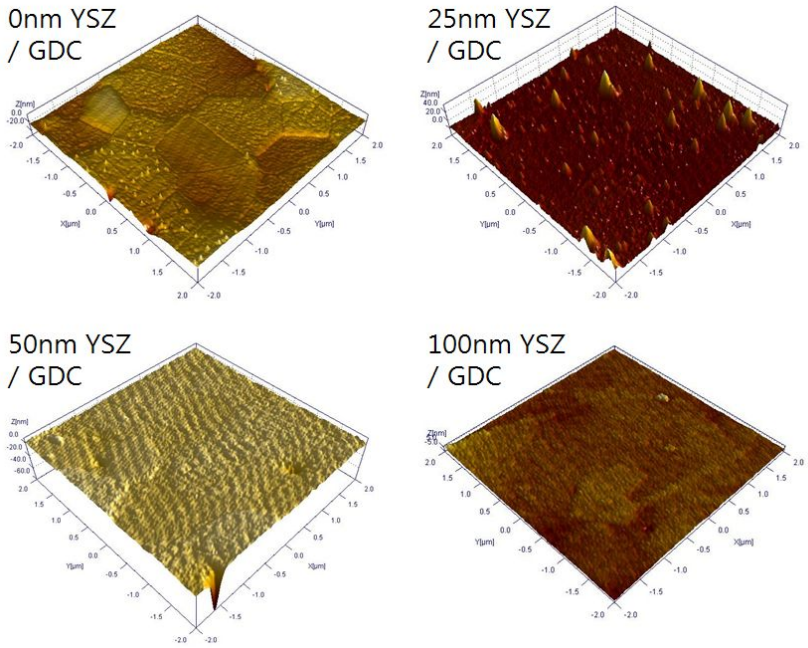

Figure 3.14 YSZ/GDC samples at 800°C air for 5 hours (x:y:z=1:1:10)

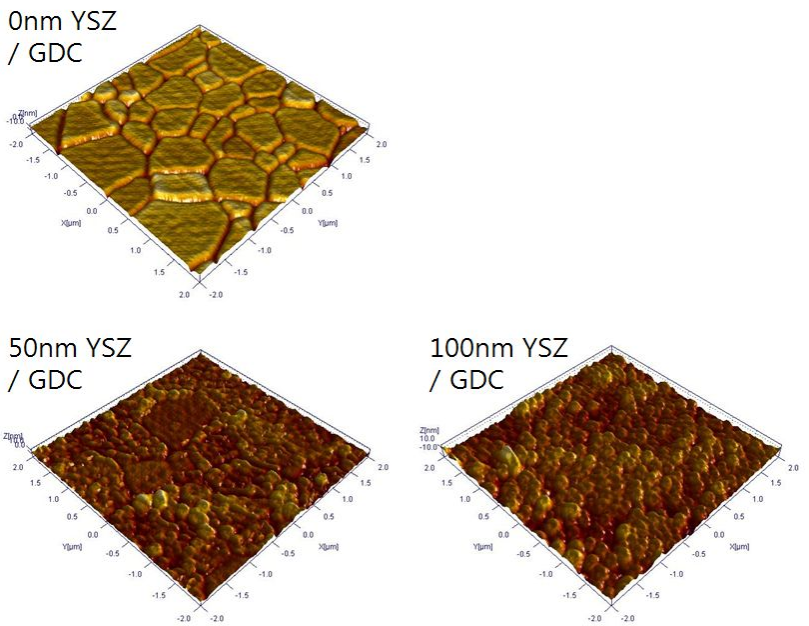

Figure 3.15 YSZ/GDC samples at 1200°C air for 5 hours (x:y:z=1:1:10)

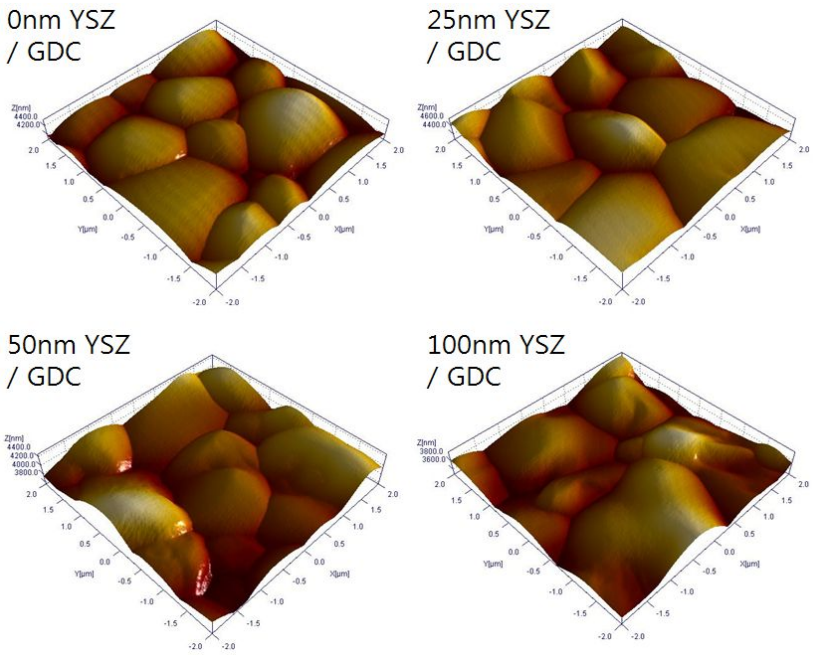

Figure 3.16 YSZ/GDC samples at 1500°C air for 5 hours (x:y:z=1:1:1)

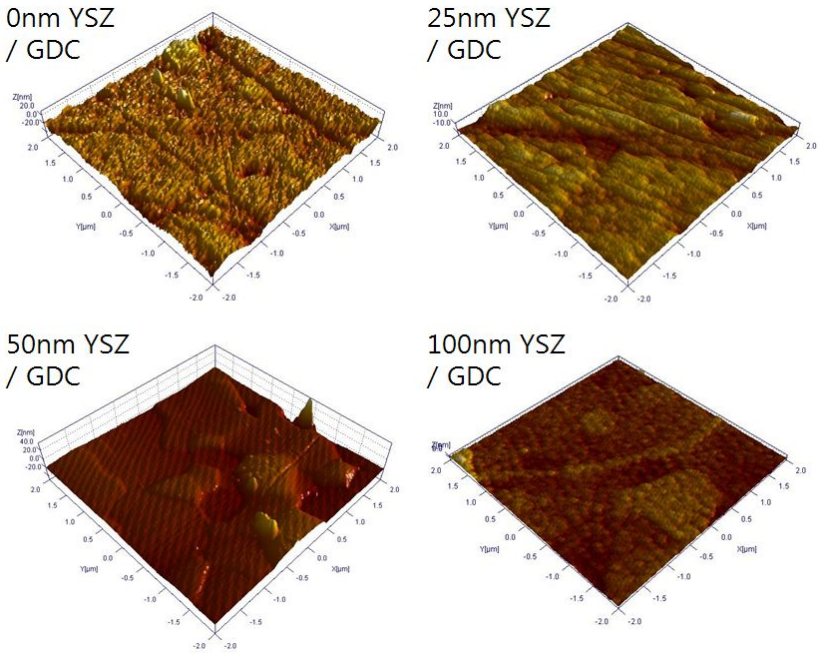

Figure 3.17 YSZ/GDC samples at 600°C H_2 for 5 hours (x:y:z=1:1:10)

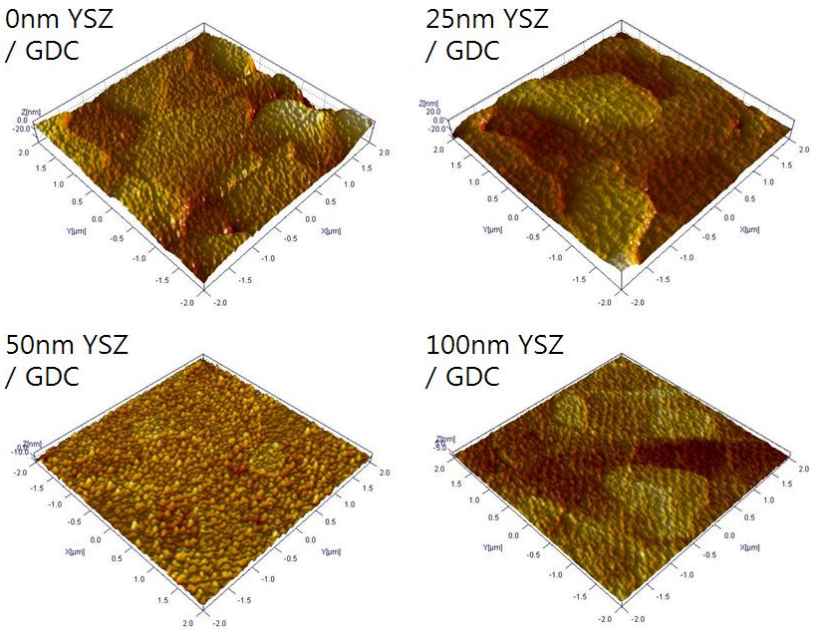

Figure 3.18 YSZ/GDC samples at 600°C H_2 for 100 hours (x:y:z=1:1:10)

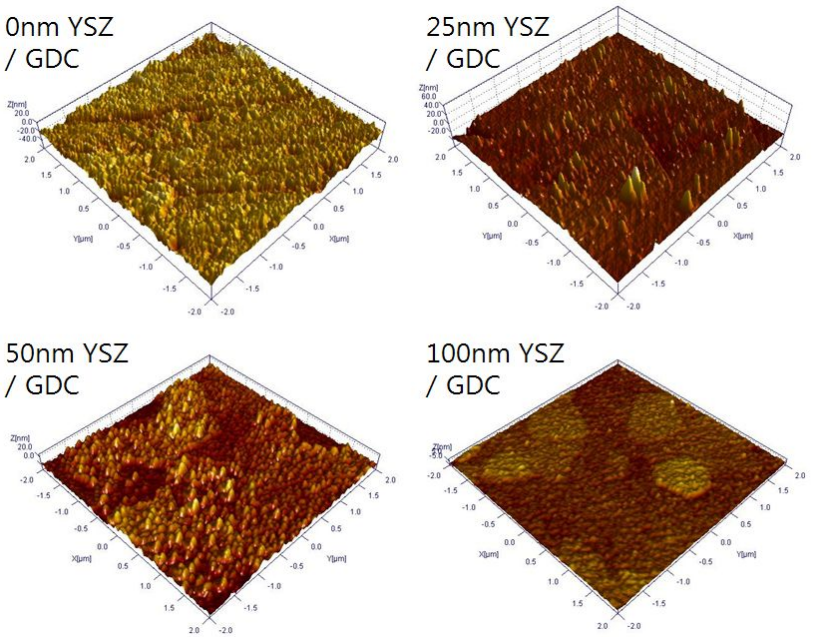

Figure 3.19 YSZ/GDC samples at 800°C H_2 for 5 hours (x:y:z=1:1:10)

3.2.3 YSZ/GDC mixing phenomenon results

There was another reason to polish GDC samples as smooth as possible. In the depth profile characterization process, a rough surface in Figure 3.20 (b) can create an illusion that the film and the substrate are mixed like Figure 3.20 (a). If the deposited layer exists in film shape on smooth substrate, we can get the depth profile in Figure 3.20 (c).

We got the XPS depth profile results from 50nm ALD-YSZ coated GDC samples exposed to ambient, 800°C, 1200°C and 1500°C air. As shown in Figure 3.21 (a) and (b), for as-deposited and 800°C samples we cannot find the components of GDC on the surfaces. But at 1200°C, there was Ce and Gd on the surface and they increased gradually with the depth. Naturally Zr and Y decreased. (Figure 3.21 (c)) Finally, the temperature of 1500°C made bi-layer entirely mixed and YSZ diffused over 200nm depth with flat composition ratio. (Figure 3.21 (d)). This trend with thin film was shown by X.D. Zhou et al. with 50:50 GDC/YSZ mixed powder. They found out the XRD peak shift that means the reaction of YSZ and GDC. [65]

Like the AFM results, these XPS results said the fabrication temperature limit would be between 800°C and 1200°C for YSZ/GDC bi-layered electrolyte SOFC again.

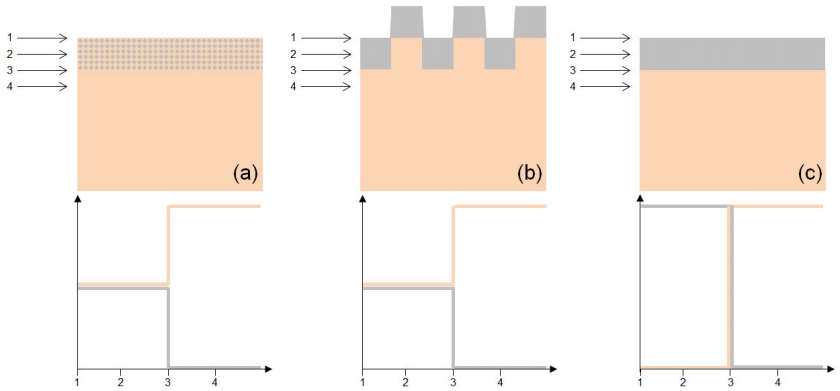

Figure 3.20 XPS depth profile results from different roughness and mixed material

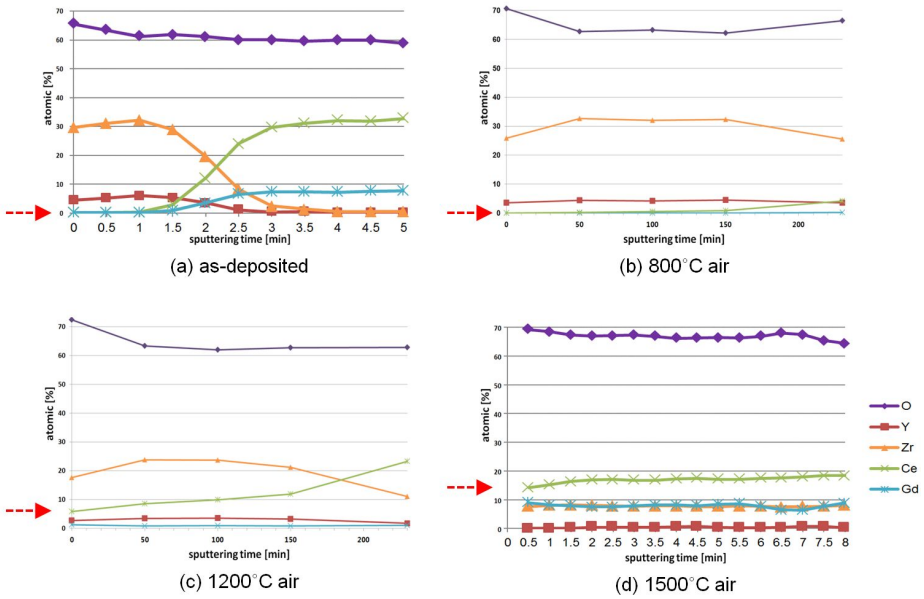

Figure 3.21 XPS depth profiles of 50nm ALD-YSZ / GDC bi-layered samples exposed to (a) embient, (b) 800°C, (c) 1200°C and (d) 1500°C air

3.3 Characterization results of PLD-YSZ cells

3.3.1 PLD-YSZ cell fabrication

To compare ALD with other thin film deposition method, we fabricated PLD-YSZ/GDC bi-layered electrolyte cells. PLD is representative PVD method so we can compare the functionality with ALD which is a kind of CVD. The differences were the Pt electrodes via sputtering, sintering bulk GDC from the powder and squared cell shape.

The fabrication process of bi-layered electrolyte supported cell via PLD follows this. We prepare GDC10 powder from NexTech Materials, Ltd. Press molding and CIP (Cold Isostatic Press) process at 2000bar followed powder preparation. We sintered compressed GDC pellet at 1500°C for 5h. Cutting, grinding and polishing made 500~1000μm thick and 2cm X 2cm GDC electrolyte pellet. Then PLD-YSZ on one side was conducted. The deposition condition at 400°C, and P_{O_2amb}=50mTorr. KrF excimer laser (λ=248nm, Complex Pro 201F, Coherent Inc.) was used as an ablation source. (laser fluence=3J/cm^2, laser frequency=5Hz, target-substrate (T-S) distance=5cm) Target was 8YSZ (TZ-8Y, Tosoh) and sintered at 1400°C for 3h. 6minutes were took to deposit 100nm YSZ, and 12 minutes were took to deposit 200nm YSZ. Pt sputtering on both sides of electrolyte completed the

fabrication process. Sputtering condition was 60mTorr Ar partial pressure, ambient temperature, 200W DC power and T-S distance=10cm.

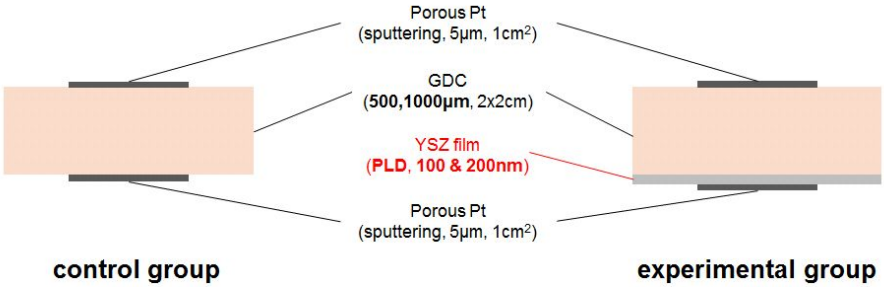

Figure 3.22 Schematics of pure GDC cell and PLD-YSZ cell

Table 3.2 PLD-YSZ conditions

	Conditions	
Substrate temp.	400°C	
P_{O2}	50mTorr	
Laser fluence	3J/cm²	
Laser frequency	5Hz	
T-S distance	5cm	
Deposition time	100nm	200nm
	6min	12min

Table 3.3 Porous Pt electrodes sputtering conditions

	Conditions
Substrate temp.	Room temp.
P_{Ar}	50mTorr
DC power	200W
T-S distance	8cm

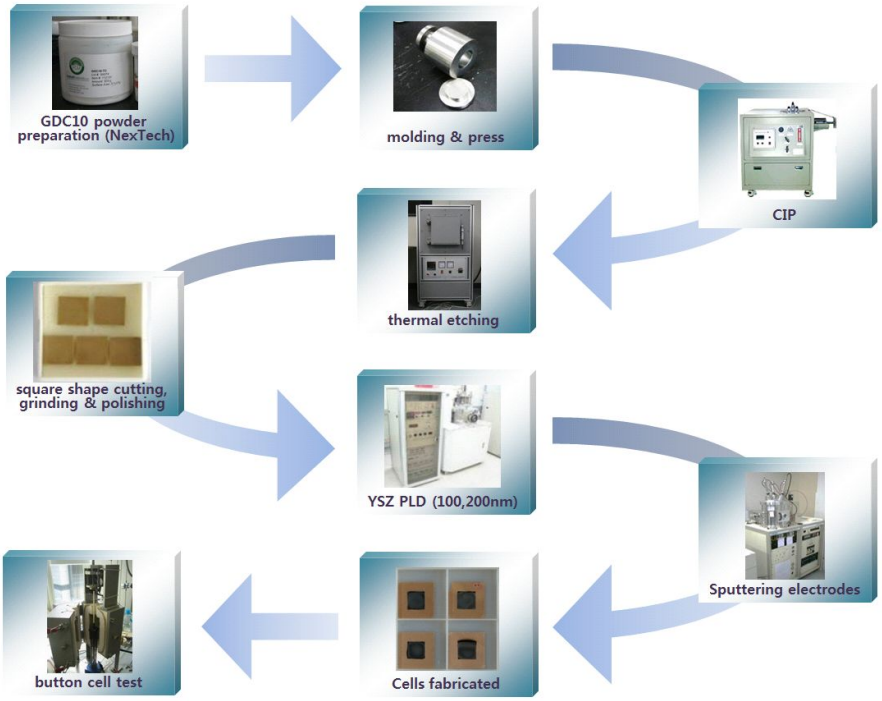

Figure 3.23 Fabrication flow of PLD-YSZ / GDC bi-layered electrolyte cells

3.3.2 iV and OCV results

Like the ALD-YSZ case, we also took the FIB-SEM images. We could ascertain that the layer shape 100 and 200nm PLD-YSZ, too. And in left picture in Figure 3.24 porous Pt was deposited in columnar shape. Figure 3.25 shows 50000 times magnified plane view of 100nm PLD-YSZ on GDC.

First we characterized 1mm cells. For the cells with the 1mm GDC thickness, 100nm PLD-YSZ coated cell in Figure 3.26 showed slightly higher OCV by 50mV gap than pure GDC cell for 10 hours with 100% H_2 at 600°C. But differ to 500μm pure GDC cell case, there was no dramatic OCV drop for 1mm pure GDC cell and OCV was higher although 500μm pure GDC cell experiment was conducted with 5% H_2. We thought that in the thickness of 1mm electron conductivity was limited by GDC itself and that 100nm PLD-YSZ layer had a little effect.

With the same 1mm GDC, iV curve and power density data at 650°C for 100nm PLD-YSZ cell could showed very small enhancement. (Figure 3.27) PLD coated cell in red showed more gentler slope only. So we concluded 100nm PLD-YSZ functioned as a GDC cracking preventer which could maintains contact resistance not as an electron insulator.

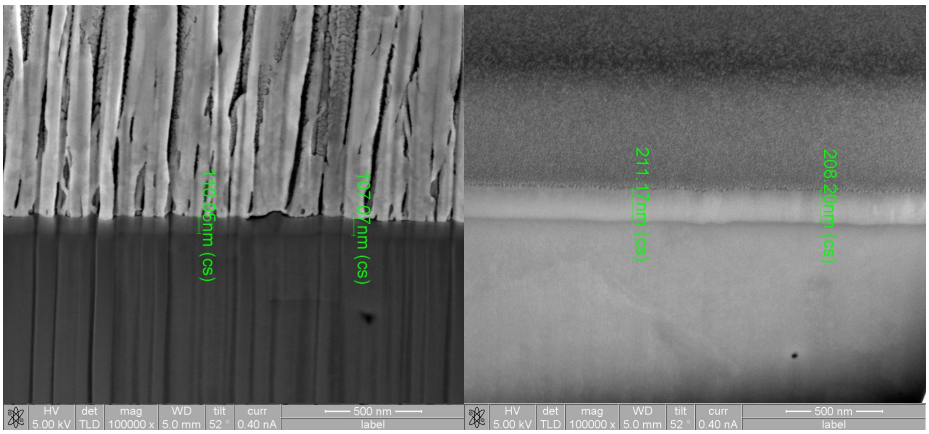

Figure 3.24 FIB-SEM cross section images of 100, 200nm PLD-YSZ layer after electrodes sputtering

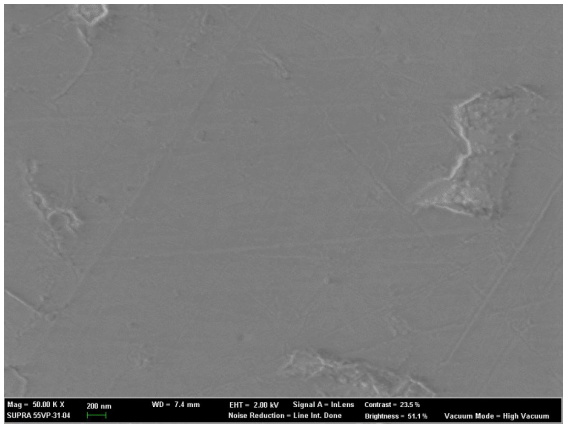

Figure 3.25 SEM plane view of 100nm PLD-YSZ layer on bulk GDC

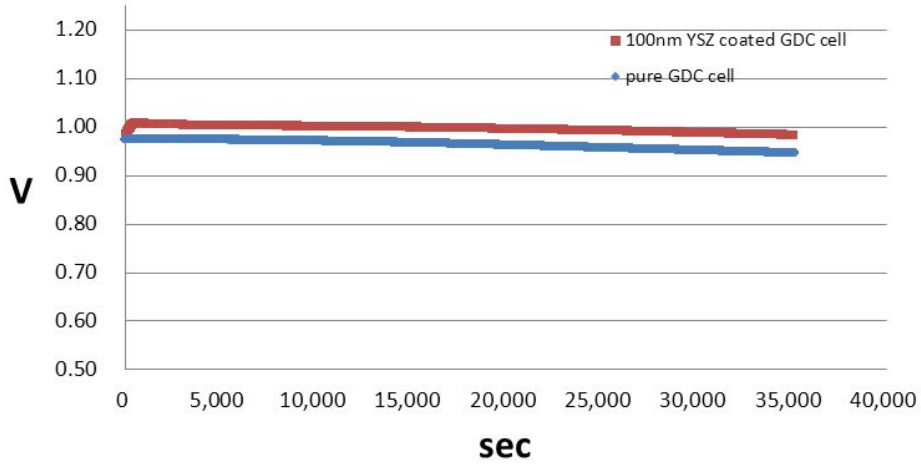

Figure 3.26 OCV transitions of 1000µm GDC cells with and without 100nm PLD-YSZ layer at 100% H_2, 600°C

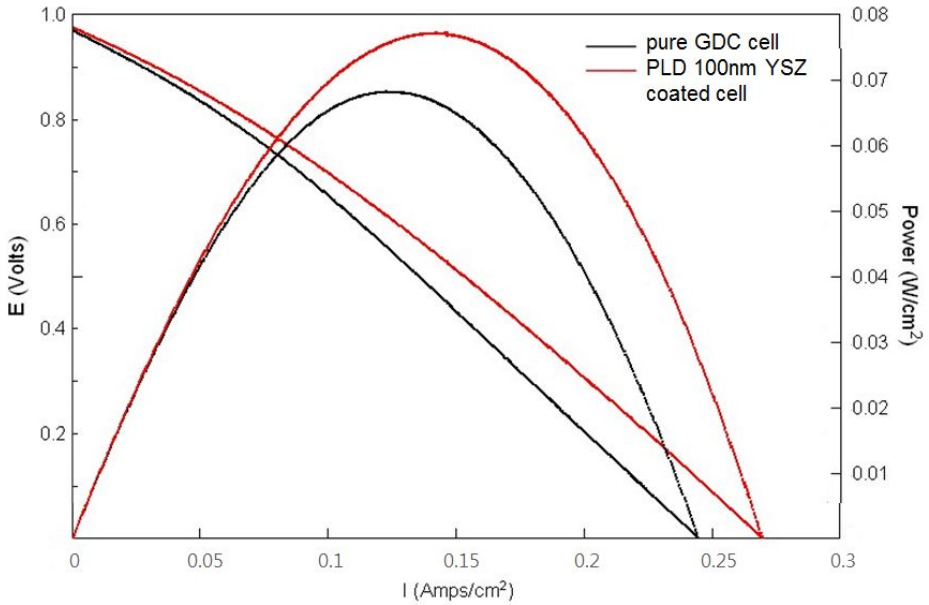

Figure 3.27 iV & power density curve comparisons of 1000µm GDC cells with and without 100nm PLD-YSZ layer at 100% H_2, 600°C

For 12.5 hours with the 500μm GDC thickness cells at 600°C OCV transition results were shown in Figure 3.28 200nm PLD-YSZ coated cell showed 0.89V~0.88V where pure GDC cell showed 0.81V~0.72V. Interestingly 100nm PLD-YSZ coated cell result (0.80V~0.66V) was little below pure GDC's. In all cases gradual drops were observed like ALD cases with 100% H_2. From these results, we found out that 200nm PLD-YSZ layer did the function we expected but it needed some more thickness due to the result under 1V and that 100nm PLD-YSZ layer thickness was meaningless like the ALD-YSZ case.

For the long term results in Figure 3.29, the black line of 200nm PLD-YSZ coated GDC cell showed gentler OCV drop than pure GDC cell for more than 2 days and. this result was similar to 100nm ALD-YSZ cell case, too.

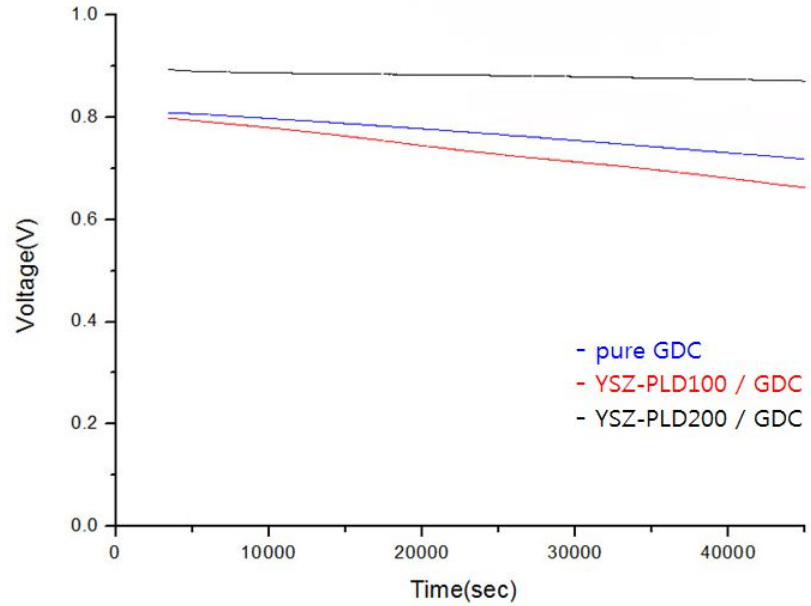

Figure 3.28 OCV transitions of 500μm GDC cells with 0, 100 and 200nm PLD-YSZ layer at 100% H_2, 600°C (12.5 hours)

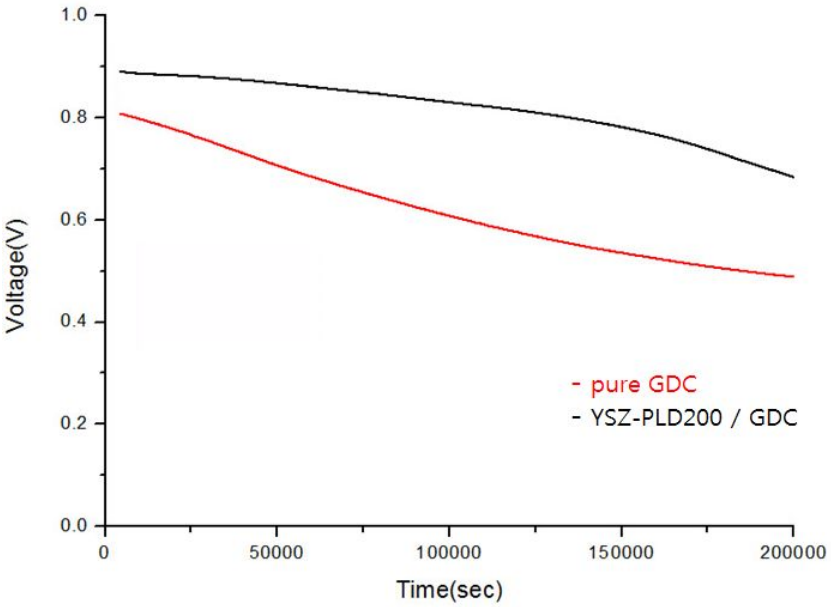

Figure 3.29 OCV transitions of 500μm GDC cells with 0 and 200nm PLD-YSZ layer at 100% H_2, 600°C (over 2 days)

With these transition graphs, we found out that the effect of ALD-YSZ layer started from 100nm where the effect of PLD-YSZ layer started from 200nm. The deposition unit of ALD is atom but the one of PLD is cluster. So the growth rate of PLD is faster but ALD has the ability of a high density with fine roughness film. Figure 3.30 shows the comparison of YSZ films from PLD and ALD methods. The voids in the TEM image of PLD-YSZ can cause the permeation of hydrogen gas to the middle of YSZ film. [66] It means the effective thickness of PLD-YSZ layer reduced to the depth of voids that can affect GDC reducing and voltage drop. But we thought relatively dense and good step covered ALD-YSZ layer blocked the hydrogen on the surface. [67] And the effective ALD-YSZ thickness was similar as the real thickness. Thus, we speculate the effective thickness of 200nm PLD-YSZ layer and 100nm ALD-YSZ layer was similar.

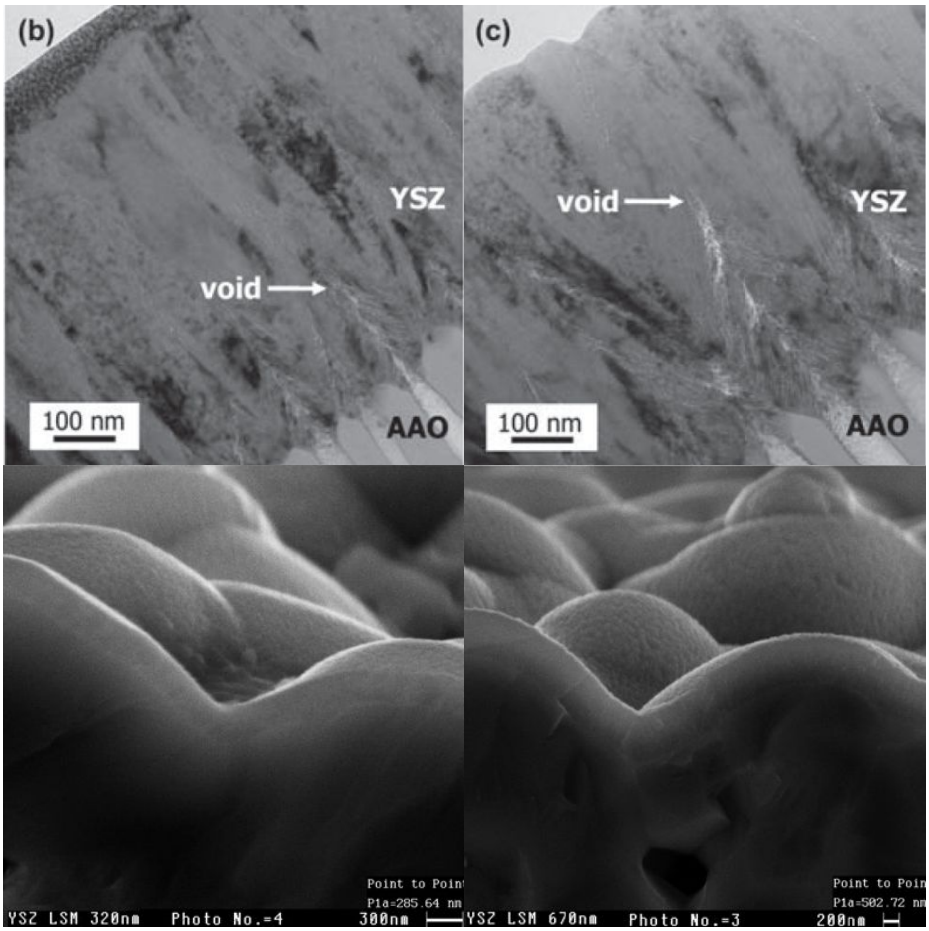

Figure 3.30 Comparison of YSZ films from (upper) PLD [66] and (lower) ALD [67] methods

We conducted a case study for the comparison of PLD and ALD for other zirconia based material (yttria doped barium zirconate, BYZ) as an electrolyte of SOFC application. [68] From the AFM images in Figure 3.31, as-deposited (400°C) PLD-BYZ showed loosely packed grain and 2.0nm roughness, where as-deposited (250°C) ALD-BYZ showed close-packed grain and 0.97nm roughness. For ALD-BYZ case, 2.0nm roughness can be achieved after the annealing process at 600°C. This can show more possibility of voids generation for PLD case. With the XRD analysis PLD-BYZ showed further crystalized structure (Figure 3.32) but the layer was more brittle than ALD-BYZ case. At this point, we found out another weakness of PLD that has more chance to crack in the process of temperature elevation or hydrogen contact. Even if a micro crack of YSZ functional layer generates, the possibility to contact with GDC or to reduce the effective YSZ thickness can rise. Thus we could conclude that an ALD-YSZ for functional layer could be advantageous than PLD-YSZ case.

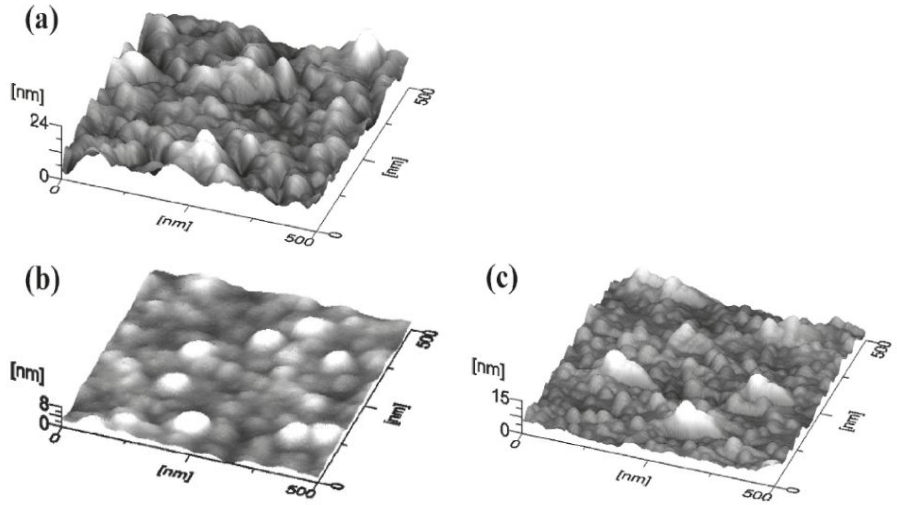

Figure 3.31 AFM images of (a) as-deposited (400°C) PLD-BYZ. (b) as-deposited (250°C) ALD-BYZ, (c) annealed (600°C) ALD-BYZ [68]

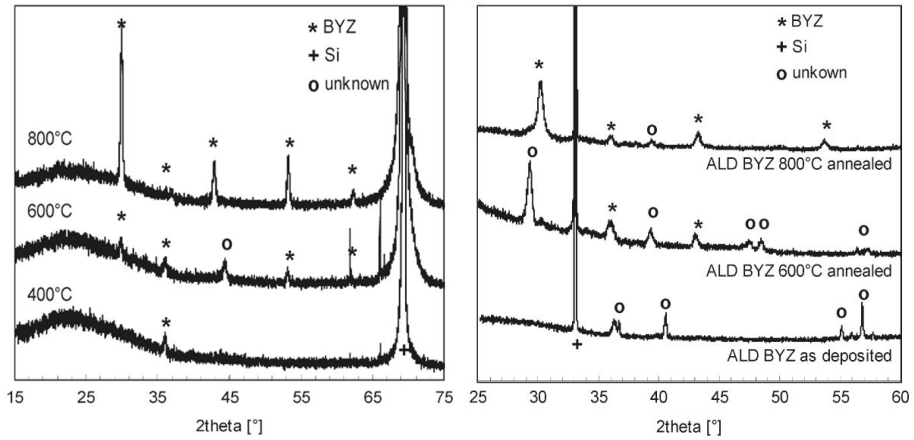

Figure 3.32 XRD graphs for (left) PLD-BYZ layer and (right) ALD-BYZ layer [68]

3.4 A free-standing thin film SOFC

3.4.1 Thin film μSOFC research status

Differ to previous bulk scale SOFC, lowering operation temperature via thin film deposition technique has been tried by a lot of research organizations. They used many deposition methods and cell structures to realize LT or IT operation maintaining the performance. Figure 3.33 shows the representative pictures of them. For most of high performance cells, their scale remained μm level. So enlargement step is actively studied.

Not only overall thin film SOFCs but also YSZ/GDC bi-layered thin film SOFC researches are reported. Huang et al. (Stanford University) sputtered 50nm GDC film on the cathode side on 50nm YSZ film. They improved the cell performance from 130mW/cm^2 to 200mW/cm^2 at 350°C. (Figure 3.34) [69] Myung et al. (Korea Institute of Science and Technology, KIST) fabricated tape-casted anode substrate with nano-structured anode functional layer using PLD. On this anode, 25nm~200nm PLD-YSZ layer and 1μm GDC-PLD layer was deposited. Without the YSZ blocking layer the OCV was about 0.6V where the OCV value was over 1V with YSZ blocking layer. And power density increased from 377mW/cm^2 to over 1W/cm^2 at 600°C. (Figure 3.35) [39]

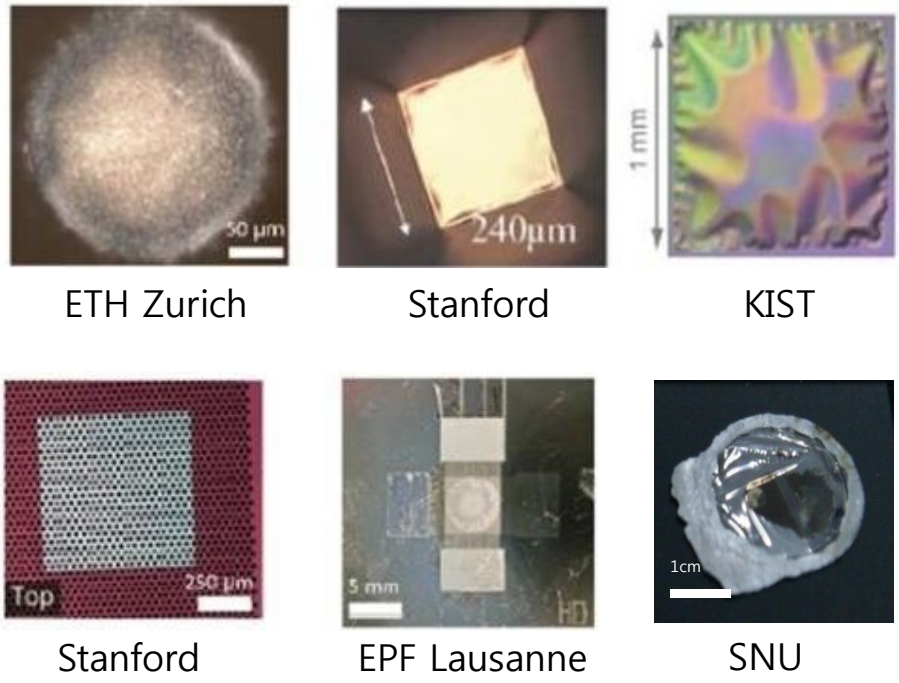

Figure 3.33 Examples of thin film SOFCs

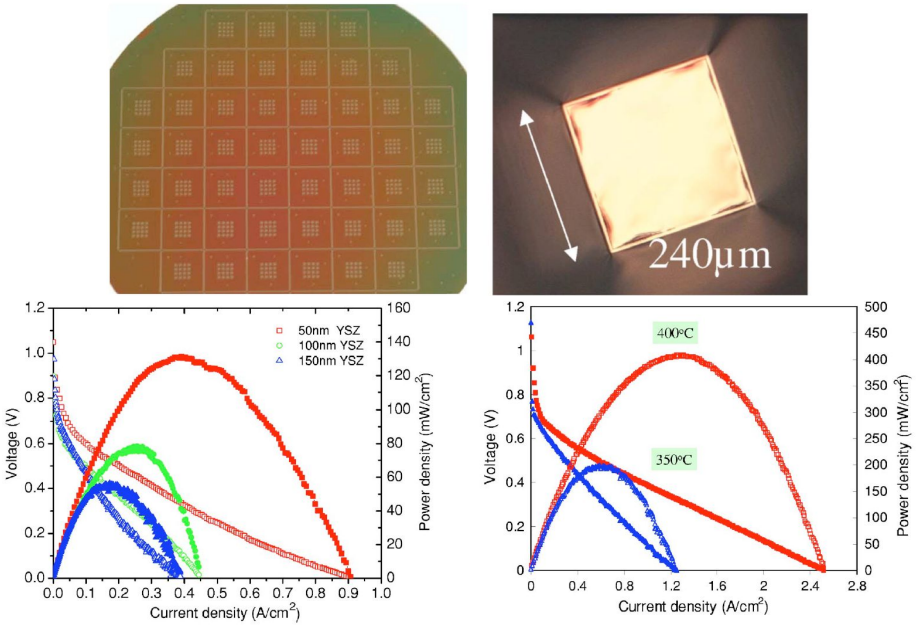

Figure 3.34 YSZ/GDC bi-layered thin film cell and performance data (Stanford University) [69]

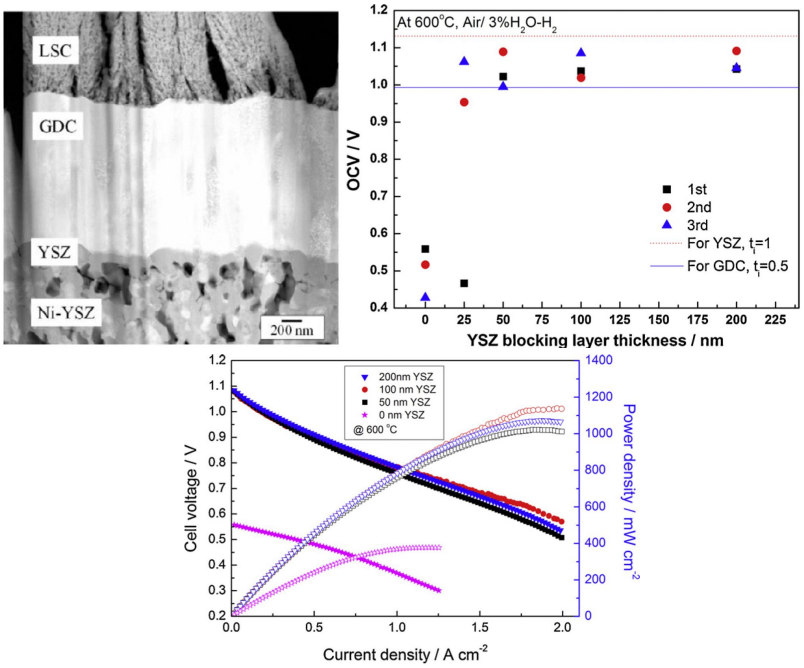

Figure 3.35 YSZ/GDC bi-layered thin film cell and performance data (KIST) [39]

3.4.2 Bi-layered thin film μSOFC fabrication

We decided to fabricate free-standing thin film YSZ-GDC bi-layered SOFC on Anodic Aluminum Oxide (AAO) substrate. Its porous (80nm pore) and columnar structure (100μm thickness) enabled easy gas permeability. Dense Pt anode deposited on AAO produced TPB lengths for electrochemical reaction and had a 10nm RMS value. After the dense Pt (anode) deposition on AAO, 60nm YSZ layer was deposited on the Pt via ALD. Then 400nm GDC layer and porous Pt were sputtered. The cell schematic is shown in Figure 3.36.

The critical points of cell fabrication were ALD-YSZ and GDC sputtering. We deposited materials in various environments and characterized them to select best conditions.

The ALD conditions were listed below Table 3.4. The carrier gas type ALD's stage temperature was set to 250°C with the chamber base pressure at 22mTorr. zirconium and yttrium precursor was heated to 40°C and 180°C respectively. Oxygen was used as an oxidant at 25°C. Although about 14% carbon contamination was detected, (Table 3.5) we deposited about 7% yttria doped zirconia layer with the cycle ratio of 7:1. The growth rates of zirconia, yttria and YSZ on Si wafer were about 0.1nm/cycle but it was lowered to 0.04nm/cycle on the Pt electrode so we conducted 1500 cycles of deposition for 60nm. (Figure 3.38)

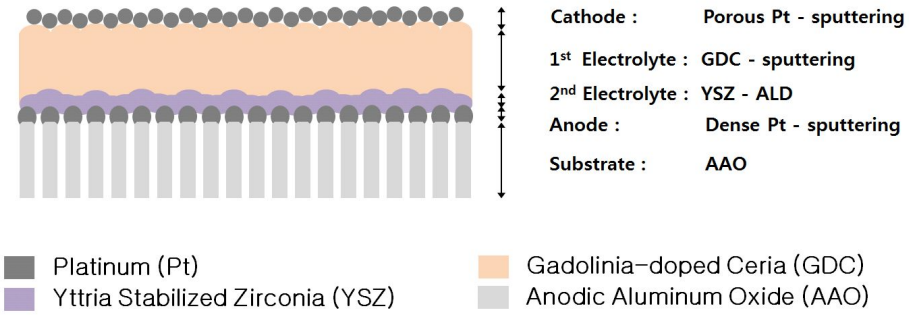

Figure 3.36 Schematics of AAO supported ALD-YSZ / sputtered GDC bi-layered electrolyte thin film SOFC

Table 3.4 ALD-YSZ conditions (carrier gas type)

	ZrO_2	Y_2O_3
Precursor	$Zr(NMe_2)_4$ @ 40°C	$Y(MeCp)_3$ @ 180°C
Flow Type	carrier gas	
Oxidant	oxygen (25°C)	
Stage Temperature	250°C	
Chamber Base Pressure	22mTorr	
Cycle ratio	Pulse / Purge: Zr Pulse (3s), O_2 Pulse (1s), Ar Purge (20s), Ar Purge (10s) — 7 times	Pulse / Purge: Zr Pulse (3s), O_2 Pulse (1s), Ar Purge (20s), Ar Purge (10s) — 1 time
Purity	14% carbon contaminant	

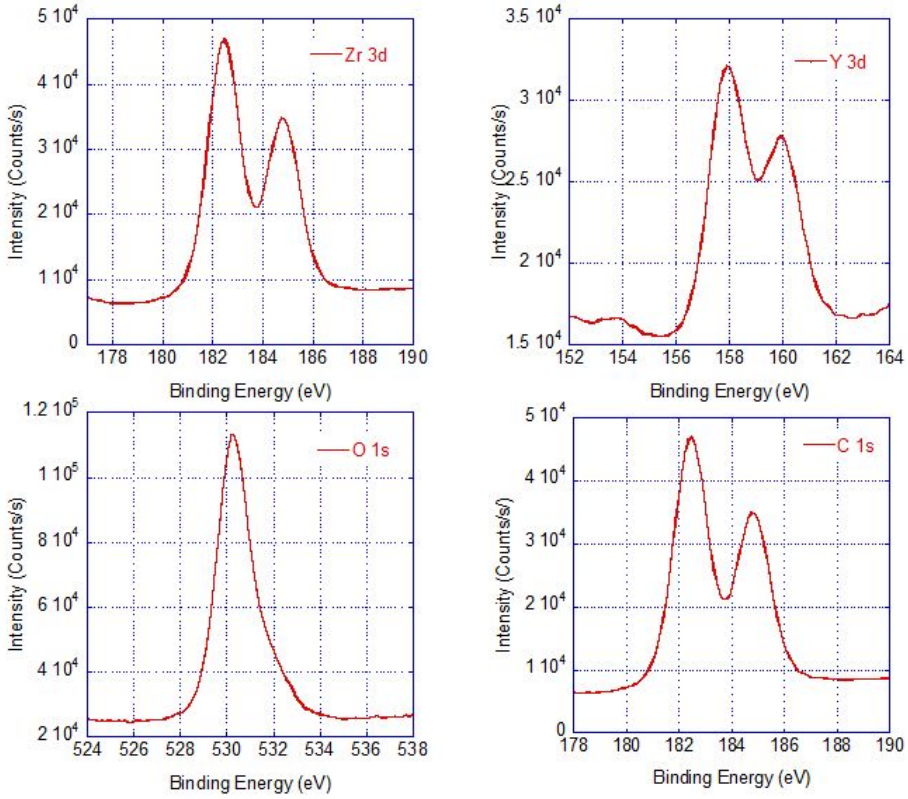

Figure 3.37 ALD-YSZ diffraction peaks (~10nm thick)

Table 3.5 Composition data of 100 cycled ALD-YSZ on Si wafer

Element	Peak Binding Energy (eV)	Atomic Concentration (%)
Zr 3d	182.5	20.9
Y 3d	157.9	3.1
O 1s	530.3	62.2
C 1s	284.9	13.8

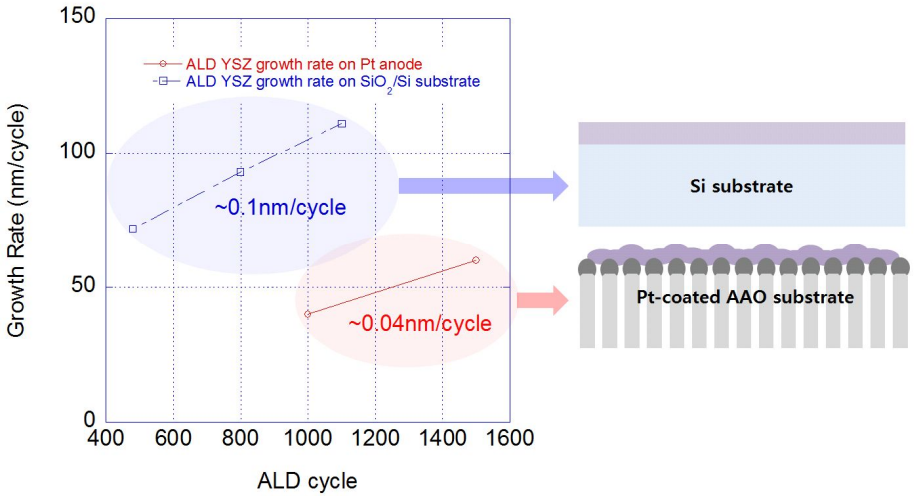

Figure 3.38 ALD-YSZ growth rates on Si wafer and dense Pt-coated AAO

To set the condition of GDC-sputtering, we deposited GDC on rotating substrate (4rpm) at 25°C, 100°C, 300°C and 500°C for 3 hours with GDC10 target. As temperature elevated, growth rate and grain size decreased but density increased with smoother surface. (Figure 3.39 and 3.40) With FE-SEM and AFM analysis, we confirmed RMS (root mean square) value and mean grain size at 500°C was 2.2 and 8.8 nm. The crystallinity also increased as temperature elevated, especially the intensity of (2 2 2) peak showed dramatic change. (Figure 3.41) Gd doping concentration showed increasing tendency but it controlled below 14%.

Table 3.6 GDC sputtering conditions

	Conditions
Substrate temp.	500˚C
Heater type	halogen
Rotating speed	1rpm
Gas composition	Ar : O_2 (80 : 20)
RF power	150W
Target composition	$Ce_{0.9}$ $Gd_{0.1}$ $O_{1.95}$
T-S distance	7.5cm
Growth rate	20nm/hour

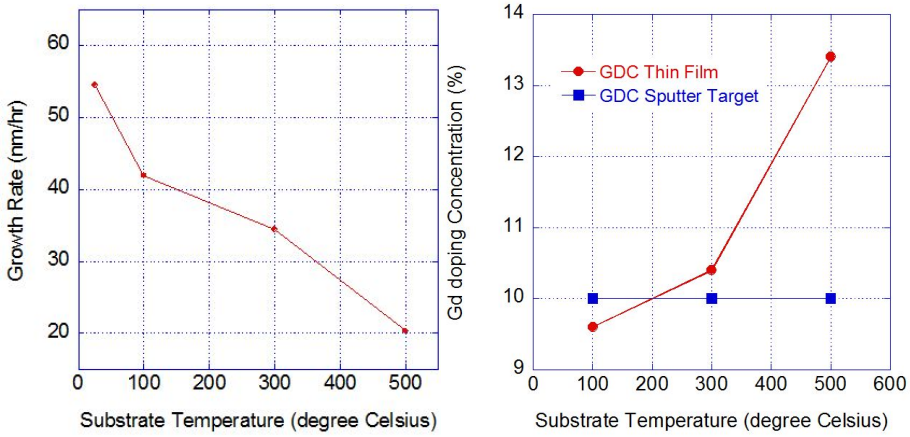

Figure 3.39 sputtered GDC growth rates and Gd doping concentration results at various temperatures

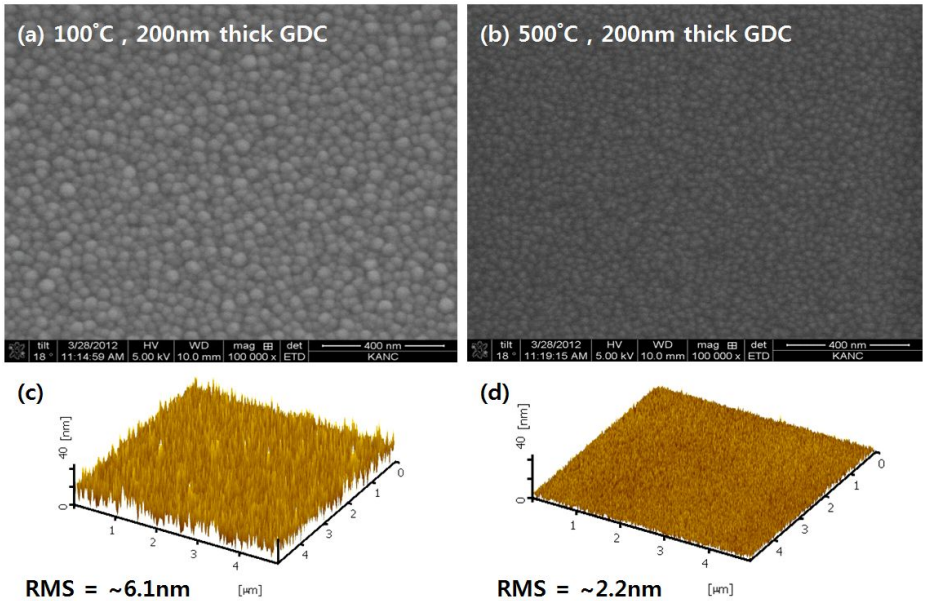

Figure 3.40 sputtered GDC surface morphology (A)(C) at 100°C and (B)(D) at 500°C

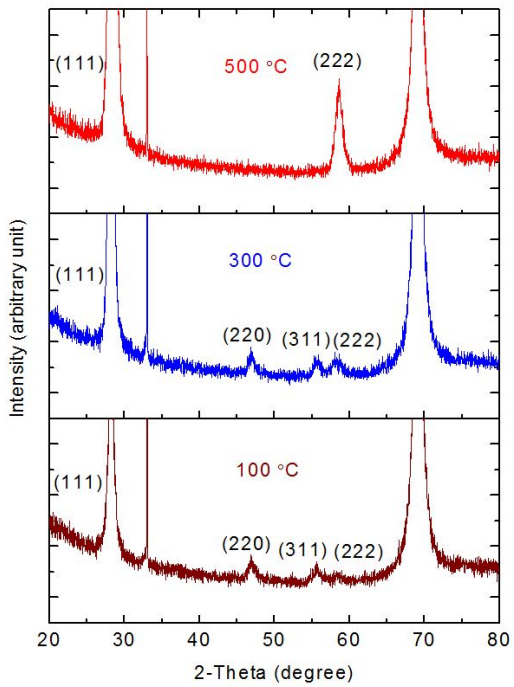

Figure 3.41 sputtered GDC X-ray diffraction peaks at various deposition temperatures

3.4.3 Experimental results

The final cell structure is shown in Figure 3.42. With the electrode area of 1mm^2, GDC-based thin film cell with 60nm ALD-YSZ showed stable performance. The OCV was over 1V and this means that gas permeation blocked well and that the ALD-YSZ layer functions as a good electron blocking layer. ASR value was 0.49Ω·cm^2 and the peak power density was measured about 77mW/cm^2 at 450°C.

With these results, we could confirm the absolute performance enhancement from the free-standing ALD-YSZ / sputtered GDC bi-layered electrolyte cell as well as ALD-YSZ / bulk GDC case.

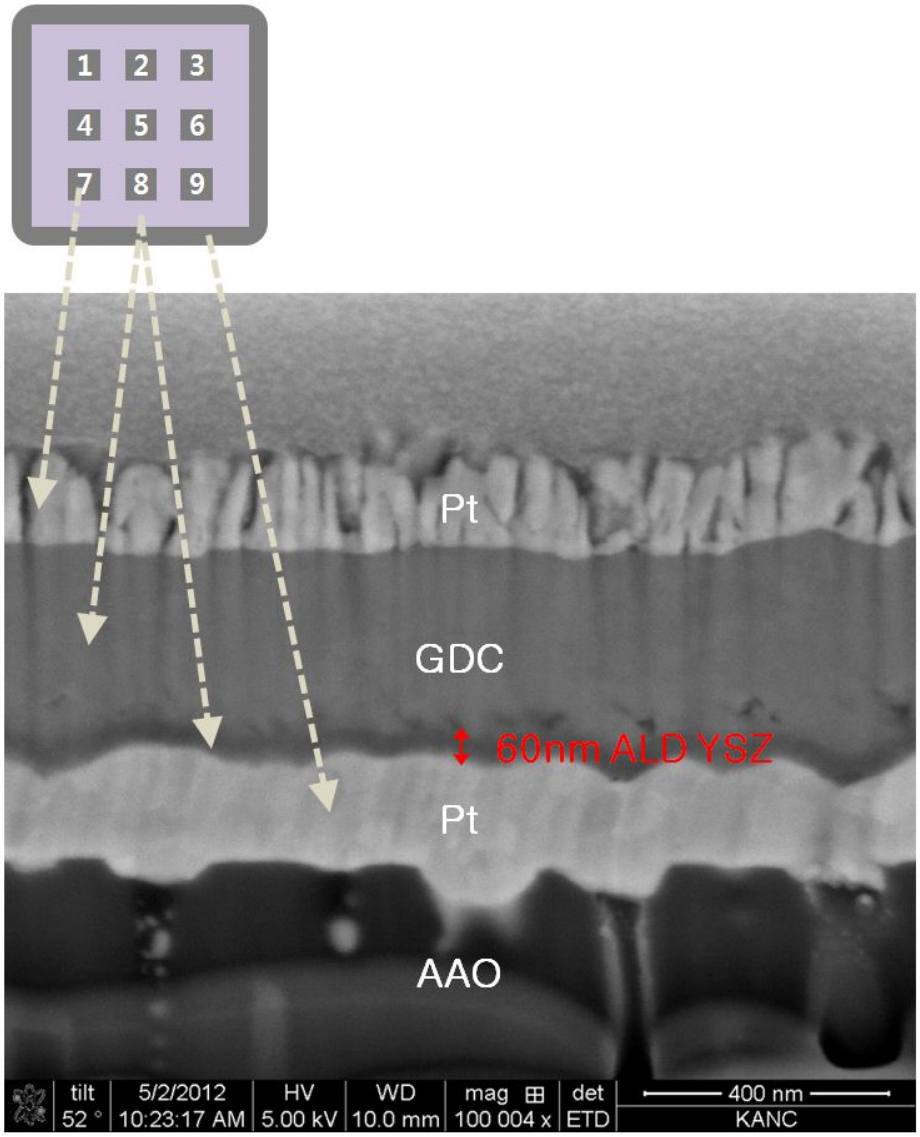

Figure 3.42 FIB-SEM image of the final structure of the free-standing bi-layered thin film cell

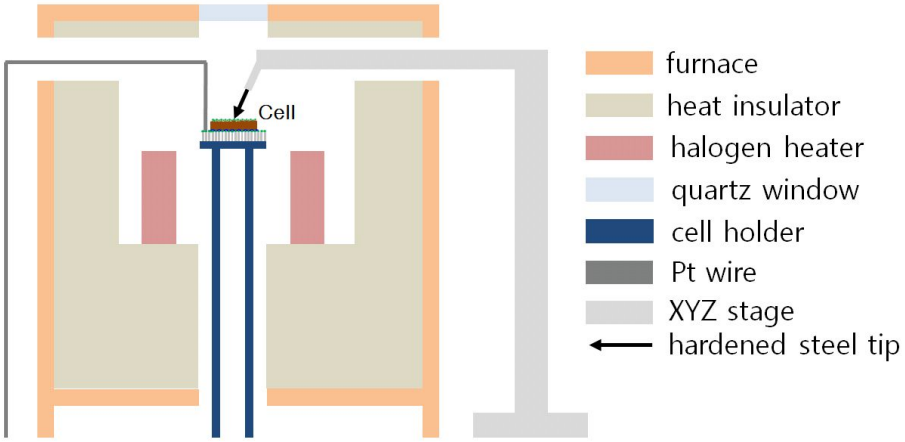

Figure 3.43 Test station for free-standing thin film SOFCs

Figure 3.44 Cathode current collections via a tip type probe

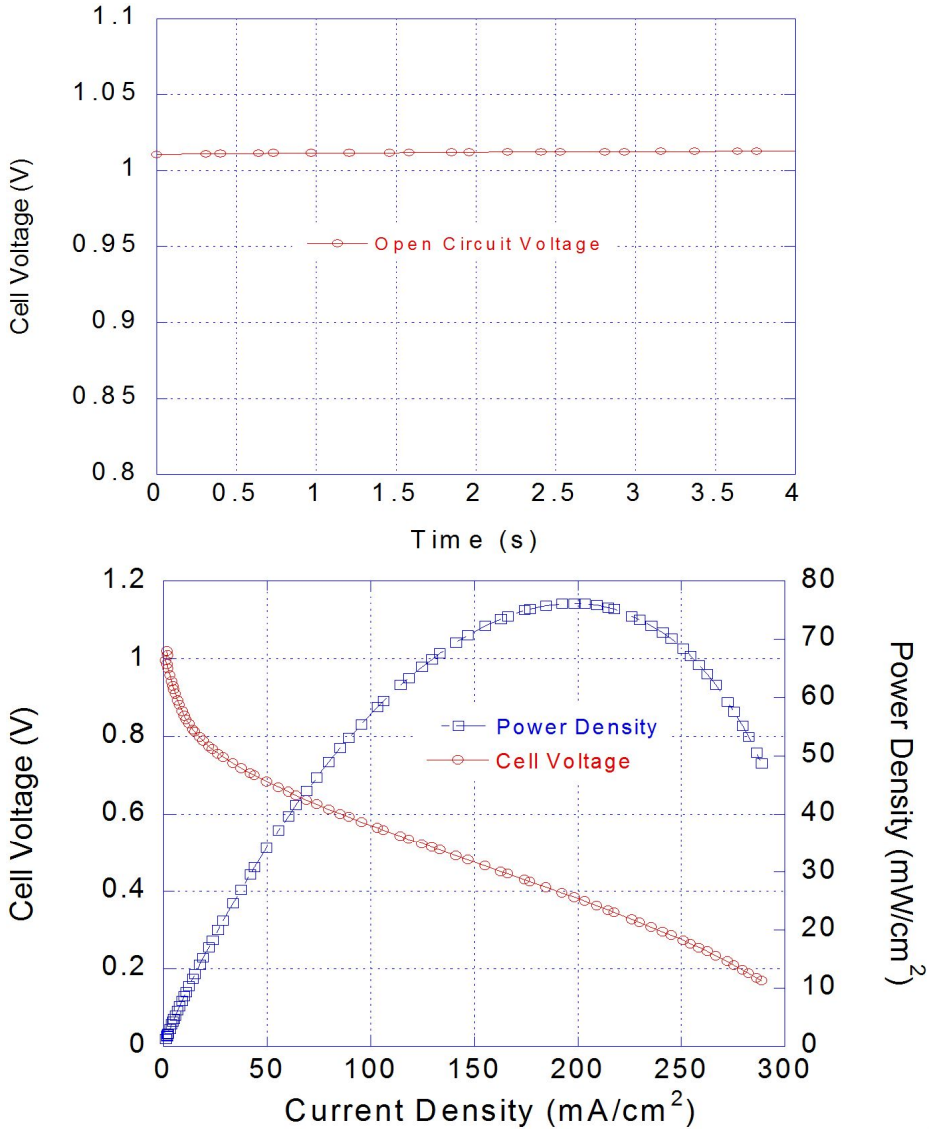

Figure 3.45 OCV and iV results of the bi-layered free-standing thin film SOFC

4. Concluding remarks

4.1 Conclusion

We started this study to lower the operation temperature of SOFCs. The attempt to fabricate YSZ/GDC bi-layered electrolyte cells via ALD method could prove great feasibility that a nano-scaled YSZ thin layer was able to enhance the performance and the durability of GDC-based SOFCs for intermediate temperature operation.

In summary,

- We deposited 50, 100, 200nm YSZ layer on bulk GDC via ALD successfully and confirmed them through FIB-SEM and XPS.
- We observed increases of over 50% in the peak power density and of about 5% in OCV at 600°C, and constant OCV over 8 hours under 5% hydrogen-concentration with the 690 cycles (about 100nm) ALD-YSZ electrolyte cell unlike the case of the pure GDC case.
- With SEM results of reduced GDC and YSZ coated GDC, we could presume that the protective ALD-YSZ layer could prevent the ceria reduction which might result in electron conductivity and micro crack generation on GDC, so that it enabled enhanced ohmic resistance.
- Through the AFM results for the surfaces of ALD-YSZ/GDC bi-layered electrolytes that were exposed various temperatures and hydrogen gas, we confirmed ALD-YSZ layer could suppress the roughness changing in

hydrogen gas and there was critical thickness limit for this functionality. (50nm at 600°C, 100nm at 800°C)

- At 1200°C the tendency that YSZ melted and moved to GDC's grain boundary started. We observed YSZ/GDC mixing with XPS depth profile analysis. Finally GDC and YSZ layer mixed entirely at 1500°C. With these results, we could know the cell fabrication temperature limit must exist between 800°C and 1200°C.
- In comparison ALD-YSZ bi-layered cells with PLD-YSZ bi-layered cells, we confirmed the effective thickness of PLD-YSZ functional layer starts from 200nm, where ALD-YSZ layer showed functionality from 100nm. This result came from the different surface morphology and the film property.
- We also confirm the availability of ALD-YSZ layer in the thin film free-standing bi-layered electrolyte cell which showed the OCV over 1V and the peak power density about 77mW/cm^2 at 450°C

In this study, we assure the high functionality of ALD-YSZ layer and the cell fabrication limit conditions for this configuration. We also found out the application could vary from bulk cell for IT operation to thin film free-standing cell for LT operation. So this research can be one of the solutions of the critical obstacle for the SOFC commercialization.

4.2 Future works

More studies are necessary to reach the solution for this research. For example, we should find optimum YSZ thickness for various deposition methods on various roughness surfaces. We also can examine sputtering, typical CVD and so on except for ALD and PLD. And the substrate roughness condition can vary the optimum thickness of YSZ layer.

We are preparing the fabrication method of anode supported ceria based cells with ALD-YSZ functional layer to compare the reasonable performance which comes necessarily from thin electrolytes. We gained the maximum power density of 55mW at 600°C and of 73.3mW at 650°C with 500μm bi-layered electrolyte supported cells. Under the simple supposition, if we reduce the electrolyte thickness to typical value of 10~20μm, we can expect much higher peak power density than the data in previous papers about bi-layered electrolyte SOFCs via various techniques. (Figure 4.1 and Table 4.1) Especially with this method, we can easily enlarge the cell size differ to our free-standing μSOFC.

On the view point of free-standing cell, area enlargement the first agent issue. Or we need to integrate the cells via optimal stacking methods. Carbon-free ALD-YSZ and micro-structural optimization of AAO-supported Pt anode are the fastest way to enhance the performance with the present setup.

Table 4.1 Performance expectations for the ALD-YSZ bi-layered SOFCs

temp.	thickness	avg. reported (mW)	ALD-YSZ iR corrected (mW)	enhancement
600°C	**500µm**	-	**55.0**	-
	100µm	250.0	275.0	10%
	50µm	422.0	550.0	30%
	20µm	582.6	1375.0	136%
650°C	**500µm**	-	**73.3**	-
	100µm	330.0	366.5	11%
	50µm	535.4	733.0	37%
	20µm	699.7	1832.5	162%

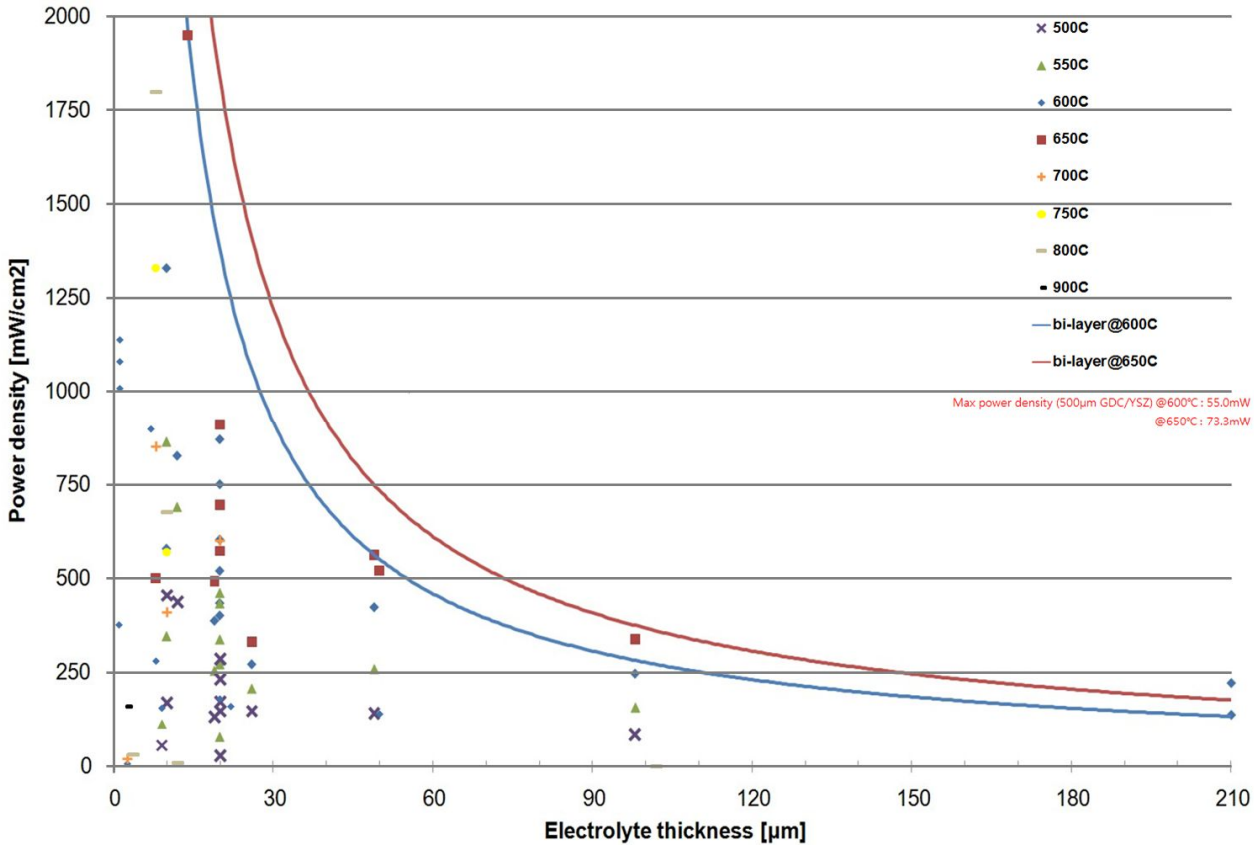

Figure 4.1 Power density expectation graphs and reported power densities of ceria based bi/single layered electrolyte SOFCs

References

1. DOE, *A demonstration of the working mechanism of a full cell*, online: http://p2library.nfesc.navy.mil/issu...5/fuelcell.jpg.

2. O'Hayre, R.P., et al., *Fuel cell fundamentals*. 2nd ed2009, Hoboken, NJ, USA: John Wiley & Sons.

3. Dicks, A. and J. Larminie, *Fuel cell systems explained*. 2nd ed2003, Hoboken, NJ, USA: SAE International and John Wiley & Sons.

4. 심준형, et al., *저온 작동 박막 고체산화물 연료전지*. 한국세라믹학회지, 2006. **43**(12): p. 751-757.

5. DOE, *Types of fuel cells*, online: http://www1.eere.energy.gov/hydrogenandfuelcells/fuelcells/fc_types.html.

6. Singhal, S.C. and K. Kendall, *High temperature solid oxide fuel cells: fundamentals, design, and applications*. 1st ed2003, Amsterdam, Netherlands: Elsevier Science.

7. 손지원, et al., *박막공정의 융합화를 통한 초소형 고체산화물 연료전지의 제작: I. Spray Pyrolysis 법으로 증착된 Ni 기반 음극과 스퍼터링으로 증착된 YSZ 전해질의 다층구조*. 한국세라믹학회지, 2007. **44**(10): p. 589-595.

8. Garcia-Barriocanal, J., et al., *Colossal ionic conductivity at interfaces of epitaxial ZrO_2:Y_2O_3/$SrTiO_3$ heterostructures*. Science, 2008. **321**(5889): p. 676-680.

9. Ohring, M., *The materials science of thin films*. 2nd ed2002, Salt Lake City, UT, USA: Academic Press.

10. Beckel, D., et al., *Thin films for micro solid oxide fuel cells*. Journal of Power Sources, 2007. **173**(1): p. 325-345.

11. LERMPS, *Schematic representation of the magnetron sputtering process. (Zoom on the magnetron cathode)*, online:

http://lermps.utbm.fr/index.php?lang=en&pge=30.

12. 고정식, *박막공정을 이용한 연료전지 MEA 구성*, in *기계항공공학부*2009, 서울대학교 대학원: 서울.

13. Aaltonen, T., *Atomic layer deposition of noble metal thin films*2005, Helsinki, Finland: University of Helsinki.

14. Kharton, V.V., F.M.B. Marques, and A. Atkinson, *Transport properties of solid oxide electrolyte ceramics: a brief review.* Solid State Ionics, 2004. **174**(1): p. 135-149.

15. Yahiro, H., et al., *High Temperature Fuel Cell with Ceria-Yttria Solid Electrolyte.* Journal of the Electrochemical Society, 1988. **135**(8): p. 2077-2080.

16. Inoue, T., et al., *Study of a solid oxide fuel cell with a ceria-based solid electrolyte.* Solid State Ionics, 1989. **35**(3-4): p. 285-291.

17. Eguchi, K., et al., *Electrical properties of ceria-based oxides and their application to solid oxide fuel cells.* Solid State Ionics, 1992. **52**(1-3): p. 165-172.

18. Virkar, A.V., *Theoretical analysis of solid oxide fuel cells with two-layer, composite electrolytes: electrolyte stability.* Journal of the Electrochemical Society, 1991. **138**(5): p. 1481-1487.

19. Mehta, K., R. Xu, and A.V. Virkar, *Two-layer fuel cell electrolyte structure by sol-gel processing.* Journal of Sol-Gel Science and Technology, 1998. **11**(2): p. 203-207.

20. Chour, K.W., J. Chen, and R. Xu, *Metal-organic vapor deposition of YSZ electrolyte layers for solid oxide fuel cell applications.* Thin Solid Films, 1997. **304**(1): p. 106-112.

21. Tsai, T., E. Perry, and S. Barnett, *Low-temperature solid-oxide fuel cells utilizing thin bilayer electrolytes.* Journal of the Electrochemical Society, 1997. **144**(5): p. L130-L132.

22. Soral, P., U. Pal, and W.L. Worrell, *Comparison of power densities and chemical potential variation in solid oxide fuel cells with multilayer and single-layer oxide electrolytes.* Journal of the

Electrochemical Society, 1998. **145**(1): p. 99-106.

23. Wachsman, E.D., *Functionally gradient bilayer oxide membranes and electrolytes.* Solid State Ionics, 2002. **152**: p. 657-662.

24. Park, J.Y. and E.D. Wachsman, *Stable and high conductivity ceria/bismuth oxide bilayer electrolytes for lower temperature solid oxide fuel cells.* Ionics, 2006. **12**(1): p. 15-20.

25. Ahn, J.S., et al., *High-performance bilayered electrolyte intermediate temperature solid oxide fuel cells.* Electrochemistry Communications, 2009. **11**(7): p. 1504-1507.

26. Chan, S.H., X.J. Chen, and K.A. Khor, *A simple bilayer electrolyte model for solid oxide fuel cells.* Solid State Ionics, 2003. **158**(1): p. 29-43.

27. Liu, Q.L., et al., *Anode-supported solid oxide fuel cell with yttria-stabilized zirconia/gadolinia-doped ceria bilalyer electrolyte prepared by wet ceramic co-sintering process.* Journal of Power Sources, 2006. **162**(2): p. 1036-1042.

28. Bi, Z., et al., *A high-performance anode-supported SOFC with LDC-LSGM bilayer electrolytes.* Electrochemical and Solid-State Letters, 2004. **7**(5): p. A105-A107.

29. Bi, Z., et al., *Electrochemical evaluation of* $La_{0.6}Sr_{0.4}CoO_3$-$La_{0.45}Ce_{0.55}O_2$ *composite cathodes for anode-supported* $La_{0.45}Ce_{0.55}O_2$-$La_{0.9}Sr_{0.1}Ga_{0.8}Mg_{0.2}O_{2.85}$ *bilayer electrolyte solid oxide fuel cells.* Solid State Ionics, 2005. **176**(7-8): p. 655-661.

30. Zhang, X., et al., *NiO–YSZ cermets supported low temperature solid oxide fuel cells.* Journal of Power Sources, 2006. **161**(1): p. 301-307.

31. Yang, D., et al., *Low temperature solid oxide fuel cells with pulsed laser deposited bi-layer electrolyte.* Journal of Power Sources, 2007. **164**(1): p. 182-188.

32. Hui, S.R., et al., *Metal-supported solid oxide fuel cell operated at 400–600°C.* Journal of Power Sources, 2007. **167**(2): p. 336-339.

33. Jang, W.S., S.H. Hyun, and S.G. Kim, *Preparation of YSZ/YDC and YSZ/GDC composite electrolytes by the tape casting and sol-gel dip-*

drawing coating method for low-temperature SOFC. Journal of Materials Science, 2002. **37**(12): p. 2535-2541.

34. Kim, S.G., et al., *Fabrication and characterization of a YSZ/YDC composite electrolyte by a sol-gel coating method.* Journal of Power Sources, 2002. **110**(1): p. 222-228.

35. Wachsman, E.D., et al., *Stable high conductivity ceria/bismuth oxide bilayered electrolytes.* Journal of the Electrochemical Society, 1997. **144**(1): p. 233-236.

36. Mehta, K., et al. *Fabrication and characterization of YSZ-coated ceria electrolytes*. in *The Third International Symposium on Solid Oxide Fuel Cells*. 1993. Honolulu: The Electrochemical Society.

37. Lim, H.T. and A.V. Virkar, *Measurement of oxygen chemical potential in Gd_2O_3-doped ceria-Y_2O_3-stabilized zirconia bi-layer electrolyte, anode-supported solid oxide fuel cells.* Journal of Power Sources, 2009. **192**(2): p. 267-278.

38. Zhang, X., et al., *Stability study of cermet-supported solid oxide fuel cells with bi-layered electrolyte.* Journal of Power Sources, 2008. **185**(2): p. 1049-1055.

39. Myung, D.H., et al., *The effect of an ultra-thin zirconia blocking layer on the performance of a 1-μm-thick gadolinia-doped ceria electrolyte solid-oxide fuel cell.* Journal of Power Sources, 2012. **206**: p. 91-96.

40. Suzuki, T., et al., *Fabrication and characterization of microtubular SOFCs with multilayered electrolyte.* Electrochemical and Solid-State Letters, 2008. **11**(6): p. B87-B90.

41. Leng, Y.J., S.H. Chan, and Q. Liu, *Development of LSCF–GDC composite cathodes for low-temperature solid oxide fuel cells with thin film GDC electrolyte.* International Journal of Hydrogen Energy, 2008. **33**(14): p. 3808-3817.

42. Zha, S., W. Rauch, and M. Liu, *Ni-$Ce_{0.9}Gd_{0.1}O_{1.95}$ anode for GDC electrolyte-based low-temperature SOFCs.* Solid State Ionics, 2004. **166**(3): p. 241-250.

43. Zha, S., et al., *GDC-based low-temperature SOFCs powered by hydrocarbon fuels.* Journal of the Electrochemical Society, 2004.

151(8): p. A1128-A1133.

44. Zhen, Y.D., et al., *Fabrication and performance of gadolinia-doped ceria-based intermediate-temperature solid oxide fuel cells.* Journal of Power Sources, 2008. **178**(1): p. 69-74.

45. Leng, Y.J., et al., *Low-temperature SOFC with thin film GDC electrolyte prepared in situ by solid-state reaction.* Solid State Ionics, 2004. **170**(1): p. 9-15.

46. Xia, C. and M. Liu, *Low-temperature SOFCs based on $Gd_{0.1}Ce_{0.9}O_{1.95}$ fabricated by dry pressing.* Solid State Ionics, 2001. **144**(3): p. 249-255.

47. Liu, Q.L., K.A. Khor, and S.H. Chan, *High-performance low-temperature solid oxide fuel cell with novel BSCF cathode.* Journal of Power Sources, 2006. **161**(1): p. 123-128.

48. Yang, M., et al., *Interaction of $La_{0.8}Sr_{0.2}MnO_3$ interlayer with $Gd_{0.1}Ce_{0.9}O_{1.95}$ electrolyte membrane and $Ba_{0.5}Sr_{0.5}Co_{0.8}Fe_{0.2}O_{3-\delta}$ cathode in low-temperature solid oxide fuel cells.* Journal of Power Sources, 2008. **185**(2): p. 784-789.

49. Misono, T., et al., *Ni-SDC cermet anode fabricated from NiO–SDC composite powder for intermediate temperature SOFC.* Journal of Power Sources, 2006. **157**(2): p. 754-757.

50. Joo, J.H. and G.M. Choi, *Micro-solid oxide fuel cell using thick-film ceria.* Solid State Ionics, 2009. **180**(11-13): p. 839-842.

51. Kim, D.J., *Lattice parameters, ionic conductivities, and solubility limits in fluorite-structure MO_2 oxide [M= Hf^{4+}, Zr^{4+}, Ce^{4+}, Th^{4+}, U^{4+}] solid solutions.* Journal of the American Ceramic Society, 1989. **72**(8): p. 1415-1421.

52. Bishop, S.R., K. Duncan, and E.D. Wachsman, *Thermo-chemical expansion of SOFC materials.* ECS Transactions, 2006. **1**(7): p. 13-21.

53. Chiang, H.W., R.N. Blumenthal, and R.A. Fournelle, *A high temperature lattice parameter and dilatometer study of the defect structure of nonstoichiometric cerium dioxide.* Solid State Ionics, 1993. **66**(1-2): p. 85-95.

54. Atkinson, A., *Chemically-induced stresses in gadolinium-doped ceria solid oxide fuel cell electrolytes.* Solid State Ionics, 1997. **95**(3): p. 249-258.

55. 박상현, *전자 덫을 이용한 세리아계 전해질의 전해질 영역 제어*, in *재료공학부* 2008, 서울대학교 대학원: 서울.

56. Shim, J.H., et al., *Atomic layer deposition of yttria-stabilized zirconia for solid oxide fuel cells.* Chemistry of Materials, 2007. **19**(15): p. 3850-3854.

57. 권태현, *중온형 고체 산화물 연료전지용 이중층 전해질의 전기화학적 특성*, in *재료공학부* 2011, 서울대학교 대학원: 서울.

58. 하승범, *Fabrication of nano-structured thin film solid oxide fuel cell by multi-deposition methods*, in *기계항공공학부* 2012, 서울대학교 대학원: 서울.

59. Moulder, J.F., et al., *Handbook of x-ray photoelectron spectroscopy: a reference book of standard spectra for identification and interpretation of* 1992, Boca Raton, FL, USA: Perkin-Elmer. 261.

60. Matsui, T., et al., *Electrochemical properties of ceria-based oxides for use in intermediate-temperature SOFCs.* Solid State Ionics, 2005. **176**(7): p. 647-654.

61. Yuan, S. and U. Pal, *Analytic solution for charge transport and chemical-potential variation in single-layer and multilayer devices of different mixed-conducting oxides.* Journal of the Electrochemical Society, 1996. **143**(10): p. 3214-3222.

62. Zhang, X., et al., *Internal shorting and fuel loss of a low temperature solid oxide fuel cell with SDC electrolyte.* Journal of Power Sources, 2007. **164**(2): p. 668-677.

63. Jung, H.Y., et al., *Fabrication and performance evaluation of 3-cell SOFC stack based on planar 10cm×10cm anode-supported cells.* Journal of Power Sources, 2006. **159**(1): p. 478-483.

64. Tsoga, A., et al., *Gadolinia-doped ceria and yttria stabilized zirconia interfaces: regarding their application for SOFC technology.* Acta Materialia, 2000. **48**(18-19): p. 4709-4714.

65. Zhou, X.D., B. Scarfino, and H.U. Anderson, *Electrical conductivity and stability of Gd-doped ceria/Y-doped zirconia ceramics and thin films.* Solid State Ionics, 2004. **175**(1): p. 19-22.

66. Kwon, C.W., et al., *High-performance micro-solid oxide fuel cells fabricated on nanoporous anodic aluminum oxide templates.* Advanced Functional Materials, 2011. **21**(6): p. 1154-1159.

67. Brahim, C., et al., *Electrical properties of thin yttria-stabilized zirconia overlayers produced by atomic layer deposition for solid oxide fuel cell applications.* Applied Surface Science, 2007. **253**(8): p. 3962-3968.

68. Shim, J.H., et al., *Intermediate-temperature ceramic fuel cells with thin film yttrium-doped barium zirconate electrolytes.* Chemistry of Materials, 2009. **21**(14): p. 3290-3296.

69. Huang, H., et al., *High-performance ultrathin solid oxide fuel cells for low-temperature operation.* Journal of the Electrochemical Society, 2007. **154**(1): p. B20-B24.

국문 초록

수소가 인류의 마지막 자원이 될 것은 이미 우리에게 익숙한 사실이다. 에너지 분야에 있어 주된 이슈는 과연 어떤 에너지 변환 장치가 미래에 살아남아 사용될 것인가에 관한 것이다. 많은 연구자들이 연료전지를 차세대 전원으로 주목한 이래, 이를 상용화하기 위한 노력이 진행 중이다.

통상적인 고분자 전해질막 연료전지가 물 관리 문제, 귀금속 촉매 사용, 전해질에 대한 특허 문제, 고가의 그라파이트 분리판 사용, 일산화탄소 피독 문제 등의 단점을 보임에 비해서, 고체산화물 연료전지는 많은 장점을 갖고 있다.

하지만 고체산화물 연료전지의 상용화에 있어 가장 큰 문제는 높은 작동에 있다. 이는 전극-전해질 결합체의 열응력, 니켈 응집, 구성물질 간의 반응, 제한된 밀봉재 선택, 고가의 분리판 물질 등의 문제를 야기시킨다. 따라서 고체산화물 연료전지의 특징 및 장점을 유지시키면서도 고온과 저온 작동의 문제점을 피할 수 있는 중온 작동 영역대의 고체산화물 연료전지에 관심을 집중시켰다.

본 연구에서는 전해질의 두께를 줄이거나 이온 전도성이 높은 물질을 전해질로 채택하는 두 가지 방법론을 모두 사용하여 작동

온도를 낮추는 것을 주제로 하여 이에 필요한 측정 장치와 지그를 제작하는 것으로 그 시작을 열었다.

높은 이온 전도도의 가돌리니아 돕트 세리아 (GDC) 상에 원자막 증착법 (ALD)을 통한 나노 단위의 이트리아 안정화 지르코니아 (YSZ) 박막을 증착한 이중층 전해질은 중온 영역 작동에서 성능과 내구성을 증대시키는 큰 가능성을 보였다.

첫째, 주사 전자 현미경 (SEM)과 X 선 광전자 분광법 (XPS) 을 통한 두께, 증착 속도, 구성 원소 비를 확인한 결과 성공적인 YSZ 의 ALD 증착을 확인할 수 있었고, 고온의 전극 소결 과정과 환원 환경에서의 작동 등에도 YSZ 박막은 건재하였다. 벌크 GDC 에 100nm 를 ALD 증착한 셀의 실험 결과 순수 GDC 전해질 셀과 달리, 50%의 출력 향상과 5% 높은 개회로 전압 (OCV)을 섭씨 600 도에서 얻을 수 있었다. 또한 5% 농도의 수소로 일정한 OCV 추이도 측정되었다. 이 원인을 밝히고자 YSZ 를 ALD 로 증착한 GDC 와 순수 GDC 를 비교 관찰한 결과, ALD 로 증착한 YSZ 막이 GDC 의 환원을 막아 전압 강하와 저항 손실을 증가시키는 전자 전도성과 미세 균열을 방지하는 것으로 밝혀졌다.

둘째, 다양한 온도와 수소에의 노출 여부를 달리하면서 GDC 상에 ALD 를 이용한 다양한 두께의 YSZ 이중층 전해질의

표면을 관찰하였다. 원자간력 현미경 (AFM)을 통해 ALD 를 이용한 YSZ 막이 수소에의 노출에 의한 표면 조도 (roughness) 변화를 막는 것을 확인하였고, 이 기능이 발현되기 시작하는 두께가 온도 별로 존재함을 알게 되었다. 섭씨 1200 도에서 박막 YSZ 막이 녹기 시작하여 GDC 결정립계로 이동하는 현상을 보였으며, XPS 깊이 방향 분석을 통해 이 온도에서 YSZ 막과 GDC 가 섞이기 시작하는 것을 확인하였다. 이로써 이중층 전해질 구조의 셀을 제작하는 온도는 섭씨 800 도와 1200 도 사이에 그 한계점이 존재하며, 이런 구조의 셀을 제작할 때 해당 온도를 거쳐야 하는 대부분의 습식법 (wet process)으로 전극을 생성하는 것을 피해야 함을 밝혔다. 수소 노출 시편 관찰 결과, 섭씨 600 도에서는 50nm 의 YSZ 막이, 섭씨 800 도에서는 100nm YSZ 막이 표면 안정성을 확보하게 함을 알게 되었다.

셋째 ALD 를 이용한 이중층 셀과 펄스 레이저 증착법 (PLD)으로 증착한 이중층 셀을 비교한 결과, 100 nm 를 ALD 로 증착한 경우와 200 nm 를 PLD 로 증착한 경우가 기능상의 유사함을 보였다. 이에 대해 ALD 와 PLD 의 증착 단위 및 과정상의 상이함으로 비롯된 표면형상과 막의 특성이 달라졌기 때문임을 문헌을 통해 알아보았다. 또한 1mm 의 GDC 에 100 nm YSZ 를

PLD 로 증착한 경우, GDC 자체가 전자 전도성을 막아 100 nm PLD 박막의 GDC 의 표면 균열을 막는 기능만을 확인하였다.

마지막으로, ALD 를 이용한 YSZ 의 기능과 셀 제작시의 제한 조건을 확인한 후 단독 지지형 박막 이중층 전해질 셀을 제작하였다. 양극산화 알루미늄 (AAO) 기판에 스퍼터링 (sputtering)으로 백금 음극 증착, ALD 로 YSZ 를 증착, sputtering 으로 GDC 증착, sputtering 으로 백금 양극 증착 순으로 섭씨 500 도가 넘지 않는 온도로 셀을 제작하였다. 해당 셀로 1V 근처의 OCV 와 77mW/cm^2 의 출력 밀도를 섭씨 450 도의 작동온도에서 얻는 만족스러운 결과를 얻었고, 이로써 본 연구의 주제가 되는 전해질 구조가 저온 작동을 하는 박막 셀에도 적용 가능함을 밝히게 되었다.

주요어: 고체산화물 연료전지 (SOFC), 중온, 가돌리니아 돕트 세리아 (GDC), 원자막 증착법 (ALD), 이중층 전해질

학번: 2008-30200